Naval Research Laboratory

Stennis Space Center, MS 39529-5004

NRL/MR/7320--05--8894

Parameterizing the High Frequency Evolution of Nearshore Waves in a Nonlinear Wave Model

KACEY EDWARDS

Ocean Dynamics and Prediction Branch
Oceanography Division

JAYARAM VEERAMONY
Advanced Systems Group
Jacob Sverdrup, Inc.
Stennis Space Center, MS

JAMES KAIHATU

Ocean Dynamics and Prediction Branch
Oceanography Division

October 7, 2005

REPORT DOCUMENTATION PAGE

Form Approved
OMB No. 0704-0188

1. REPORT DATE *(DD-MM-YYYY)*	**2. REPORT TYPE**	**3. DATES COVERED** *(From - To)*
7-10-2005	Memorandum Report	

4. TITLE AND SUBTITLE

Parameterizing the High Frequency Evolution of Nearshore Waves in a Nonlinear Wave Model

5a. CONTRACT NUMBER

5b. GRANT NUMBER

5c. PROGRAM ELEMENT NUMBER
PE0601153N

6. AUTHOR(S)

Kacey Edwards, Jayaram Veeramony,* and James Kaihatu

5d. PROJECT NUMBER

5e. TASK NUMBER

5f. WORK UNIT NUMBER
73-8580-05

7. PERFORMING ORGANIZATION NAME(S) AND ADDRESS(ES)

Naval Research Laboratory
Oceanography Division
Stennis Space Center, MS 39529-5004

8. PERFORMING ORGANIZATION REPORT NUMBER

NRL/MR/7320--05-8894

9. SPONSORING / MONITORING AGENCY NAME(S) AND ADDRESS(ES)

Office of Naval Research
800 N. Quincy St.
Arlington, VA 22217-5660

10. SPONSOR / MONITOR'S ACRONYM(S)
ONR

11. SPONSOR / MONITOR'S REPORT NUMBER(S)

12. DISTRIBUTION / AVAILABILITY STATEMENT

Approved for public release; distribution is unlimited.

13. SUPPLEMENTARY NOTES

*Advanced Systems Group, Jacob Sverdrup, Inc., Stennis Space Center, MS

14. ABSTRACT

Waves propagating through the shoaling and surf zones exhibit properties not characteristic of linear sinusoidal waves. Nonlinear wave-wave interactions act to transfer energy between the different harmonics of the peak frequency; this transfer is most apparent from the peak frequency of the spectrum to higher harmonics of the peak. As a result of these nonlinear interactions, the shape of a wave is altered making it asymmetrical vertically (skewness) and horizontally (asymmetry). The effects of nonlinear interactions are most easily seen in wave spectra, and the accuracy of a model's frequency dispersion relation greatly effects nonlinear interactions. Therefore, the frequency domain version of a nonlinear mild slope equation gives a very good representation of the propagation of waves through the shoaling and surf zones. However, such models are computationally expensive. In order to reduce the computational cost of the nonlinear mild slope equation model, it is combined with the high-wavenumber Toba range parameterization of Smith and Vincent (2003) to form a hybrid model, thus constraining the high frequencies to a specified energy level. The hybrid model reduces the number of frequency components explicitly modeled by the nonlinear mild slope equation so that the one-dimensional model satisfactorily replicates chosen experiments in minutes, rather than hours. However, important wave parameters, like skewness and asymmetry, disagree with observations and full model results. Further work is needed to improve the hybrid model's energy level computation for the parameterized portions of spectra and the model's ability to produce results capable of adequately replicating important wave parameters.

15. SUBJECT TERMS

Nonliner waves; Wave parameters; Hybrid model

16. SECURITY CLASSIFICATION OF:			**17. LIMITATION OF ABSTRACT**	**18. NUMBER OF PAGES**	**19a. NAME OF RESPONSIBLE PERSON**
a. REPORT	**b. ABSTRACT**	**c. THIS PAGE**			Kacey Edwards
Unclassified	Unclassified	Unclassified	UL	100	**19b. TELEPHONE NUMBER** *(include area code)* (228) 688-5077

Standard Form 298 (Rev. 8-98)
Prescribed by ANSI Std. Z39.18

TABLE OF CONTENTS

LIST OF ILLUSTRATIONS

Figure

LIST OF TABLES

Table

PARAMETERIZING THE HIGH FREQUENCY EVOLUTION OF NEARSHORE WAVES IN A NONLINEAR WAVE MODEL

CHAPTER 1

INTRODUCTION

Waves propagating through the nearshore environment present a unique set of problems. As depth decreases, the waves interact with the bottom. As a result, the wave speed decreases and the wave height increases. This process is called shoaling. In addition to changes in wave shape, shoaling also causes reflection and refraction. As the waves propagate further shoreward, they become unstable due to the continued increase in wave height and decrease in wave speed, causing the waves to break. Nonlinear effects in general dominate waves that are shoaling or breaking. Areas of strong nonlinearity usually coincide with regions of weak frequency dispersion.

The measure of nonlinearity is given by the relative waveheight, a/h, where a is wave amplitude and h is water depth. For $a/h << 1$, nonlinearity is weak. An additional nondimensional parameter is relative depth, kh, where k is wavenumber. Relative depth is a measure of frequency dispersion with $kh << 1$ indicating weak dispersion.

Nonlinear Waves

The nonlinearity of waves propagating in intermediate and shallow water ranges acts to exchange energy with other wave components (Madsen & Sørensen, 1993). The transfer of energy from the fundamental (peak) frequency to harmonics of the fundamental frequency (Kirby, 1997; Kaihatu, 2003) is the most pronounced, though these interactions occur across all frequencies.

Manuscript approved July 13, 2005.

The effects of nonlinear interactions between waves are easily seen in frequency or wavenumber spectra. Frequency spectra of shoaling waves are characterized by amplified harmonics of spectra's peak frequencies (Bredmose, 2002). Therefore, these spectra have multiple peaks. This phenomenon has been observed in data (Smith & Vincent, 2003) and model results, including Chen, Guza, and Elgar (1997), Herbers, Russnogle, and Elgar (2000), Eldeberky and Battjes (1996), and Herbers and Burton (1997).

Furthermore, dissipation of energy at high frequency components caused by breaking encourages the transfer of energy from low frequencies to high frequencies. The combined effects of dissipation and nonlinear interactions result in "broad" and "featureless" surf zone spectra with a single peak at the fundamental frequency (Herbers & Burton, 1997) but with more high frequency energy in general than was present in the offshore spectrum. This shape is sustained in the surf zone where dissipation and nonlinear interactions equilibrate.

For decades, it has been known that fully developed seas in the presence of wind also exhibit equilibrium between dissipation and input energy. Such equilibrium has allowed for parametric descriptions of wave spectra in deep water. However, little effort has been put into developing a parameterization for the observed equilibrium range of surf zone wave spectra (Smith & Vincent, 2003). Following early work of Thornton (1977) and more recent work of Zakharov (1999), Smith and Vincent developed a parameterization for the equilibrium range of surf zone wave spectra "in terms of a power law in wavenumber" (p. 3374).

In transferring energy among different frequencies, nonlinear interactions not only cause an equilibrium range in wave spectra but also change the wave shape. During the shoaling phase of wave evolution, wave crests become narrower and more peaked while wave troughs become broader and flat. This vertical asymmetry is termed skewness. An additional result of nonlinear interactions is the horizontal asymmetry (termed asymmetry) of the wave shape described as a pitched-forward sawtooth (Kirby, 1997).

History of Nonlinear Wave Models

Because of the nonlinear behavior of waves in the nearshore environment, linear theory is inadequate for describing shoaling waves and waves in the surf zone (Smith & Vincent, 2003; Kirby, 1999). Various types of nonlinear wave models have been developed.

Airy began the study of nonlinear waves in 1845. His work resulted in the Airy or Nonlinear Shallow Water Equations. These equations govern the evolution of nondispersive, nonlinear waves. Other early contributions were made by Boussinesq in1872 and Kortweg and de Vries in 1895 (Kirby, 1997).

In 1967 Peregrine derived a model of depth averaged velocity and surface elevation. Using his Boussinesq-type model, Peregrine (1967) performed the first calculation of wave shoaling and evolution (Kirby, 1997).

Development of Boussinesq models continued through the 1970's and 1980's. However, classical Boussinesq models are confined to shallow water areas of weak nonlinearity and dispersion (Bredmose, 2002; Kirby, 2003). With the increased availability of computers (Kirby, 1997), efforts were made to

improve classical Boussinesq models enabling them to represent wider ranges of relative depth (kh) (Kirby, 2003) resulting in the development of “extended” Boussinesq models. Extended Boussinesq models give valid results for deeper water by approximating the dispersion relation from fully-dispersive linear theory. Close to wave breaking, the waves are more nonlinear and developing fully nonlinear forms of Boussinesq models (Kirby, 2003) extends the validity of the Boussinesq model up to the breaking region. Fully nonlinear versions of extended Boussinesq models are accurate but the improved dispersion only “mimics” the behavior of full dispersion (Kaihatu, 2001) often by “tuning” the dispersion relation with free parameters (Kaihatu, 2003). Madsen and Sørensen (1993) emphasize that an accurate linear dispersion relation is essential in describing nonlinear interactions.

An additional complication of Boussinesq models is that they evolve the free surface in the time domain. Depending on the complexity of the time-domain equation, a transformation of extended Boussinesq models to the frequency domain often results in a model that produces different wave properties than the corresponding time domain model (Kaihatu, 2003).

An alternative to Boussinesq models is the mild slope equation. The mild slope equation retains full linear dispersion while simulating refraction, shoaling, and diffraction over a mildly sloping bottom. The derivation of a nonlinear mild slope equation results in a fully dispersive, weakly nonlinear model capable of operating in areas of wave shoaling and breaking (Kaihatu and Kirby, 1995).

An additional advantage to modeling waves with the nonlinear mild slope equation is that it evolves amplitudes, rather than the free surface (Kaihatu,

2003). Thus, these models are frequency domain models that directly provide information on nonlinearity (Kirby, 1997). Kaihatu (2003, p. 67) reports that nonlinear mild slope equation models "appear to be more accurate than frequency domain transformed extended Boussinesq models explored [within his study]." Furthermore, spatial resolution can be coarser than necessary with time domain equations.

Unfortunately, results of nonlinear mild slope equation models come at a high price. Like fully nonlinear extended Boussinesq models, nonlinear mild slope equation models are computationally expensive (Bredmose, 2002; Kaihatu, 2003); this is because the individual nonlinear interactions result in $O(N^2)$ operations, where N is the number of frequency components. Kaihatu (2001) shows that increasing the number of frequencies retained in a calculation improves the higher order moments, asymmetry and skewness, which result from nonlinear interactions. However, increasing frequency components increases the computational requirements (Kaihatu, 2003).

Significance of Study

This study focuses on utilizing the equilibrium range of surf zone wave spectra to reduce the computational expense of modeling with a nonlinear mild slope equation. To accomplish this task, a hybrid model is formulated so that the equilibrated portion of a spectrum is determined by Smith and Vincent's (2003) parameterization. Thus, the number of frequency components explicitly modeled by the nonlinear mild slope equation is reduced while retaining a significant number of frequency components in the spectra. A full description of the model

is given in the next chapter. The success of the hybrid model will be determined not only by its ability to replicate measured wave spectra but also by its ability to accurately give important wave properties like root-mean-squared waveheight (H_{rms}), skewness and asymmetry. Hybrid model results and corresponding wave properties are given in Chapter 4 followed by a discussion of the conclusions and future work in Chapter 5.

CHAPTER 2

THE MODEL

The hybrid wave model described in this chapter combines a nonlinear frequency domain model with a parameterization of the energy distribution of high frequency components. Kaihatu and Kirby (1995) derived and tested the nonlinear frequency domain model, and Smith and Vincent (2003) developed the parameterization. Sections below describe each entity of the hybrid model.

The Nonlinear Frequency Domain Model

This section describes the nonlinear frequency domain model, which explicitly calculates the evolution of the spectra at frequencies below the parametric cutoff. The model, first derived by Kaihatu and Kirby (1995) starts from the boundary value problem expressed in terms of the velocity potential (Φ) (e.g. Dean & Dalrymple, 1991). The governing equation and boundary conditions are

$$\nabla_h^2 \Phi + \Phi_{zz} = 0, \qquad -h \le z \le \eta \tag{2.1}$$

$$\Phi_z = -\nabla_h h \cdot \nabla_h \Phi, \qquad z = -h \tag{2.2}$$

$$\eta_t - \Phi_z + \nabla_h \eta \cdot \nabla_h \Phi = 0, \qquad z = \eta \tag{2.3}$$

$$g\eta + \Phi_t + \frac{1}{2}(\nabla_h \Phi)^2 + \frac{1}{2}(\Phi_z)^2 = 0, \qquad z = \eta. \tag{2.4}$$

η denotes free surface elevation relative to the still water level where the vertical coordinate $z = 0$. Upward from the still water level, z is positive; h denotes water depth. The subscript h denotes operation in the x and y directions, and the subscripts z and t represent differentiation in the respective dimensions.

Linear equations include the Laplace equation (equation 2.1) and the bottom boundary condition (equation 2.2). However, the surface boundary conditions (equations 2.3 and 2.4) not only are nonlinear but also are applied at the free surface, which is unknown. To retain nonlinearity, Kaihatu and Kirby expand the free surface boundary conditions about $z = 0$ and keep terms to $O(\varepsilon^2)$, where $\varepsilon = ka$ is the non-dimensional parameter that scales the nonlinear terms. Combining the dynamic and kinematic free surface boundary conditions results in a free surface boundary condition (equation 2.5) with the free surface variable eliminated.

$$\Phi_z = -\frac{1}{g}\left[\Phi_{tt} + \frac{1}{2}(\nabla_h \Phi)_t^2 + \frac{1}{2}(\Phi_z)_t^2 - \frac{1}{2g}(\Phi_t)_{zt}^2 + \nabla_h \cdot (\Phi_t \nabla_h \Phi)\right], \qquad z = 0. \quad (2.5)$$

Formulation of the boundary value problem requires assumptions that place limitations on the model. The Laplace equation (and existence of the velocity potential) requires that the fluid be inviscid and irrotational. In turn, the assumption of an inviscid flow requires that equation 2.2 use the free slip condition at the bottom. Therefore, with respect to the bottom, velocities are assumed to be tangential, realistically limiting frictional shear stress to an extremely thin layer. Furthermore, equation 2.4 (and consequently equation 2.5) assumes that no difference between the fluid's pressure and the atmospheric pressure exists, only gravity restores a displacement in the water surface.

From the boundary value problem, Kaihatu and Kirby (1995) take steps toward a parabolic approximation of a weakly nonlinear mild slope equation in the frequency domain. Although each transformation toward the desired model positively affects the modeling of waves in the surf zone, each imposes

restrictions. For the derivation of the two dimensional mild slope equation, transformation to the frequency domain and the parabolic approximation, see Kaihatu and Kirby. Here, only the discussion of the resulting effects and restrictions are provided.

The linear mild slope equation given as a function of wavenumber (k), phase speed (C), and group velocity (C_g) is written

$$\nabla \cdot (CC_g \nabla \hat{\Phi}) + k^2 CC_g \hat{\Phi} = 0 . \tag{2.6}$$

It combines shoaling, refraction and diffraction, including reflection (Battjes, 1994; Dingemans, 1997). In addition, it conserves energy of periodic gravity waves (Battjes). Although weakly nonlinear, the two dimensional mild slope equation retains several linear wave properties, including the linear depth dependence and dispersion relation given by

$$f_n(k_n, h, z) = \frac{\cosh k_n (h+z)}{\cosh k_n h} \quad \text{and} \tag{2.7}$$

$$\omega^2 = g k_n \tanh k_n h \text{, respectively.} \tag{2.8}$$

Because Kaihatu and Kirby (1995) seek a frequency domain model the time dependence is removed from the weakly nonlinear mild slope equation by two processes. First, Kaihatu and Kirby assume that the waves are periodic in time.

$$\Phi = \sum_{n-1}^{N} \frac{\Phi_n}{2} e^{-i\omega_n t} + \frac{\Phi_n^*}{2} e^{i\omega_n t} \tag{2.9}$$

where the asterisk denotes complex conjugate.

Second, they utilize resonant triad interactions between frequency components (Phillips, 1980) to factor out the time dependence from the nonlinear

term. The triad interactions result from the products of Fourier series applied to the nonlinear terms. Because the mild slope equation retains full linear dispersion, the accurate computation of phase mismatch and resulting energy transfer follows (Madsen & Sørensen, 1993). While the equation benefits from linear dispersion and remains free of time dependence, it remains elliptic.

Elliptic equations require specification of all boundaries and simultaneous solution of all points everywhere in the domain. To ease computational requirements and boundary specification, Kaihatu and Kirby (1995) employ a parabolic approximation (e.g. Radder, 1979). The parabolic approximation transforms the boundary value problem into an initial value problem requiring input at only the offshore boundary, marching the solution forward in space. The transformation requires that the wave field be primarily progressive in the positive x-direction; therefore, losing the ability to model backward-reflected waves (Battjes, 1994) or waves approaching at highly oblique angles to the x-direction (Kirby, 1986). In addition, the parabolic approximation inherently assumes that amplitudes vary slowly in the y-direction while "retaining fast wave-like variations in (only) the x-direction" (Kaihatu & Kirby, 1995, p. 1906). Kaihatu and Kirby fulfill these requirements by assuming

$$\hat{\Phi}_n(x,y) = -\frac{ig}{\omega_n} A_n(x,y) e^{i\int k_n(x,y)dx} \quad \text{and} \tag{2.10}$$

$$\hat{\Phi}_n(x,y) = \frac{ig}{\omega_n} A_n(x,y) e^{-i\int k_n(x,y)dx} \tag{2.11}$$

At this point, Kaihatu and Kirby (1995) scale the two dimensional equation and reduce it to a one dimensional, frequency domain mild slope equation. The resulting equation is

$$A_{nx} + \frac{\left(kCC_g\right)_{nx}}{2\left(kCC_g\right)_n} A_n = -\frac{i}{8\left(kCC_g\right)_n} \cdot \left[\sum_{l=1}^{n-1} RA_l A_{n-l} e^{i\int \left(k_l + k_{n-1} - k_n\right) dx} + 2\sum_{l=1}^{N-n} SA_l \; A_{n+l} e^{i\int \left(k_{n+l} - k_l - k_n\right) dx} \right], \tag{2.12}$$

referred to as the "fully dispersive nonlinear shoaling model" (Kaihatu, 1994, p. 19). Refer to Kaihatu and Kirby for a definition of the coefficients, R and S. Although equation 2.12 retains shoaling, refraction, and diffraction, the mild slope equation does not inherently account for energy losses resulting from friction or breaking (Berkhoff, 1972).

In order for the model to accurately propagate waves through the surf zone, it needs a dissipation mechanism. Kaihatu and Kirby (1995) employ the "'simple' probabilistic dissipation model" (p.1909) of Thornton and Guza (1983) given by

$$\beta(x) = \frac{3\sqrt{\pi}}{4\sqrt{gh}} \frac{B^3 f_{peak} H_{rms}^5}{\gamma^4 h^5}, \tag{2.13}$$

with the root-mean-square waveheight

$$H_{rms} = 2\sqrt{\sum_{n=1}^{N} \left|A_n\right|^2}. \tag{2.14}$$

and free parameters $B = 1$ and $\gamma = 0.6$. The dissipation model is based on probability because it describes the averaged dissipation of a population of waves, and as such no single breakpoint adequately describes the breaking

location of this random wavefield (Thornton & Guza). Rather than describe the initiation of breaking as a point, a breaking zone describes this area of the domain (Horikawa, 1988). At any one point in the breaking zone, some waves break while others remain unbroken, with waves of greater wave heights breaking offshore and smaller waves breaking closer to shore (Thornton & Guza).

The formulation of Thornton and Guza (1983) depends on the lumped characteristics of the spectrum without accounting for its frequency dependence. Kaihatu and Kirby (1995) distribute the dissipation model (equation 2.13), constant for all waves at each depth, over the frequency range of the spectrum in order to implement it in the model (Kaihatu, 2003). Following the approach of Mase and Kirby (1992), Kaihatu and Kirby split the distribution of the dissipation model between a frequency-squared function and a frequency-independent function. The dissipation mechanism is described by

$$\alpha_n = \alpha_{n0} + \left(\frac{f_n}{f_{peak}} \right)^2 \alpha_{n1} \text{ , where} \tag{2.15}$$

$$a_{n0} = F\beta(x) \text{ and} \tag{2.16}$$

$$\alpha_{n1} = \left[\beta(x) - \alpha_{n0} \right] \frac{f_{peak}^2 \sum_{n=1}^{N} |A_n|^2}{\sum_{n=1}^{N} f_n^2 |A_n|^2} . \tag{2.17}$$

N is the total number of frequency components retained by the model, and F is a free parameter that determines what percentage of the dissipation model (equation 2.13) is distributed to the frequency independent function (equation 2.16) (Kaihatu and Kirby). $F = 0$ provides full frequency-squared dependence. If

$F = 1$, the mechanism weights the dissipation according to the energy level in each frequency bin with no regard to frequency. According to Kaihatu and Kirby, giving the frequency-squared and frequency-independent functions the same weight produces the best results; therefore, $F = 0.5$. It is noted here that Kirby and Kaihatu (1996) provide physical reasoning for $F = 0$. The nonlinear frequency domain mild slope equation with dissipation is given by

$$A_{nx} + \frac{\left(kCC_g\right)_{nx}}{2\left(kCC_g\right)_n} A_n + \alpha_n A_n = -\frac{i}{8\left(kCC_g\right)_n} \cdot \left[\sum_{l=1}^{n-1} RA_l A_{n-l} e^{i\int \left(k_l + k_{n-1} - k_n\right) dx} + 2\sum_{l=1}^{N-n} SA_l \; A_{n+l} e^{i\int \left(k_{n+l} - k_l - k_n\right) dx} \right]. \quad (2.18)$$

Eldeberky and Madsen (1999) criticize Kaihatu and Kirby's (1995) transformation between amplitudes of Φ and amplitudes of η. The transformations, equations 2.10 and 2.11, are derived from the first order dynamic free surface boundary condition, which does not include the nonlinearity of equation 2.4 (Kaihatu, 2003). Kaihatu (2001) includes a second order correction to the transformation between amplitudes of Φ and amplitudes of η and reports that the correction is essential in correctly determining the free surface, especially for the high frequencies.

The Parameterization

The models discussed in the previous section describe the nonlinear evolution of waves in great detail. An alternative way of describing the nonlinear evolution of waves is to look for trends in the spectral shape and express these trends in terms of several parameters. This parameterization approach has been

applied in deep and finite depth wave models (Booij, Ris, & Holthuijsen, 1999). Like the equilibrium range of deepwater and finite depth wave spectra, the equilibrium range of surf zone wave spectra develop because nonlinear interactions transfer energy predominantly from low to higher harmonics. In addition, the parameterization of the surf zone equilibrium range follows a power law in wavenumber. Resio, Pihl, Tracy, and Vincent (2001) define this power law to be

$$S(k) = \beta k^n \,, \tag{2.19}$$

where $S(k)$ is the wavenumber spectrum. For waves in deep and finite water depth, β depends on wind speed, and $n = -5/2$. Resio et al. found the power law as applied to waves in deep and finite water depth to be valid for a range of wavenumbers from 1.5 to $3f_p$.

Smith and Vincent (2003) developed the parameterization of the surf zone equilibrium range using data from several laboratory and field experiments. The data used represented many combinations of several wave field and domain characteristics.

In developing their parameterization of the equilibrium range of surf zone wave spectra, Smith and Vincent (2003) showed that the equilibrium range consists of two subranges, referred to as the Toba range and the Zakharov range. While the parameterization of the Zakharov range describes the portion of the wavenumber spectra between $2.5k_p$ and $k = 1/h$, the Toba parameterization describes the area between $k = 1/h$ and $6k_p$. k_p is the wavenumber of maximum energy.

Smith and Vincent (2003) based the parameterization of the Toba range on data from two laboratory experiments and one set of field data totaling 109 spectra. The resulting mathematical formulation of the parameterization for the Toba range was found to be

$$S(k) = \beta_{Toba} k^{-5/2} \text{ , for } kh \geq 1 . \quad (2.20)$$

where $\beta_{Toba} = \alpha_{Toba} h^{0.5}$ with $\alpha_{Toba} = 0.0103$. In addition to the data used for the Toba parameterization, Smith and Vincent based the Zakharov parameterization on a second data set collected in the field. In total they used 227 spectra to find the parameterization. It is described mathematically by

$$S(k) = \beta_{Zak} k^{-4/3} \text{ , for } k_p < kh < 1 . \quad (2.21)$$

where $\beta_{Zak} = \alpha_{Zak} h^{1.67}$ with $\alpha_{Zak} = 0.0102$.

It is seen in equations 2.19 and 2.20 that the power transform of the Toba range and the power transform given by Resio et al. (2001) share the same slope. The difference between deep and finite depth wave spectra and surf zone wave spectra lies in the coefficient of the power transform. While the β of deep and finite depth wave spectra parameterizations depends on wind speed, the β of surf zone parameterizations depends on a more important surf zone parameter, depth.

Analysis of the parameterizations of the surf zone equilibrium subranges by Smith and Vincent (2003) confirm the parameterizations' depth dependences. As the waves propagate into shallow water, the Zakharov parameterization describes a larger part of the spectrum. In contrast if $k_p > 1/h$, only the Toba range exists.

The Hybrid Model

The hybrid model is a version of Kaihatu and Kirby's (1995) one dimensional nonlinear mild slope equation with the second order correction of Kaihatu (2001). In this model, complex amplitudes for the region of a spectrum where $k < 1/h$ are determined in the manner of Kaihatu and Kirby. For the $k \geq 1/h$ area of a spectrum, the hybrid model utilizes the Toba parameterization of Smith and Vincent (2003).

The difference in the domains of Kaihatu and Kirby (1995) and the Toba parameterization (Smith & Vincent, 2003) complicates the combining of the two models. Kaihatu and Kirby is a frequency domain model, and the parameterization is a function of wavenumber. Because Kaihatu and Kirby retain the linear dispersion relation, it is easy to employ equation 2.8 to obtain a wavenumber for each frequency of the wavefield. Since each frequency corresponds to a particular wavenumber and vice versa, only the component number determines the point in a spectrum where $k = 1/h$.

As the hybrid model marches forward in space, amplitudes for frequencies in the region outside the Toba range are explicitly calculated using equation 2.18, and equation 2.20 gives energy for each wavenumber inside the Toba range. For instances where $k_p > 1/h$, the Toba range defines the region of a spectrum where $k > k_p$. The relation

$$S(f) = \frac{S(k)\Delta k}{\Delta f} \tag{2.22}$$

transforms a wavenumber spectrum to a frequency spectrum. Since

$$S(f) = \frac{2|A_n|^2}{\Delta f}, \tag{2.23}$$

the amplitudes for each frequency in the Toba range are given by

$$A_n = \sqrt{\frac{S(f)\Delta f}{2}} e^{i\Theta} \text{ , where} \tag{2.24}$$

Θ is a random phase.

CHAPTER 3

TESTING DOMAINS AND METHODS

This chapter describes two domains used in the development of the hybrid model and for testing the hybrid model's performance; in addition, it covers the methods used for these tasks. The two domains of choice are a long, mildly sloping domain and the domain of Mase and Kirby's (1992) case two experiment. Observations exist only for the experiment of Mase and Kirby.

A Long, Mildly Sloping Domain (long slope)

This idealized testing domain replicates 1,292 m of a nearshore environment with a bottom slope of 0.01 (Figure 3.1). The long slope configuration roughly resembles the bathymetric profile at Duck, North Carolina, home of the U.S. Army Engineering Field Research Facility. At the offshore boundary the depth is 13 m. The input spectrum was determined from a time series, which was in turn determined from a random-phase decomposition of a TMA spectrum (Bouws, Gunther, Rosenthal, & Vincent, 1985) using the method of Cox, Kobayashi, and Wurjanto (1991). The TMA spectrum had a significant waveheight of 1 m with a peak frequency (f_p) of 0.1 Hz. The peakedness parameter for the TMA spectrum used was $\tilde{\gamma} = 20$, representative of a narrow-banded spectrum suited to swell. The energy at the peak frequency lies in a region of intermediate water depth, and the deep water region (higher frequencies) contains significant energy. The sampling interval of the time series is 0.5 s.

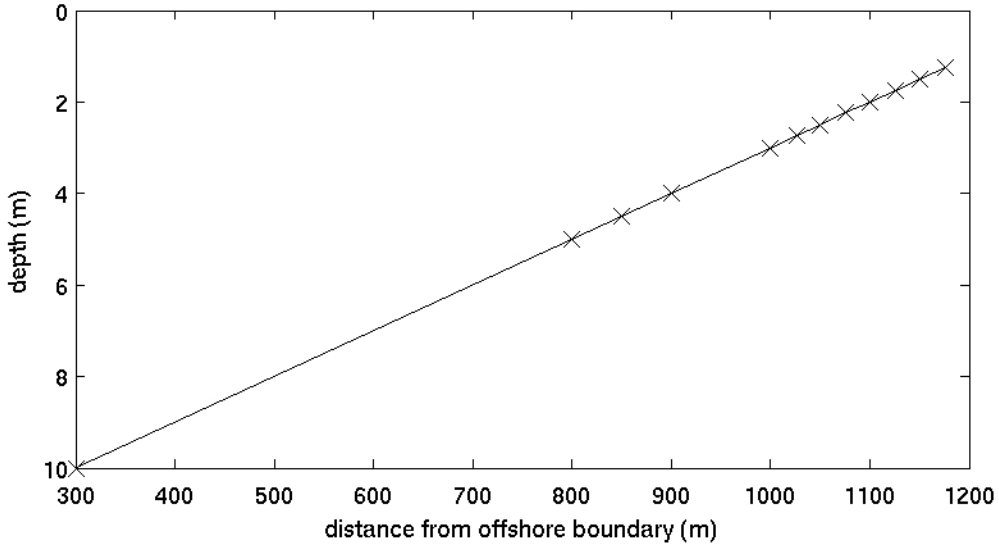

Figure 3.1 Long, mildly sloping (long slope) domain. Red x's denote the locations considered in comparisons.

Although no experimental data exist for this domain, it encompasses the characteristics of an "ideal" domain for the model of Kaihatu and Kirby (1995), which has been shown to possess sufficient skill in determining spectra for such a domain. Results of Kaihatu and Kirby provide spectra for the testing of the hybrid model.

Mase and Kirby's (1992) Domain (MK92)

Mase and Kirby (1992) set up a wavetank experiment that spanned 1,090 cm with a bottom slope of 0.05 (Figure 3.2). During their Case 2 experiment, they propagated random waves through the domain and collected time series data of free surface at depths of 47, 35, 30, 25, 20, 17.5, 15, 12.5, 10, 7.5, 5, and 2.5 cm. The Case 2 experiment of Mase and Kirby utilized a sampling interval of 0.05 s resulting in a time series of 15,000 points at each observation location (Mase & Kirby, 1992; Kaihatu, 1994).

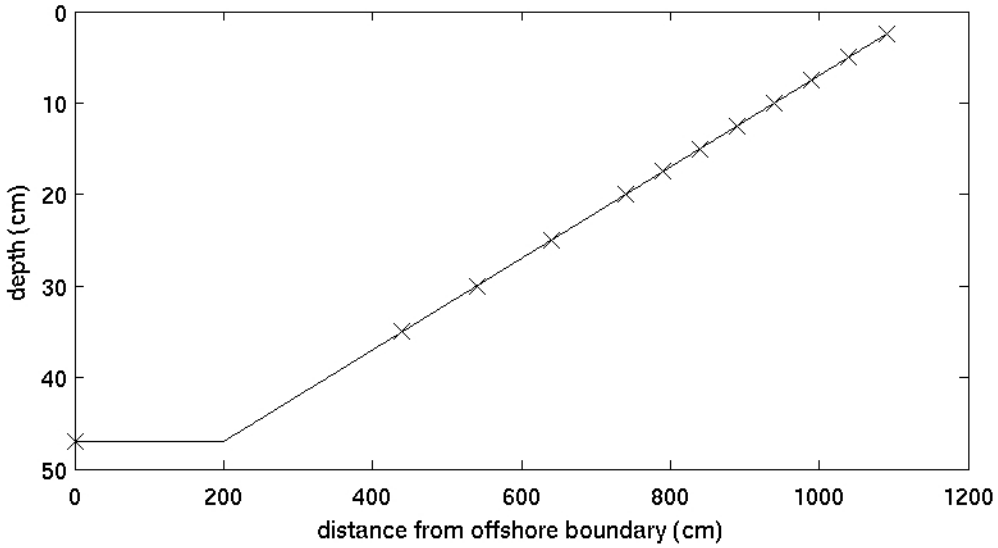

Figure 3.2 The domain of Mase and Kirby's (1992) case two experiment (MK92). Red x's denote locations considered in comparisons.

Mase and Kirby (1992) created random waves for case two of their experiment with a Pierson-Moskowitz spectrum at the offshore boundary. The energy at the input spectrum's f_p of 1.0 Hz resides in intermediate water depth at the wavemaker. Because the f_p is in intermediate water depth (Kaihatu, 1994; Kaihatu & Kirby, 1995; Kaihatu, 2003) putting significant energy in deep water (Kaihatu, 1994) (Figure 3.3), Case 2 of the experiment provides a demanding test for nonlinear models which purport to span the range from deep to shallow water (Kaihatu, 2003).

Model Input and Output

The model of Kaihatu and Kirby (1995) and the hybrid model propagate waves in one direction. To simulate the transformation of waves coming from offshore, the models require input at the most offshore location in the domain. In

addition, because both models are formulated in the frequency domain, the input takes the form of the amplitudes of the wave components in a wave train. Given a time series, these amplitudes are derived using Fast Fourier Transforms (FFT). The FFT algorithm is more efficient if the number of points is a power of two. Additionally, for statistical certainty, we wish to average spectra from multiple realizations of the time series. Therefore, the time series is divided into a number of segments (*m*), each containing a power of two number of points (*n*), and in this study, we choose *n*=2048. The FFT then results in *m*-segments of 1024 frequency components each. However, because computational time depends on the number of frequency components, the length of each segment is usually truncated. While this truncation affects skewness and asymmetry, it has little effect on the total energy (Kaihatu, 1994). The full and hybrid models handle the segments individually.

For the gently sloping domain, the time series that results from the TMA spectrum was divided into eight segments of 2,048 points apiece. Given the sampling interval 0.5 s, the frequency interval is 1/1,024 Hz. Only 500 frequency components were retained for each segment.

For the Mase and Kirby (1992) domain, the time series of surface elevation measured at a depth of 47 cm was used as input for the models. Therefore, the time series is divided into seven segments of 2,048 points. With 2,048 points recorded at a sampling interval of 0.05 s, the frequency interval is 1/102.4 Hz. The segment length was truncated to include only the first 500 Fourier coefficients, which retained roughly 99.9% of the total energy (Kaihatu & Kirby, 1996)..

Because the models work on each segment individually, the output is given as truncated segments, like the input. Several steps were taken to obtain the frequency and wavenumber spectra from the model results.

Frequency spectra were determined by Bartlett averaging over the number of segments for each domain. Furthermore, eight adjoining frequency bands were averaged in the spectra. The total averaging process resulted in 128 degrees of freedom for the long slope domain and 112 degrees of freedom for the MK92 domain.

Because model results represent half of two sided spectra, the one-sided frequency spectra are given by

$$S(f) = \frac{2|A_n|^2}{\Delta f}, \tag{3.1}$$

where $S(f)$ represents a frequency spectrum, A_n are the complex amplitudes, and Δf is the frequency interval. Furthermore, the wavenumber spectrum is related to the frequency spectrum by

$$S(f)\Delta f = S(k)\Delta k, \tag{3.2}$$

where $S(k)$ represents a wavenumber spectrum and Δk is the wavenumber interval. Since wavenumber is related to the frequency via the dispersion relation (equation 2.8) and the time series is sampled at constant intervals, the frequency interval is constant, and the wavenumber interval varies.

Evaluating individual parts of the hybrid model

For the hybrid model to successfully replicate measurements, the parametric component and the explicitly modeled component of the model must

show the capability of reproducing the wave field evolution. For the long slope domain, results of Kaihatu and Kirby (1995) provide a basis for testing in the domain; therefore, at this time only the parameterization of the Toba range is explored. Kaihatu and Kirby (p. 1909) report, "…the nonlinear mild-slope model compares very well to the (MK92) data for much of the frequency range throughout most of the domain." Therefore, for the MK92 domain, the Toba range parameterization is compared to observations recorded by Mase and Kirby (1992) during the second case of their experiment.

Both graphical and numerical comparisons were used to determine the extent of the Toba range parameterization's ability to describe the Kaihatu and Kirby (1995) results for the long slope domain and the observations for the MK92 domain. Graphical comparisons were conducted by simply superimposing the parameterization (equation 2.20) onto the full model results for the long slope domain and onto the observations collected in the MK92 domain. To support the graphical comparisons, regression analysis was performed on the model results and observations. Resulting estimates of the regression coefficients were numerically compared to the Toba range parameterization.

Lines of regression were "fit" to each spectrum by first taking a power transformation of the Toba range parameterization such that equation 2.20 becomes

$$\ln(S(k)) = \ln(\beta_{Toba}) - \frac{5}{2}\ln(k) \tag{3.3}$$

resembling the slope-intercept form of a line, where the intercept is $\ln(\beta_{Toba})$ and

the slope is $-5/2$. Next, the method of least squares was utilized given the independent variable

$$x = \ln(k) \tag{3.4}$$

and the dependent variable

$$y = \ln(S(k)) \tag{3.5}$$

to obtain an estimate of the slope and intercept for each spectrum's Toba range. Several methods were used to determine that the regressions adequately represent the observed and modeled spectra's Toba ranges. The methods and results are presented in the Appendix.

Finally, confidence intervals were determined for the slope of each spectrum's Toba range given by the regression model. These ranges were compared to Smith and Vincent's (2003) range of one standard deviation (0.15) around the slope in equation 2.20. Based on a *t*-distribution, the confidence intervals were determined for a significance level of 5%. Although an estimate of each spectrum's intercept was determined, β_{Toba} was calculated by a different method, which is described below.

Evaluating the Hybrid Model

Four implementations of the hybrid model were tested over the long slope and the MK92 domains. These differ in the parameterization's value of β_{Toba}. For the first case, Smith and Vincent's (2003) formulation of β_{Toba}, $\beta_{Toba} = 0.0103h^{0.5}$, was used. It is referred to as β_{SNV}. Results of the second case were reached using a depth independent (constant) β_{Toba}. This value of β_{Toba}

was determined from the energy of the input spectra's Toba ranges, and it is referred to as β_{con}. The method used to determine β_{con} is referred to as energy matching and is described below. Rather than determine β_{Toba} from the input spectrum's Toba range, the third case uses the input spectrums Toba range to determine α_{Toba} so that $\beta_{Toba} = \alpha_{Toba} h^{0.5}$ is depth dependent. This case of β_{Toba} is referred to as β_{emat}, and the value of α_{Toba} determined from the input spectrum is referred to as α_{emat}. Finally, the relation $\beta_{Toba} = \alpha_{Toba} h^{0.5}$ was used, where

$$\alpha_{Toba} = C \frac{H_{rms}}{h}. \tag{3.6}$$

H_{rms} / h is a dimensionless parameter, and the constant C was determined from the relation

$$C = \alpha_{emat} \frac{h_0}{H_{rms,0}}, \tag{3.7}$$

where h_0 and $H_{rms,0}$ are values of depth and waveheight, respectively, at the offshore boundary. H_{rms} is given in equation 2.14. The final case is referred to as β_{alf}.

For the long slope domain, hybrid model results were compared to results of Kaihatu and Kirby (1995). For the MK92 domain, hybrid model results were compared to the observations collected by Mase and Kirby (1992). Comparisons were conducted graphically by superposition, and numerical comparisons utilized mean square error (MSE) to determine the degree of agreement between a hybrid model and either full model results or observations, depending on the domain. MSE is defined as

$$MSE = \frac{1}{n-2}\sum \varepsilon^2 \,, \tag{3.8}$$

where n is the sample size and ε is the residual of the comparison.

Energy Matching to Determine β_{con}

To determine β_{con}, it was assumed that there was no difference between the total energy of the Toba range parameterization and the total energy of the input spectra's Toba range so that

$$\int_{k=1/h}^{k_N} \beta_{Toba} k^{-5/2} dk = \int_{k=1/h}^{k_N} S(k)_{in}\, dk \,. \tag{3.9}$$

The right hand side is the total energy of the Toba range parameterization (equation 2.20), and the left hand side is the total energy of the input spectra's Toba range. $S(k)_{in}$ is the input wavenumber spectrum. β_{Toba} is constant for a particular depth, so equation 3.9 becomes

$$\beta_{Toba} = \frac{\int_{k=1/h}^{k_N} S(k)_{in}\, dk}{\int_{k=1/h}^{k_N} k^{-5/2} dk} \,. \tag{3.10}$$

Energy Matching to Determine α_{emat}

Determining α_{emat} follows from the previous section. Because $\beta = \alpha h^{0.5}$, equation 3.10 is rewritten as

$$\alpha_{emat} h_0^{0.5} = \frac{\int_{k=1/h}^{k_N} S(k)_{in}\, dk}{\int_{k=1/h}^{k_N} k^{-5/2} dk} \text{ so that} \tag{3.11}$$

$$\alpha_{emat} = \frac{\int_{k=1/h}^{k_N} S(k)_{in}\, dk}{h_0^{0.5} \int_{k=1/h}^{k_N} k^{-5/2} dk}, \tag{3.12}$$

where h_0 is water depth at the offshore boundary. Now, $\beta_{emat} = \alpha_{emat} h^{0.5}$, for every depth in a domain.

Determining Wave Parameters

In addition to graphical and numerical comparisons of model results, wave parameters were calculated for all of the model results and available data. H_{rms} (equation 2.14), skewness, and asymmetry provide additional quantitative measures for comparison. Skewness and asymmetry, whose physical meanings are described in the introduction, are given by equations 3.13 and 3.14, respectively.

$$Skewness = \frac{\left|\eta^3\right|}{\left|\eta^2\right|^{3/2}} \tag{3.13}$$

$$Asymmetry = \frac{\left|(H(\eta))^3\right|}{\left|\eta^2\right|^{3/2}} \tag{3.14}$$

$H(\eta)$ represents the Hilbert transform of the free surface.

CHAPTER 4

RESULTS

This chapter addresses the results of our analysis. We begin by demonstrating the need for nonlinear interactions in the modeling of shoaling and surf zone waves. Because modeling with nonlinear interactions requires substantial computational time (as established in chapter 1), the parameterization of Smith and Vincent (2003) is explored as a means of reducing the computational expense of modeling waves through the surf zone. The hybrid model results are presented following an examination of the β_{Toba} formulations used in the parametric component of the hybrid model. Finally, wave parameters computed from model results are given.

Modeling Shoaling and Surf Zone Waves without Nonlinear Interactions

Removing nonlinear interactions from the full model (Kaihatu & Kirby, 1995) results in a linear model and reduces computational time from over 2.5 hr to approximately 6 min in the MK92 domain and from approximately 23 hr to approximately 12 min in the long slope domain. However, poor results negate any benefits gained by the reductions in computational expense.

In both domains, neglecting nonlinear interactions suffices until the point where secondary peaks begin to form (Figures 4.1-4.8). In fact, in the MK92 domain, where $h < 15$ cm, neglecting nonlinear interactions gives the same, if not better, results as the full model, which overestimates high frequency energy through the entire domain; this overestimation suggests that the model does not have a uniformly valid deep water asymptote. The linear model performs well in

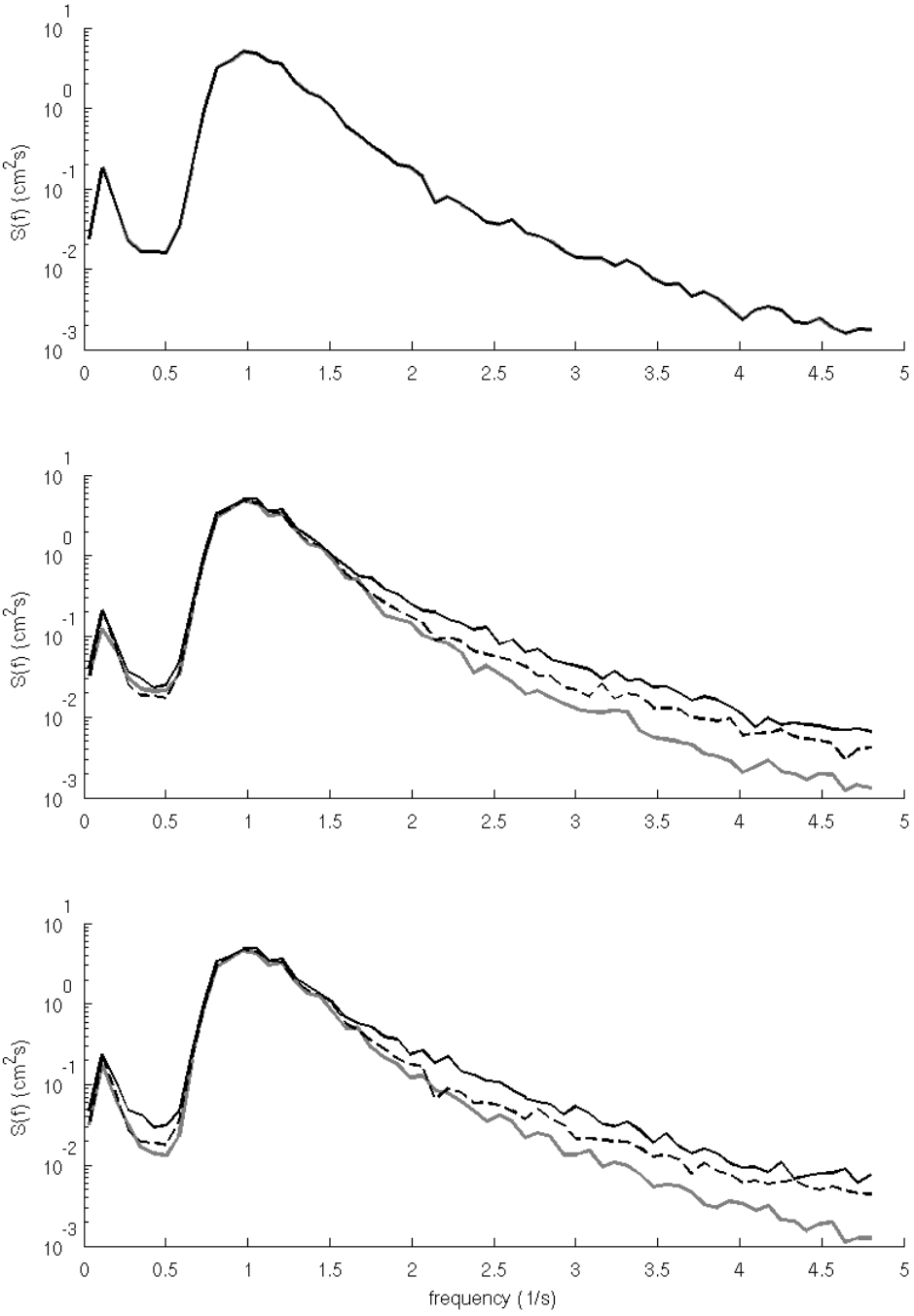

Figure 4.1 Comparison of observations (gray line), full model (black solid), and linear model (black dash). Comparisons are for the MK92 domain (top) 47cm, (middle) 35 cm, and (bottom) 30 cm.

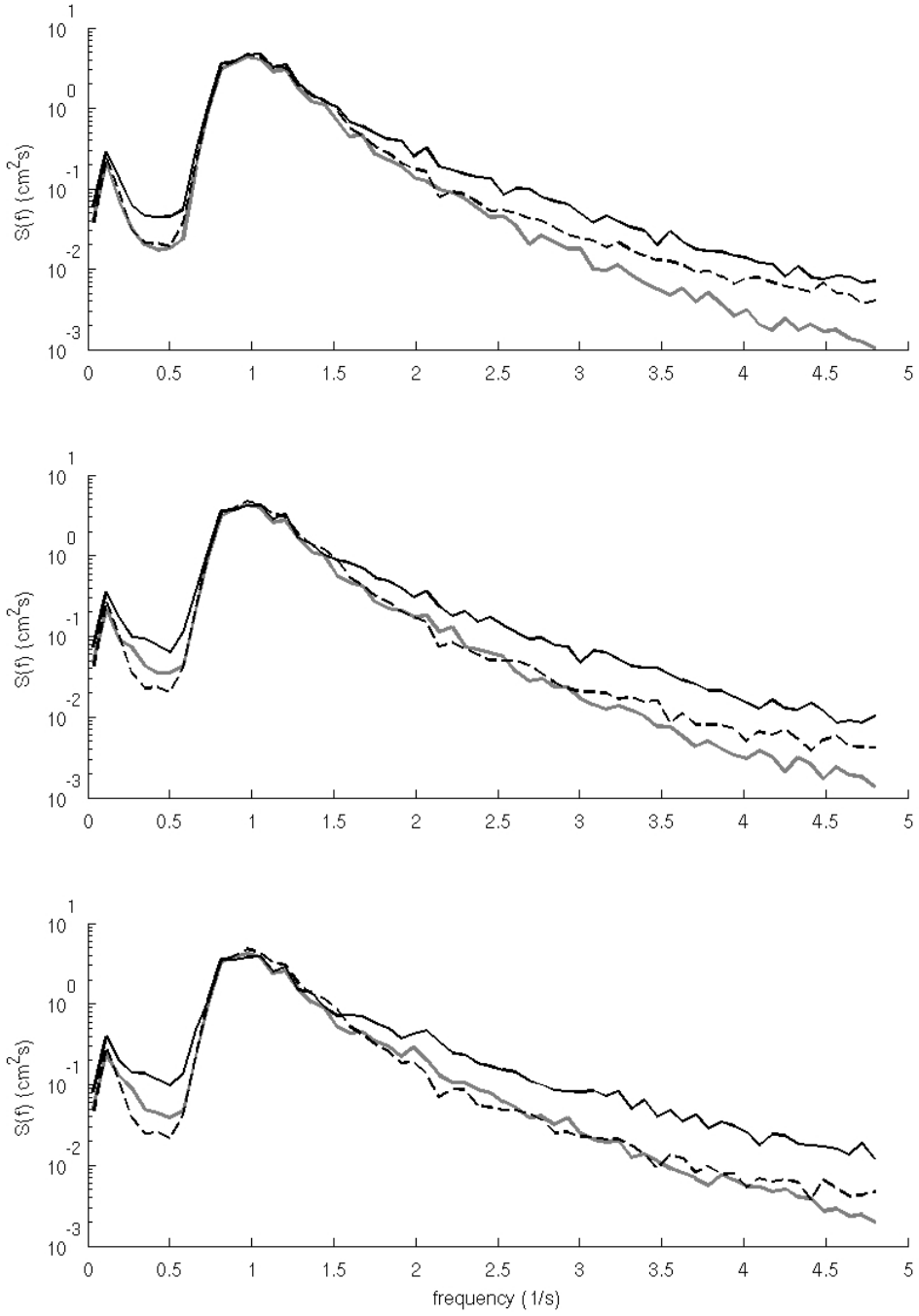

Figure 4.2 Comparison of observations (gray line), full model (black solid) and linear model (black dash). Comparisons are for the MK92 domain (top) 25 cm, (middle) 20 cm, and (bottom) 17.5 cm.

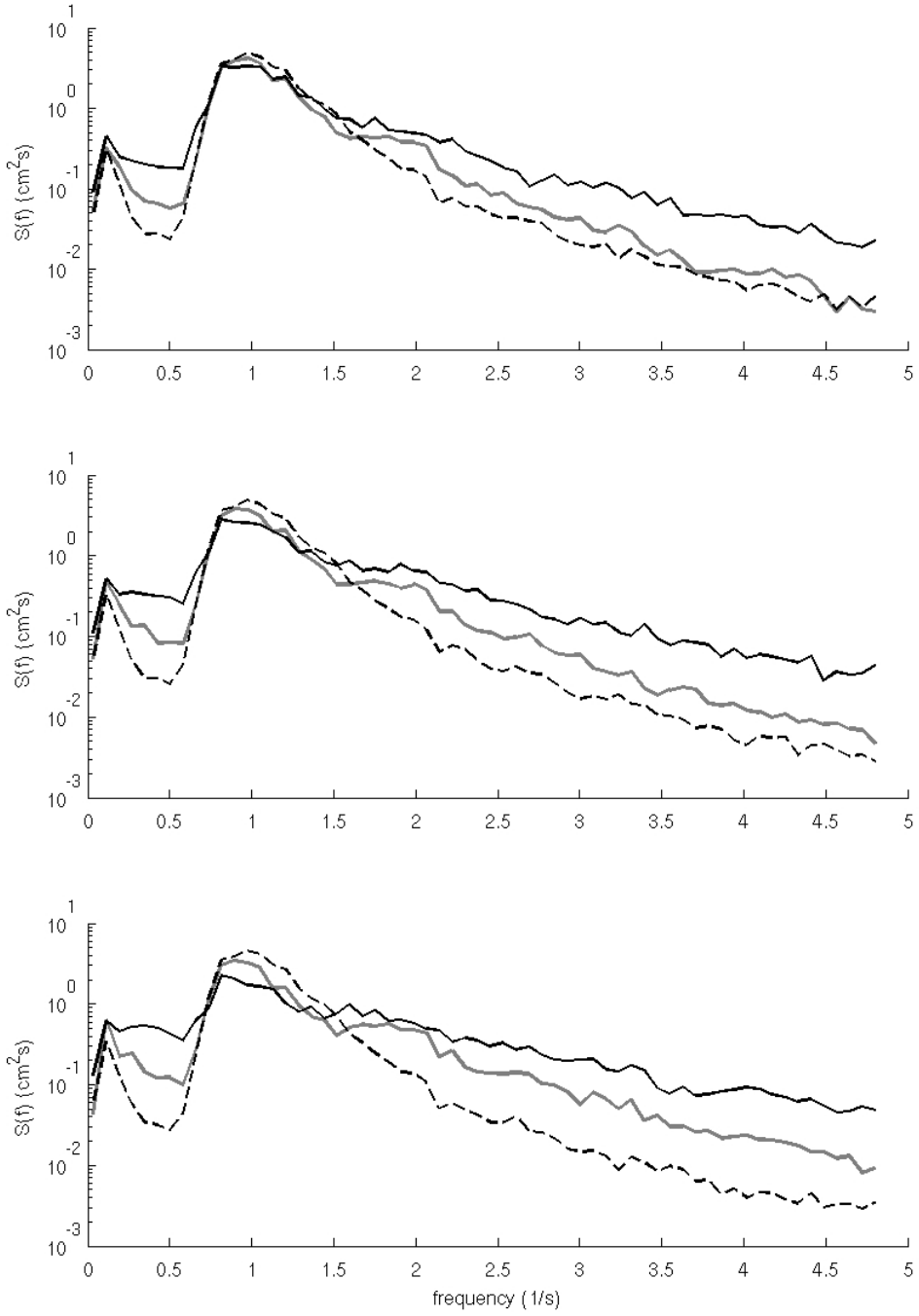

Figure 4.3 Comparison of observations (gray line), full model (black solid) and linear model (black dash). Comparisons are for the MK92 domain (top) 15 cm, (middle) 12.5 cm, and (bottom) 10 cm.

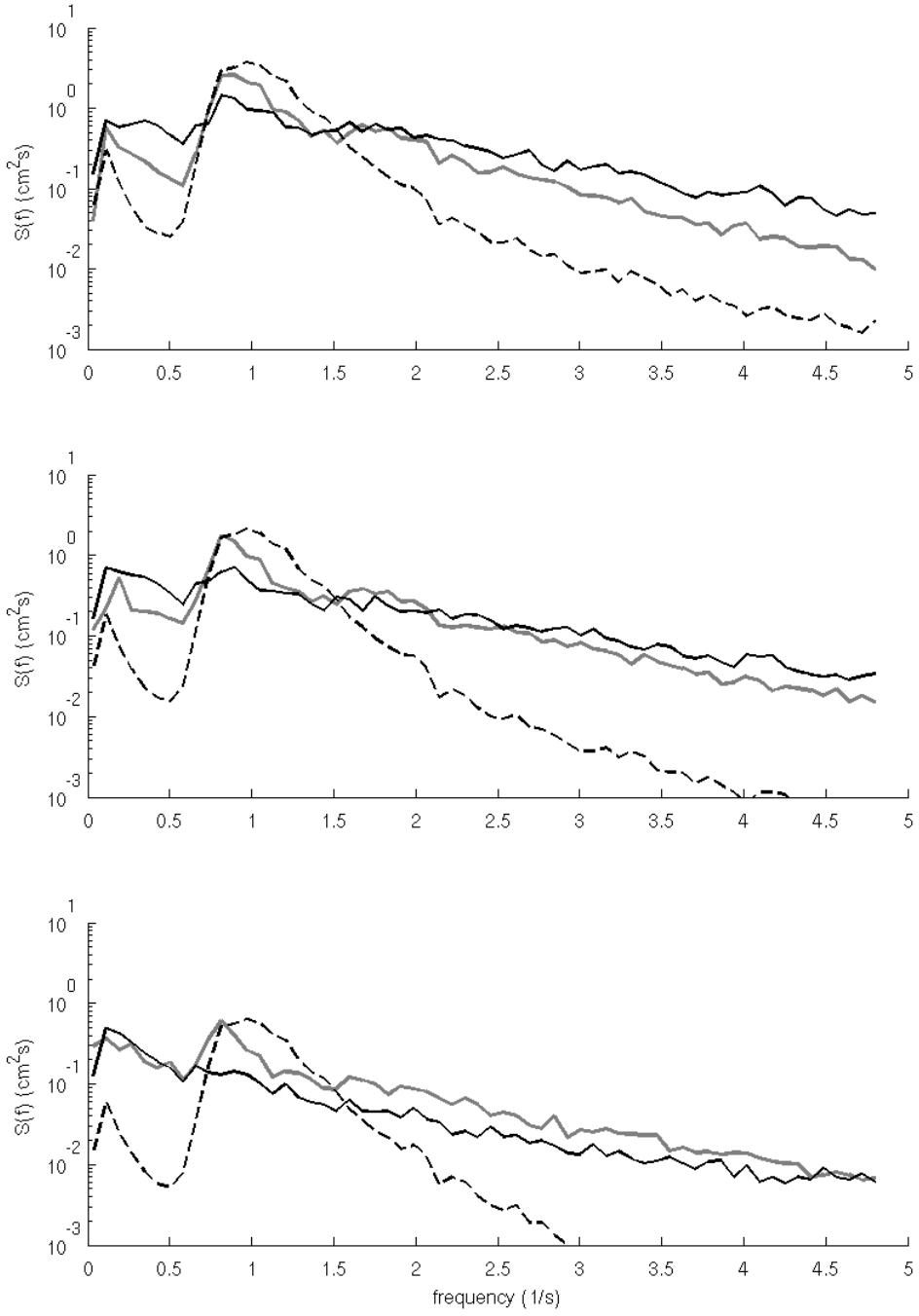

Figure 4.4 Comparison of observations (gray line), full model (black solid) and linear model (black dash). Comparisons are for the MK92 domain (top)7.5 cm, (middle) 5 cm, and (bottom) 2.5 cm.

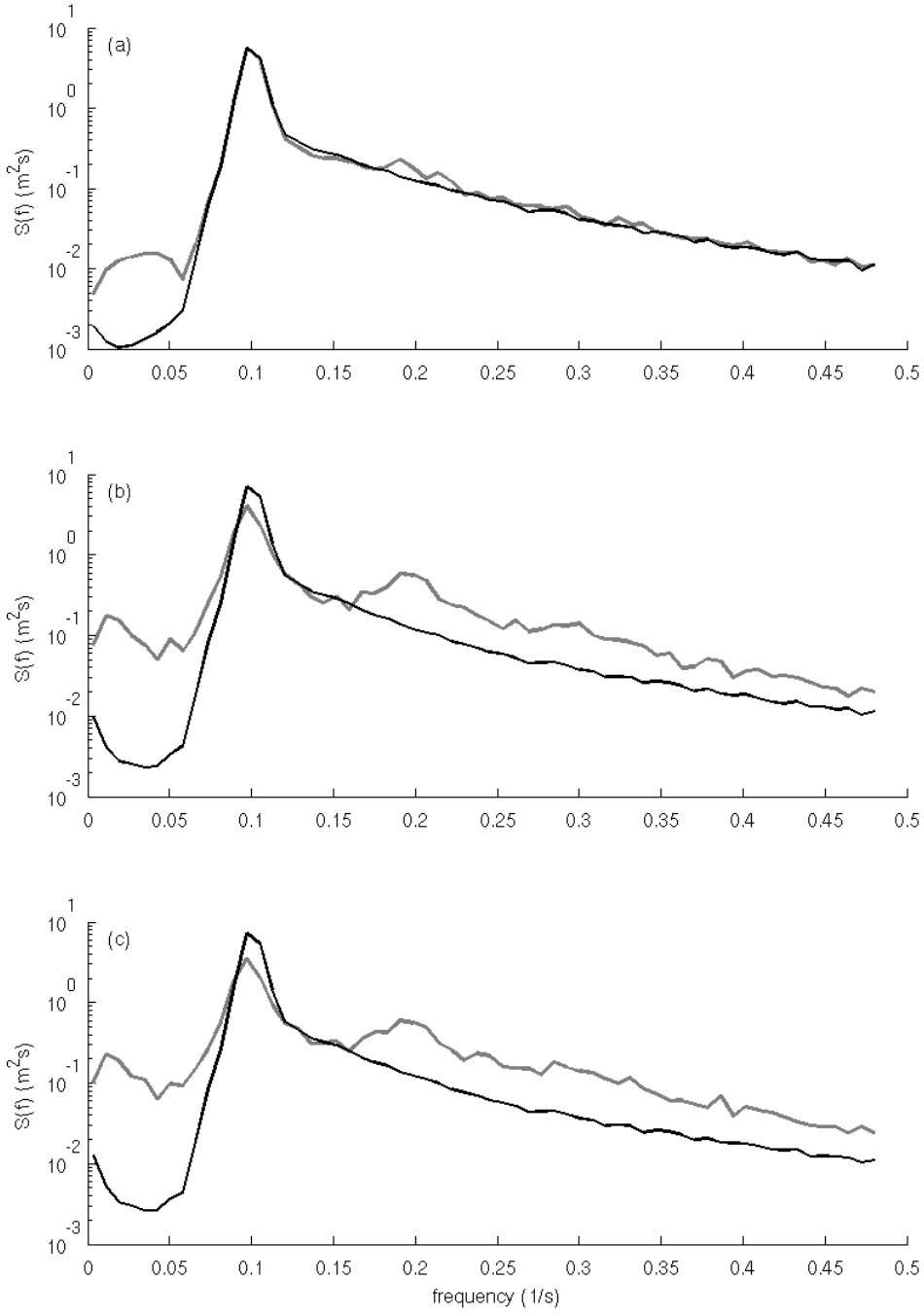

Figure 4.5 Comparison of full model (gray solid) and linear model (black solid). Comparisons are for the long slope domain (top) 10 m, (middle) 5 m, and (bottom) 4.5 m.

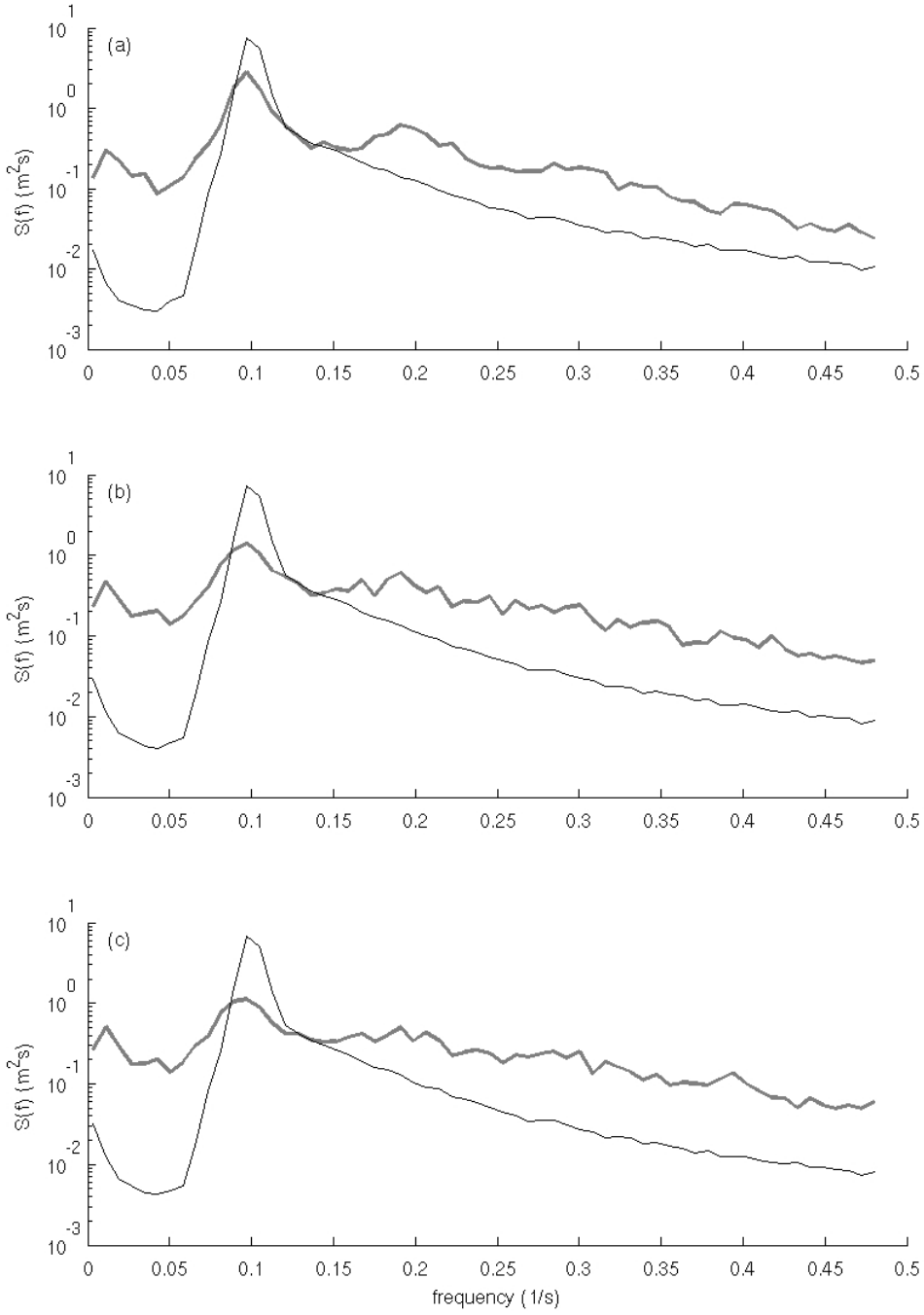

Figure 4.6 Comparison of full model (gray solid) and linear model (black solid). Comparisons are for the long slope domain (top) 4 m, (middle) 3 m, and (bottom) 2.75 m.

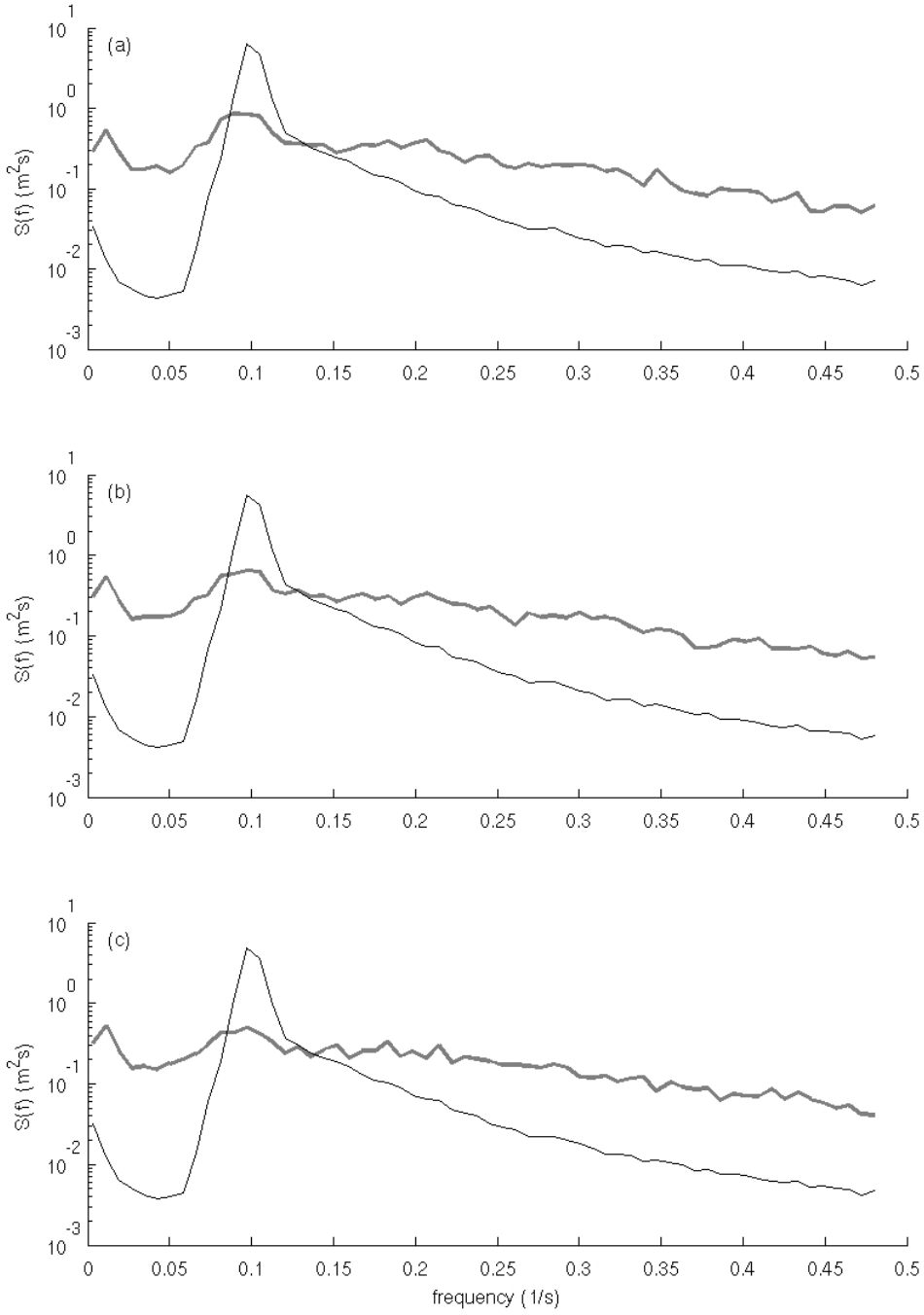

Figure 4.7 Comparison of full model (gray solid) and linear model (black solid). Comparisons are for the long slope domain (top) 2.5 m, (middle) 2.25 m, and (bottom) 2 m.

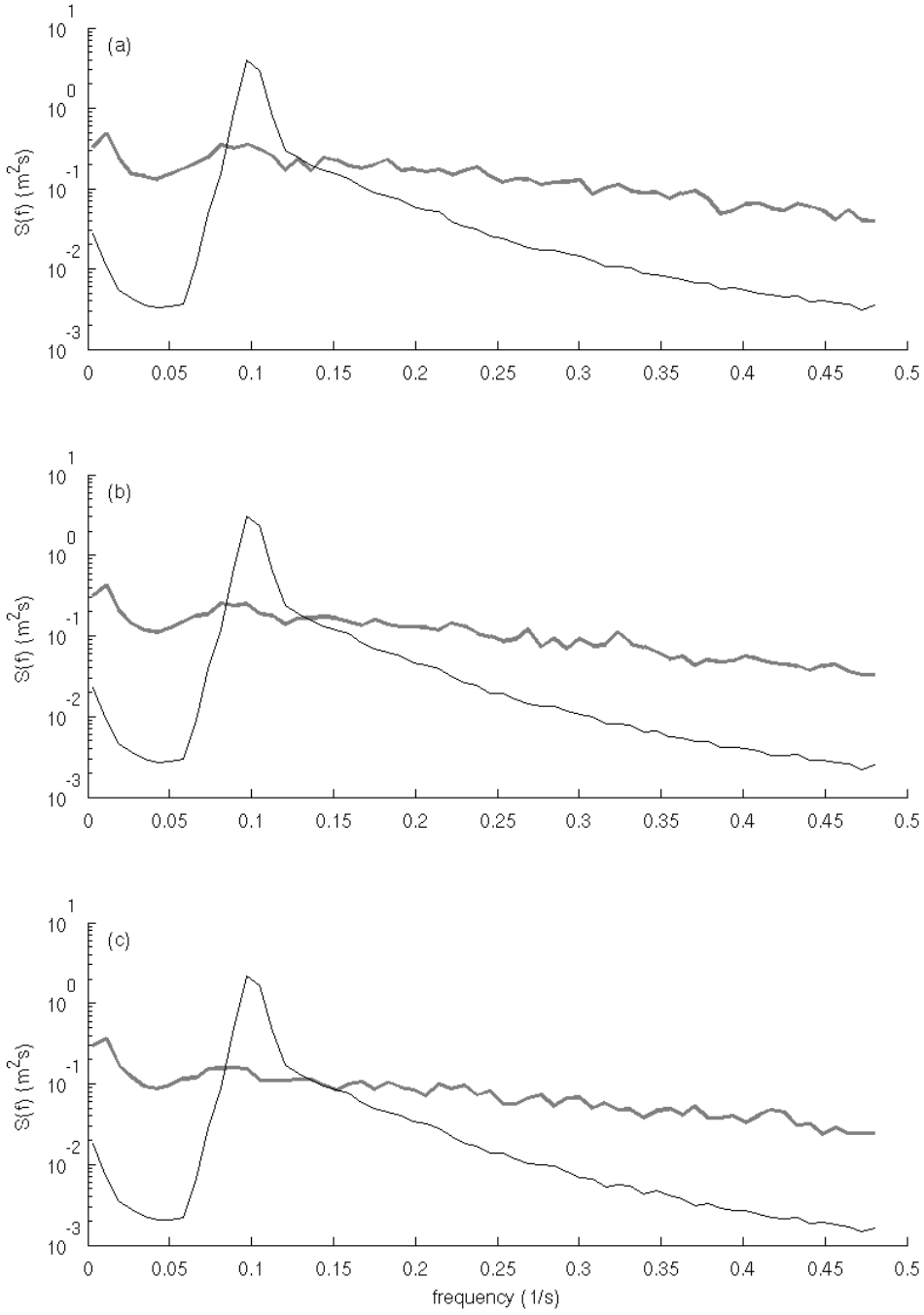

Figure 4.8 Comparison of full model (gray solid) and linear model (black solid). Comparisons are for the long slope domain (top)1.75 m, (middle) 1.5 m, and (bottom) 1.25 m.

deep water where the effects of nonlinear interactions are small. When waves shoal, however, nonlinear interactions intensify. Furthermore, in the surf zone, breaking waves result in turbulence that dissipates energy at high frequencies and, in turn, promotes energy transfer from low to high frequencies via nonlinear interactions. Once the nonlinear interactions and dissipation jointly serve to change the shape of the spectrum, linear theory is insufficient because it does not change the shape.

Toba Parameterization Evaluation

Visual comparisons of the Toba parameterization to spectra's Toba ranges in the MK92 (Figure 4.9) and long slope (Figure 4.10) domains show that in regions where valid, the parameterization appears to adequately represent the spectra.

As mentioned in chapter 3, the MK92 domain's k_p is in intermediate water for most of the domain. Furthermore, $k_p h > 1$ for depths greater than approximately 25 cm. If $k_p > 1/h$, then the Zakharov range ($k_p < k < 1/h$) is nonexistent. In addition, at a depth of approximately 10 cm, k_p enters shallow water, thus allowing the two distinct subranges to coexist.

For the first half of the MK92 domain, where $k_p h > 1$ or $k_p h \approx 1$, the slope of the Toba parameterization is flatter than the slopes of the spectra's Toba ranges. As mentioned previously in chapter 2, wind is an important factor outside the surf zone, and the Toba range slope of a wind wave spectrum is the same as the Toba range slope of a surf zone spectrum. However, the laboratory wave spectra recorded by Mase and Kirby (1992) do not include the effects of

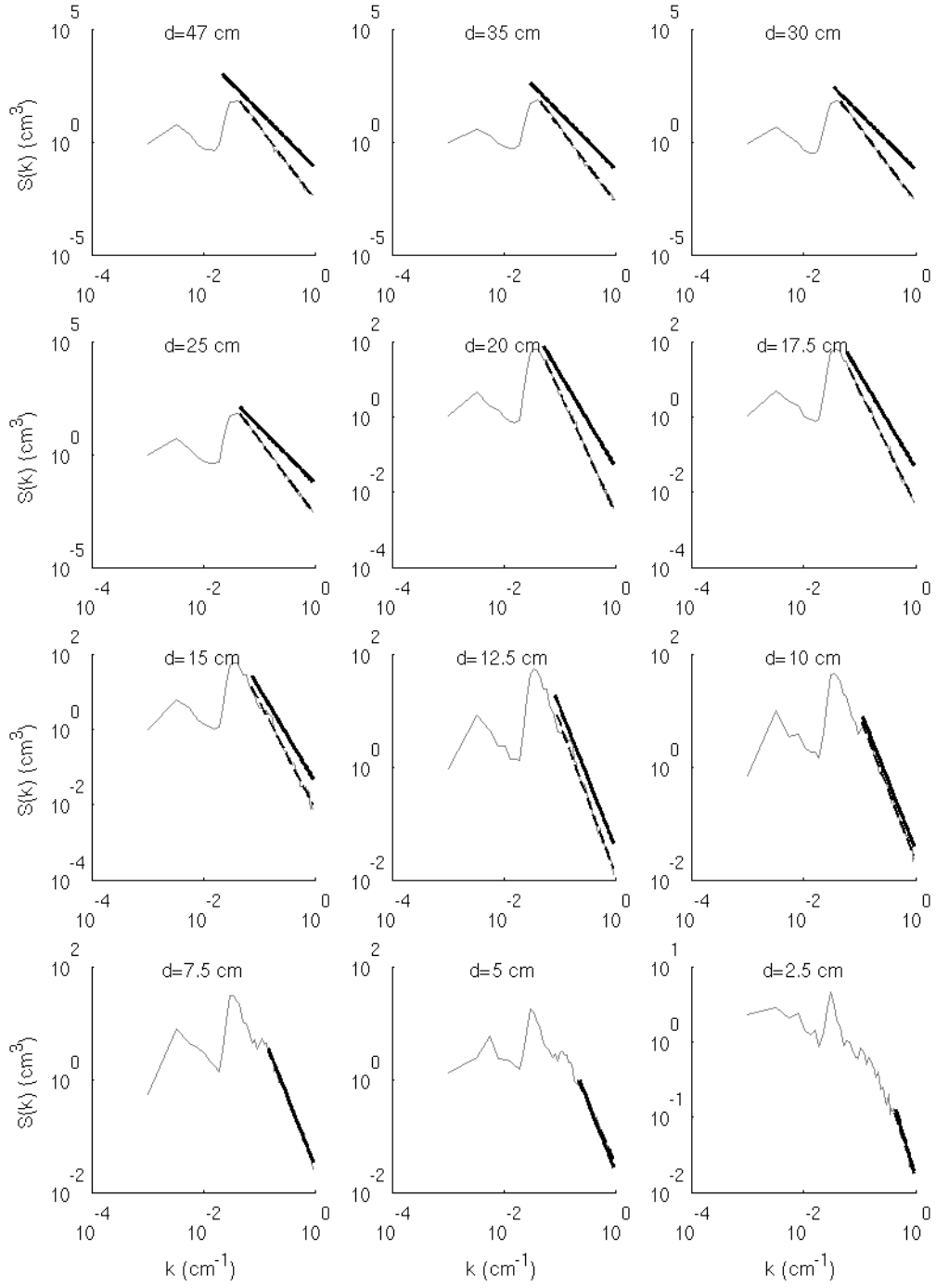

Figure 4.9 Comparison of Smith and Vincent's (2003) Toba parameterization (black solid) and wavenumber spectra resulting from the full model (gray line) in addition to the lines "fit" to the spectra (black dash). Comparisons are given at different depths (d) in the MK2 domain.

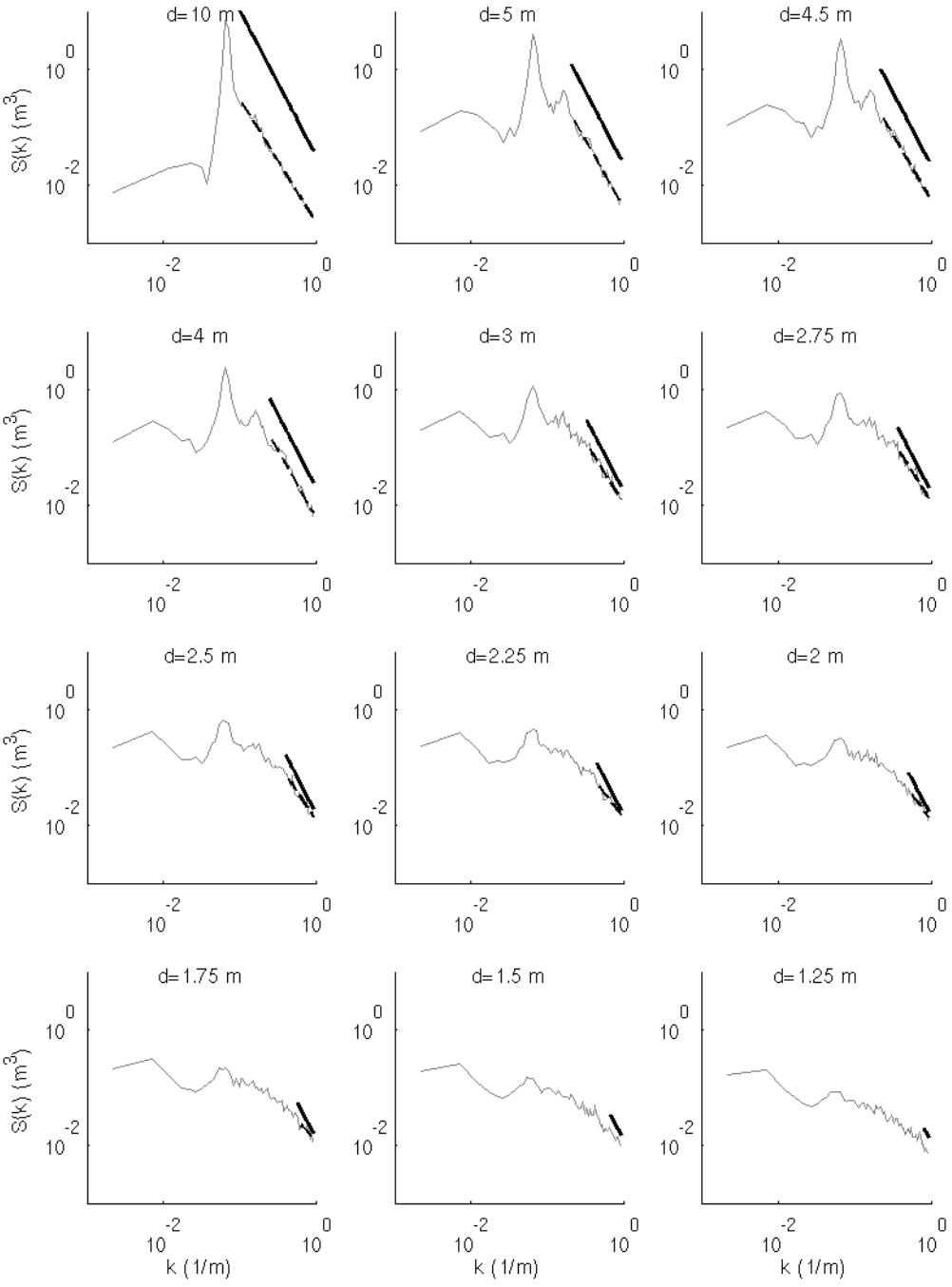

Figure 4.10 Comparison of Smith and Vincent's (2003) Toba parameterization (black solid) and wavenumber spectra resulting from the full model (gray line) in addition to the lines "fit" to the spectra (black dash). Comparisons are given at different depths (d) in the long slope domain.

wind, which works to increase energy of high wavenumbers and make the spectral slope less steep.

Waves begin to shoal at a depth of approximately 15 cm placing emphasis on a depth dependence, rather than wind. Shoaling increases spectral energy and thus promotes energy transfer primarily from the k_p causing the formation of a secondary energy peak. Because energy is lost from the k_p and transferred to the secondary peak, the spectrum's Toba slope comes more into agreement with the parameterization's slope. Finally, the waves break and turbulence dissipates energy at the high wavenumbers, enhancing energy transfer from the low wavenumbers and thus flattening the spectra's Toba range slopes. Therefore, in the surf zone (i.e. $H_{rms} / h > 0.4$ per Smith and Vincent (2003)) where $h < 15$ cm, the spectral Toba range slopes agree with the slope of the Toba range parameterization.

It appears that at depths where the slopes agree, the parameterization adequately represents the energy level of the spectra's Toba range. Furthermore, it appears that a gentler spectral slope, as suggested by the parameterization, is capable of bringing the energy levels of spectra outside the shoaling and surf zones into closer agreement with the parameterization.

In the long slope domain, k_p enters the shallow water range at a depth of approximately 5 m. With $k_p \mathrm{h} << 1$, both subranges exist (Smith & Vincent, 2003). As depth decreases, however, $k_p h$ and the number of wavenumbers that satisfy $k \geq 1/h$ decreases. Eventually, the range $k_p h \geq 1$ (Toba) vanishes, and the Zakharov range ($k_p < k < 1/h$) dominates.

For most of the long slope domain, the slope of the parameterization is steeper than the slope of the spectra's Toba ranges. In contrast to spectra of the MK92 domain, spectra in the intermediate water range are relatively narrow with well defined peaks indicative of a lack of wind effects. Again, a lack of wind effects in the intermediate water spectra appears to prohibit the parameterization from adequately representing the slope of these spectra.

Once shoaling begins, depth effects dominate, and nonlinear interactions cause the formation of the secondary peak. The parameterization now adequately represents the spectral slope. However, as waves enter the shallow water range, the wavenumber satisfying $kh = 1$ moves toward the high wavenumber range, and thus spectra have fewer wavenumbers in the Toba range. Because the boundary between the Toba and Zakharov range is more likely to be a range than a single point (Smith & Vincent, 2003), the flatter slope of the Zakharov range becomes more important. Numerical comparisons show that the slopes of the Toba parameterization and range agree at approximately 4 m depth.

For depths less than approximately 3 m, the parameterization adequately represents the energy of the spectra. At other depths, as with the slope, the narrow, sharp spectral peak prevents the parameterization from adequately representing the energy level. Because the spectral peak is of much greater energy than surrounding wavenumbers, the resulting secondary peak is well defined, and relatively little energy is transferred to wavenumbers around the harmonic of the peak wavenumber. Thus, the spectra fail to relax to the broad

featureless shape indicative of equilibrated spectra, and the energy levels do not agree.

Evaluation of the Hybrid Model

In this section, results from the hybrid model are given in relation to each other, the full model, and in the case of the MK92 domain, observations. However, before the hybrid model results are given, values of β_{Toba} given by Smith and Vincent (2003) and determined from the input spectra's Toba range energy are reported.

Values of β_{Toba}

As described in Chapter 3, the hybrid model was executed four times for each domain, with each execution using a different representation of β_{Toba} (Table 4.1) in the parameterization. The four values of β_{Toba} differ for both domains.

For the long slope domain, the four values of β_{Toba} used in the hybrid models differ from β_{SNV} by an order of magnitude (Table 4.2). Despite the difference in value, β_{SNV} and β_{emat} tend to decrease with a decrease in water depth and overestimate the input spectrum's Toba range energy (Figure 4.11). β_{emat} represents the energy better than β_{SNV}. β_{alf} falls between the energy matched values (β_{con} and β_{emat}) and β_{SNV} at the offshore boundary. It increases into shallow water until the depth is approximately 2.25 m (Table 4.2).

Table 4.1

Formulations of β_{Toba} Used in the Hybrid Model

Symbol	Formula ($\beta = \alpha h^{0.5}$)	Description
β_{SNV}	$\alpha_{SNV} = 0.0103$	β as determined by Smith and Vincent (2003)
β_{con}	$\beta = constant$	β determined by matching the energy of the input spectrum; constant
β_{emat}	$\alpha_{emat} = \frac{\int_{k=1/h}^{k_N} S(k)_{in}\, dk}{h_0^{0.5} \int_{k=1/h}^{k_N} k^{-5/2}\, dk}$	β determined by matching the energy of the input spectrum; depth dependent
β_{alf}	$\alpha_{alf} = C\frac{H_{rms}}{h}$; $C = \alpha_{emat}\frac{h_0}{H_{rms,0}}$	β determined as a function of waveheight, depth, and α_{emat}; depth dependent

Table 4.2

Values of β_{Toba} Used in Determining Wave Evolution in the long slope domain with the Hybrid Model.

Depth (m)	β_{SNV}	β_{con}	β_{emat}	β_{alf}
10.00	*0.0326*	*0.0041*	*0.0036*	*0.0128*
5.00	*0.0230*	*0.0041*	*0.0025*	*0.0194*
4.50	*0.0218*	*0.0041*	*0.0024*	*0.0206*
3.50	*0.0193*	*0.0041*	*0.0021*	*0.0234*
3.00	*0.0178*	*0.0041*	*0.0020*	*0.0246*
2.74	*0.0170*	*0.0041*	*0.0019*	*0.0251*
2.50	*0.0163*	*0.0041*	*0.0018*	*0.0253*
2.24	*0.0154*	*0.0041*	*0.0017*	*0.0254*
2.00	*0.0146*	*0.0041*	*0.0016*	*0.0250*
1.74	*0.0136*	*0.0041*	*0.0015*	*0.0243*
1.50	*0.0126*	*0.0041*	*0.0014*	*0.0232*
1.24	*0.0115*	*0.0041*	*0.0013*	*0.0219*

Unlike the values of β_{Toba} used in propagating waves with the hybrid model through the long slope domain, values of β_{Toba} used in the MK92 domain are similar in value (Figure 4.12). However, with the exception of β_{alf}, values used in the hybrid model differ greatly from values determined from observations,

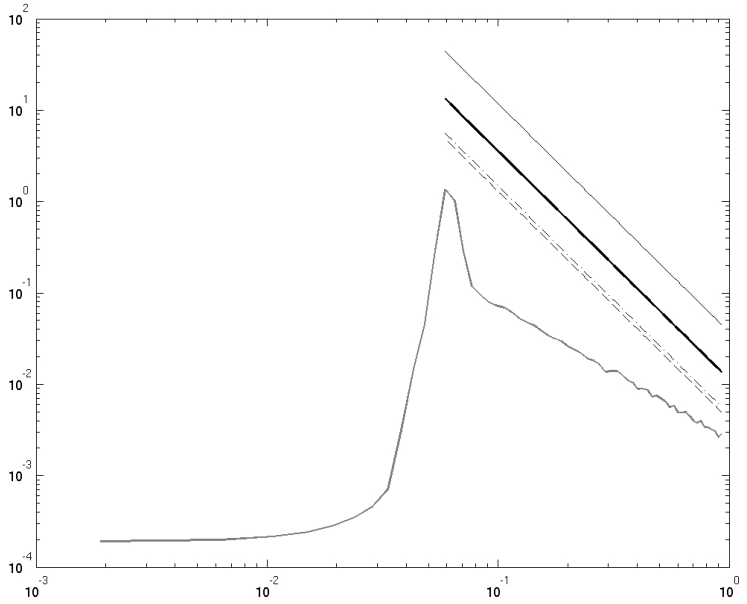

Figure 4.11 A comparison of the long slope domain's input spectrum (gray line) to Toba range parameterizations used in the hybrid model. The parameterizations differ in β_{Toba} values, where the three are (a) Smith and Vincent (2003) (black solid), (b) the constant value (black dash), (c) energy matched (black dotted), and (d) energy matched with the nonlinearity parameter (bold black solid).

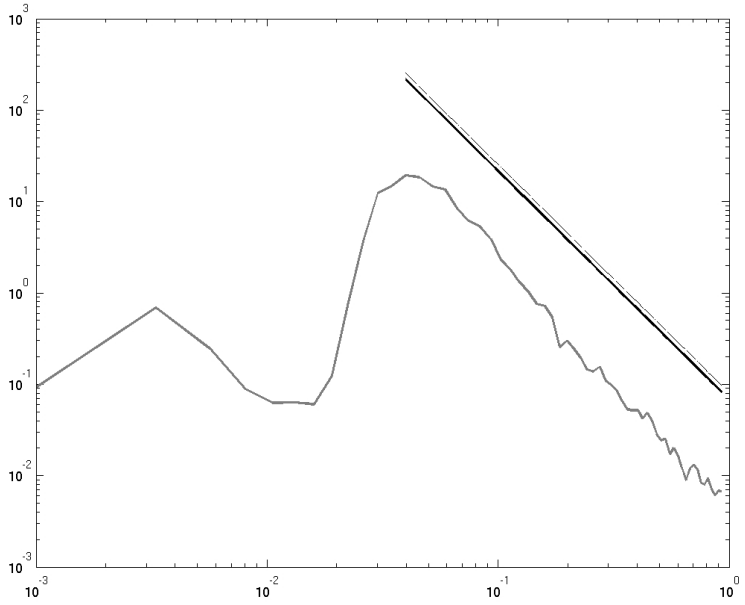

Figure 4.12 A comparison of the MK92 domain's input spectrum (gray line) and the Toba range parameterizations used in the hybrid model. The parameterizations differ in their value of β_{Toba}. The three values are (a) Smith and Vincent's (2003) (black solid), (b) constant (black dash), (c) energy matched (black dotted), and energy matched with the nonlinearity parameter (bold black solid).

Table 4.3

Values of β_{Toba} Used in the Hybrid Model to Propagate Waves through the MK92 Domain.

Depth (cm)	β_{obs}	β_{SNV}	β_{const}	β_{emat}	β_{alf}
47.0	*0.0804*	*0.0706*	*0.0804*	*0.0804*	*0.0680*
35.0	*0.0772*	*0.0609*	*0.0804*	*0.0694*	*0.0759*
30.0	*0.0775*	*0.0564*	*0.0804*	*0.0642*	*0.0805*
25.0	*0.0765*	*0.0515*	*0.0804*	*0.0587*	*0.0865*
20.0	*0.0851*	*0.0461*	*0.0804*	*0.0525*	*0.0956*
17.5	*0.0909*	*0.0431*	*0.0804*	*0.0491*	*0.1023*
15.0	*0.0955*	*0.0399*	*0.0804*	*0.0454*	*0.1105*
12.5	*0.0940*	*0.0364*	*0.0804*	*0.0415*	*0.1189*
10.0	*0.1108*	*0.0326*	*0.0804*	*0.0371*	*0.1306*
7.5	*0.1441*	*0.0282*	*0.0804*	*0.0321*	*0.1358*
5.0	*0.1224*	*0.0230*	*0.0804*	*0.0262*	*0.1325*
2.5	*0.0725*	*0.0163*	*0.0804*	*0.0185*	*0.1233*

β_{obs} , in the domain (Table 4.3). β_{obs} remains fairly constant through the domain, with almost all changes consisting of an increase with decreased depth. β_{alf} follows the same trend. Because β_{SNV} and β_{emat} depend on depth, their values decrease with a decrease in water depth. Although β_{alf} overestimates the energy at the offshore boundary (Figure 4.12), it represents the energy the best.

Qualitative Hybrid Model Results

This section reports hybrid model results relative to full model results and, in the case of the MK92 domain, observations. Hybrid model results are referenced as follows:

Case 1 is the hybrid model with β_{SNV} .

Case 2 is the hybrid model with β_{con} .

Case 3 is the hybrid model with β_{emat} .

Case 4 is the hybrid model with β_{alf} .

Qualitative and quantitative comparisons of model results are given for the two domains. Beginning with qualitative comparisons, first are results for the long slope domain, where the hybrid model reduces computational time from approximately 23 hr to approximately 1 hr.

Although case 1 replicates the Toba range well for spectra with energy transfer to higher harmonics, (Figure 4.13 (b) and (c) and Figure 4.14 (a)), it overestimates the range in deeper water (Figure 4.13 (a)) and underestimates it at depths shallower than 4 m (Figures 4.14, 4.15, and 4.16). Outside of the Toba range, case one overestimates the spectra's energy until a depth of

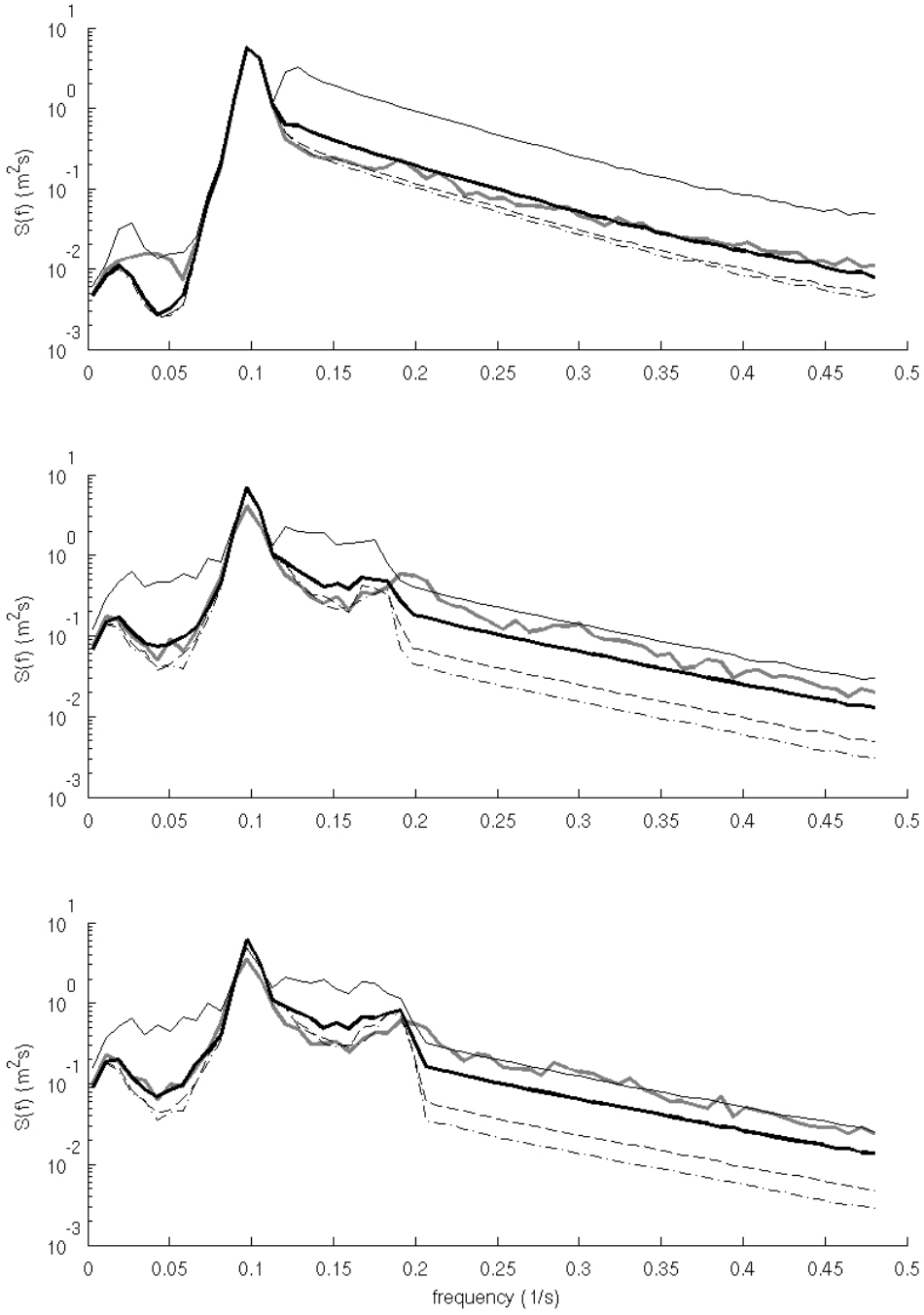

Figure 4.13 Comparison of full model (gray line) and hybrid model results (case 1, black solid; case 2, black dashed; case 3, black dash dotted; case 4 bold black solic). Results are given for the long slope domain (a) 10 m, (b) 5 m, and (c) 4.5 m.

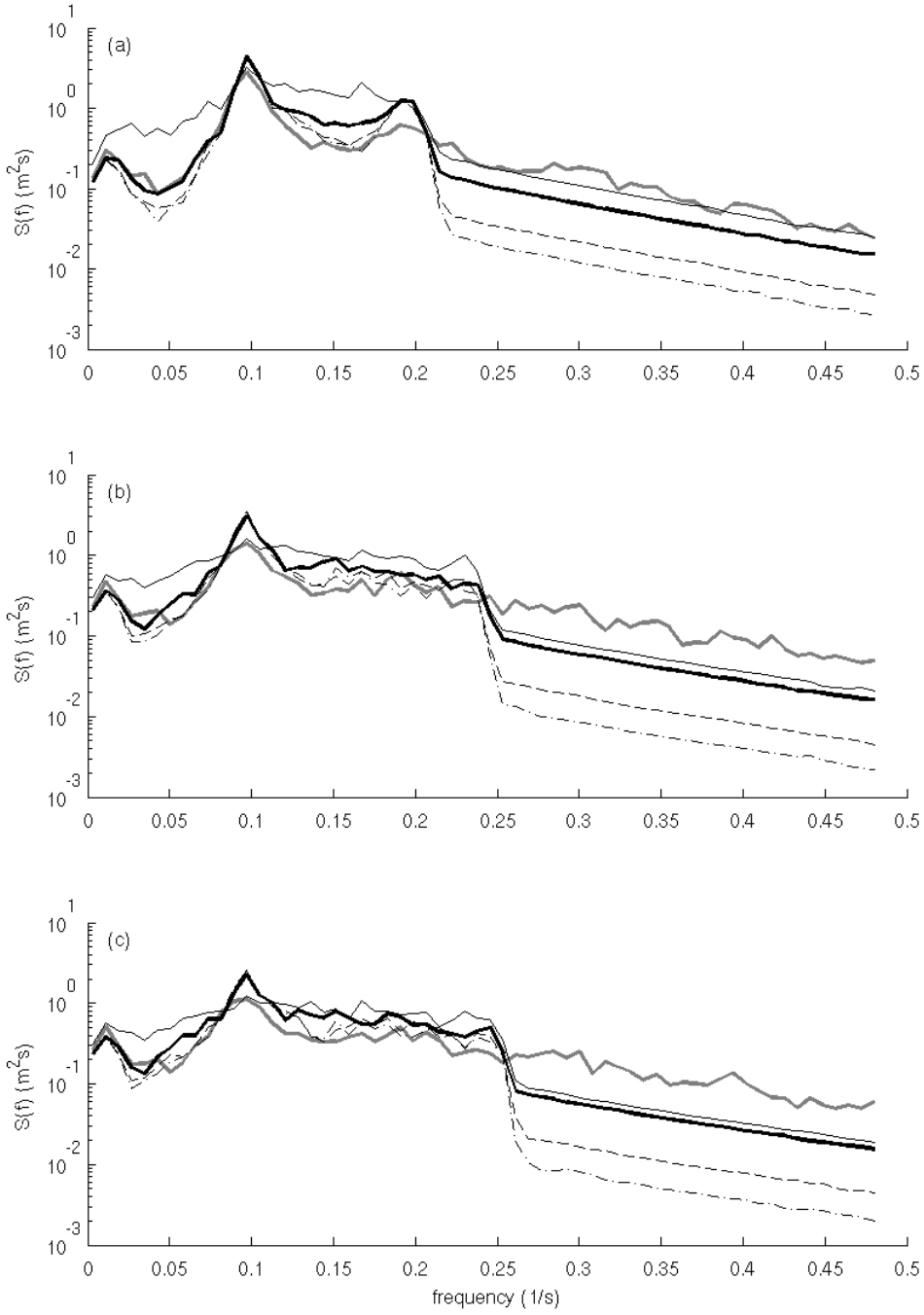

Figure 4.14 Comparison of full model (gray line) and hybrid model results (case 1, black solid; case 2, black dashed; case 3, black dash dotted; case 4 bold black solid). Results are given for the long slope domain (a) 4 m, (b) 3 m, and (c) 2.75 m.

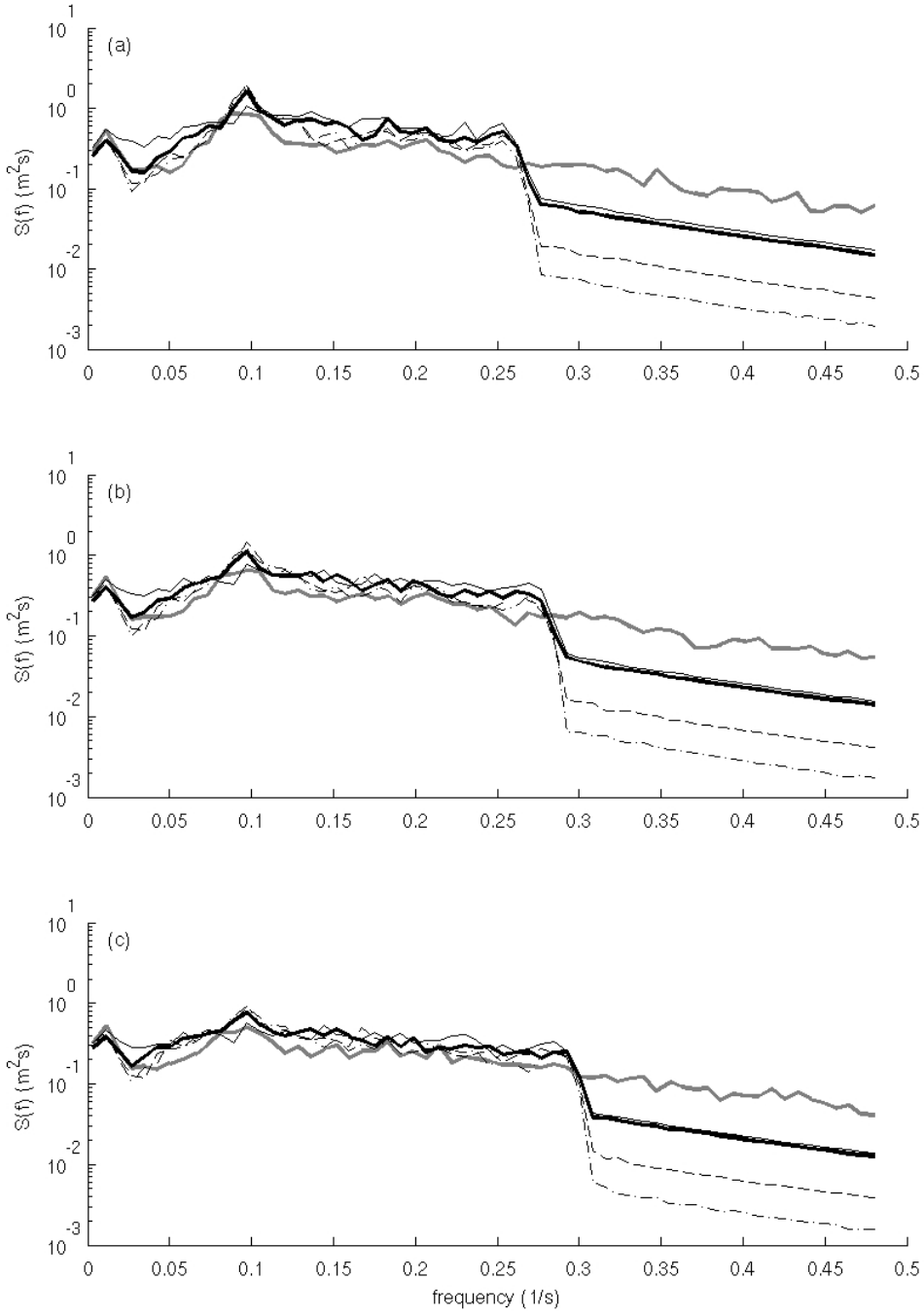

Figure 4.15 Comparison of full model (gray line) and hybrid model results (case 1, black solid; case 2, black dashed; case 3, black dash dotted; case 4 bold black solid). Results are given for the long slope domain (a) 2.5 m, (b) 2.25 m, and (c) 2 m.

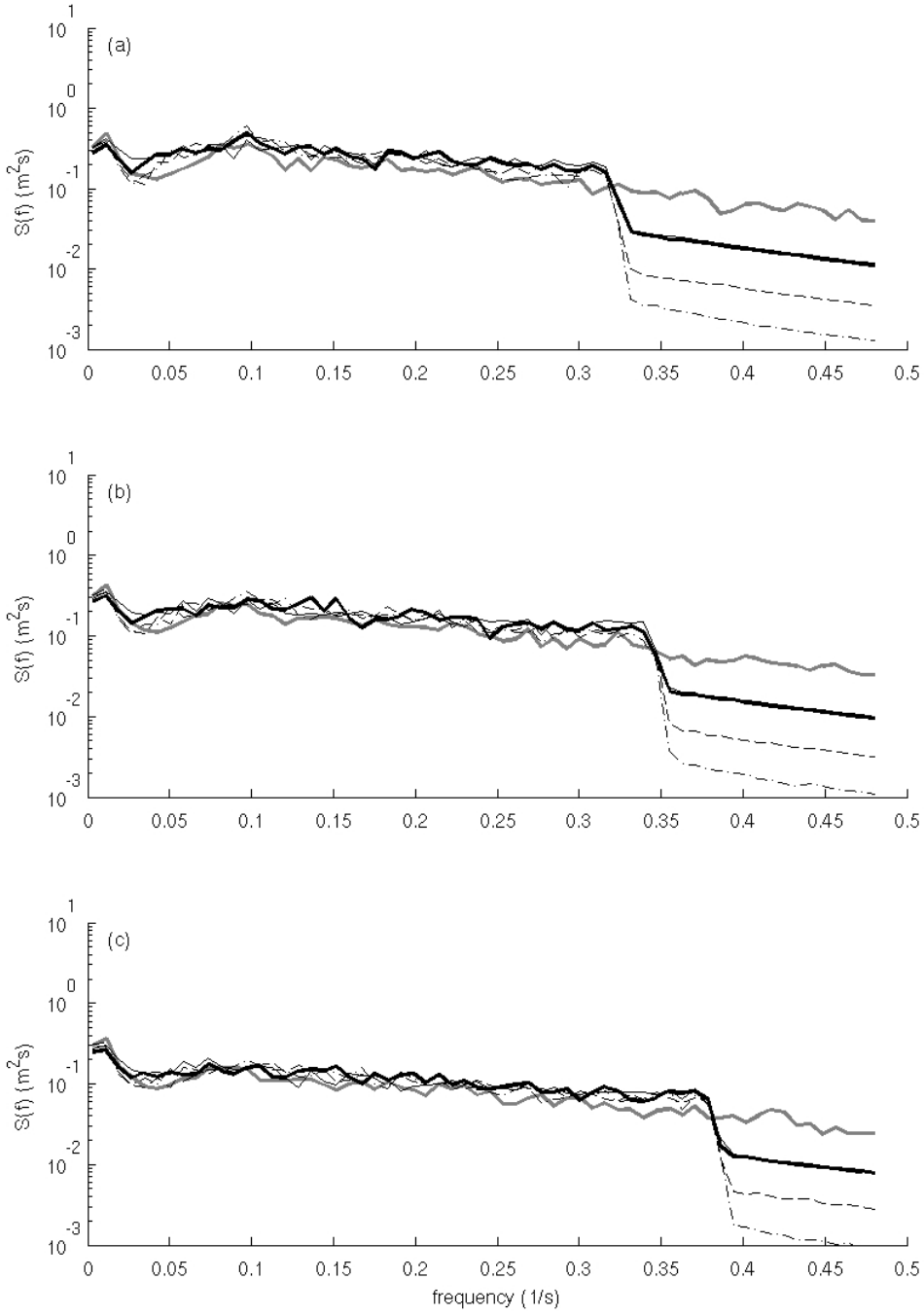

Figure 4.16 Comparison of full model (gray line) and hybrid model results (case 1, black solid; case 2, black dashed; case 3, black dash dotted; case 4 bold black solid). Results are given for the long slope domain (a) 1.75 m, (b) 1.5 m, and (c) 1.25 m.

approximately 1.75 m (Figure 4.16 (a)), where the spectrum's peak disappears, and energy is distributed more evenly across all frequencies. The initial overestimation of energy outside the Toba range results because the Toba parameterization overestimates energy at the high frequencies forcing too much energy to the low frequencies of the spectra.

Because they initially represent the Toba range well, cases 2 and 3 perform exceptionally better than case 1 outside the Toba range (Figures 4.13—4.16). However, the spectra's Toba ranges are underestimated at depths shallower than approximately 10 m. Case 2 replicates the energy in the spectra's Toba ranges slightly better than case 3, with the difference increasing as depth decreases.

At locations of shallower depths β_{SNV} and β_{alf} are within the same order of magnitude; therefore, case 4 performs similar to case 1 predicting the Toba range better than cases 2 and 3 (Figures 4.14—4.16). However, at offshore locations, case 4 performs similarly to cases 2 and 3 in the Toba range (Figure 4.13 (a)). Because case 4 refrains from overestimating the Toba range of offshore spectra, the final case replicates areas outside the Toba range where the energy is overestimated by case 1.

For the MK92 domain, the hybrid model reduces computational time from over 2.5 hr to approximately 0.5 hr. Results from the four cases of the hybrid model are similar in deeper water (Figure 4.17 (b) and (c)). The energy is overestimated by all cases, and the slope is flatter than the slope of the spectra's Toba ranges.

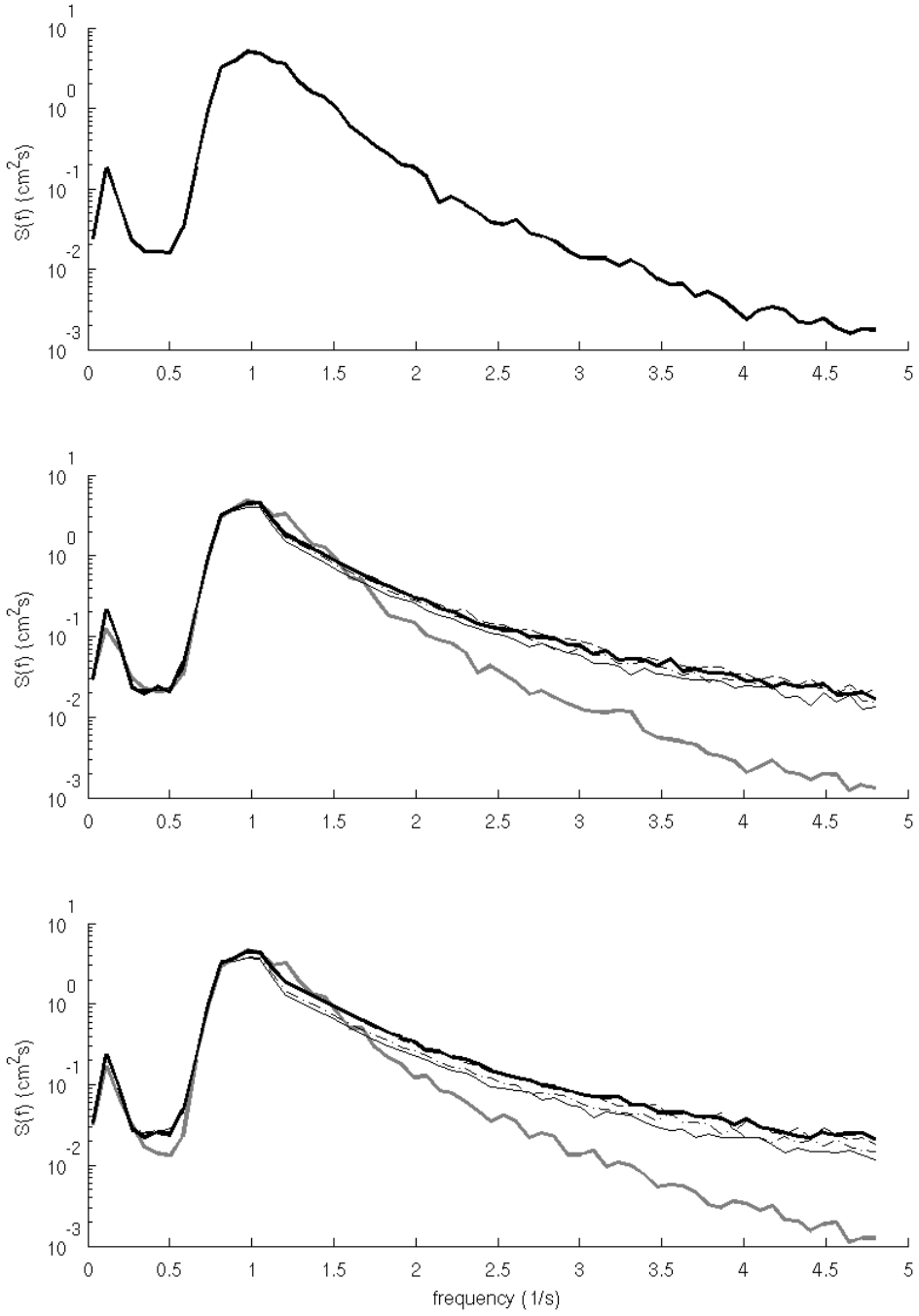

Figure 4.17 Comparison of observations (gray line) and hybrid model results (case 1, black solid; case 2, black dashed; case 3, black dash dotted; case 4 bold black solid). Results are given for the MK92 domain (a) 47 cm, (b) 35 cm, and (c) 30 cm.

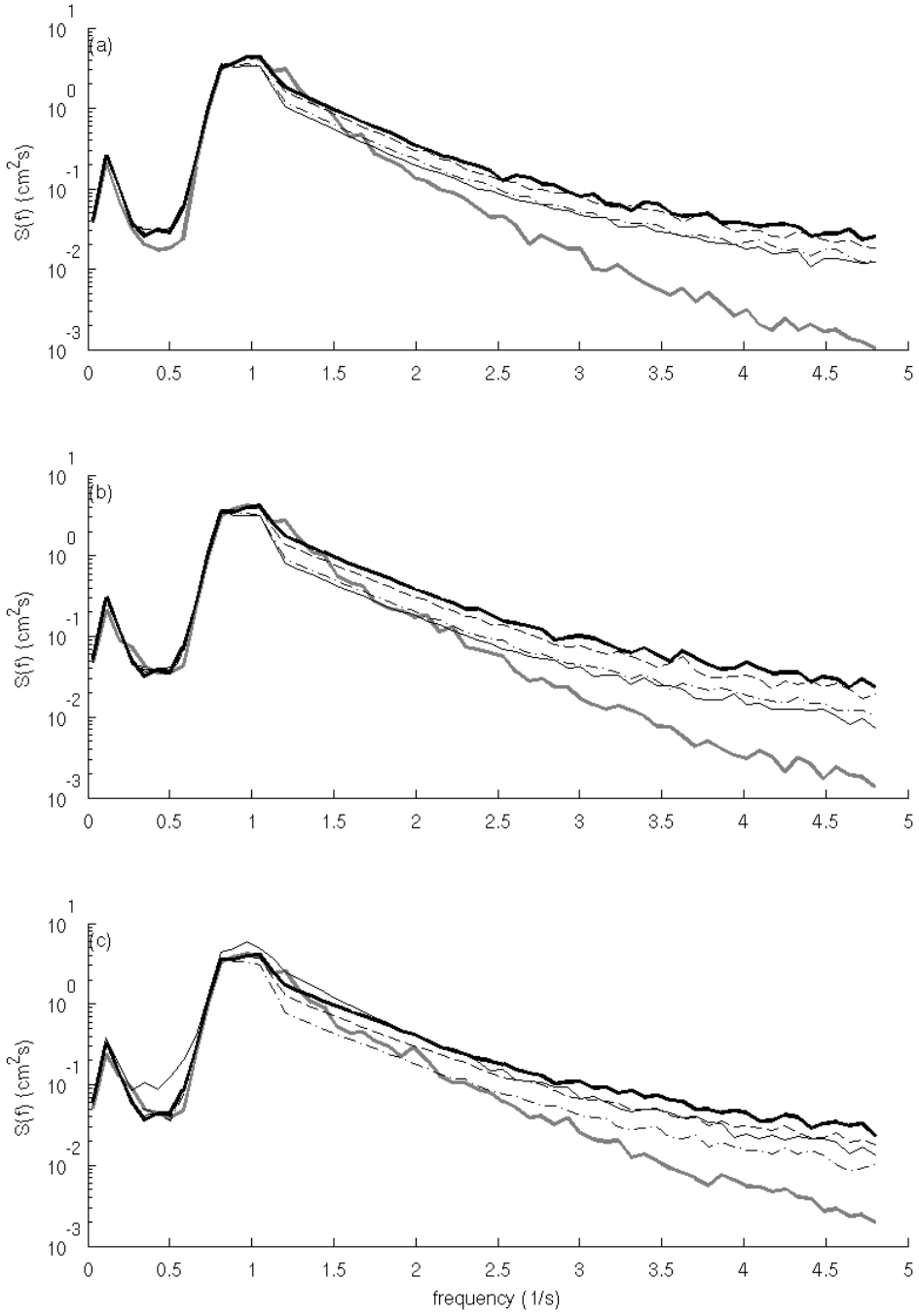

Figure 4.18 Comparison of observations (gray line) and hybrid model results (case 1, black solid; case 2, black dashed; case 3, black dash dotted; case 4 bold black solid). Results are given for the MK92 domain (a) 25 cm, (b) 20 cm, and (c) 17.5 cm.

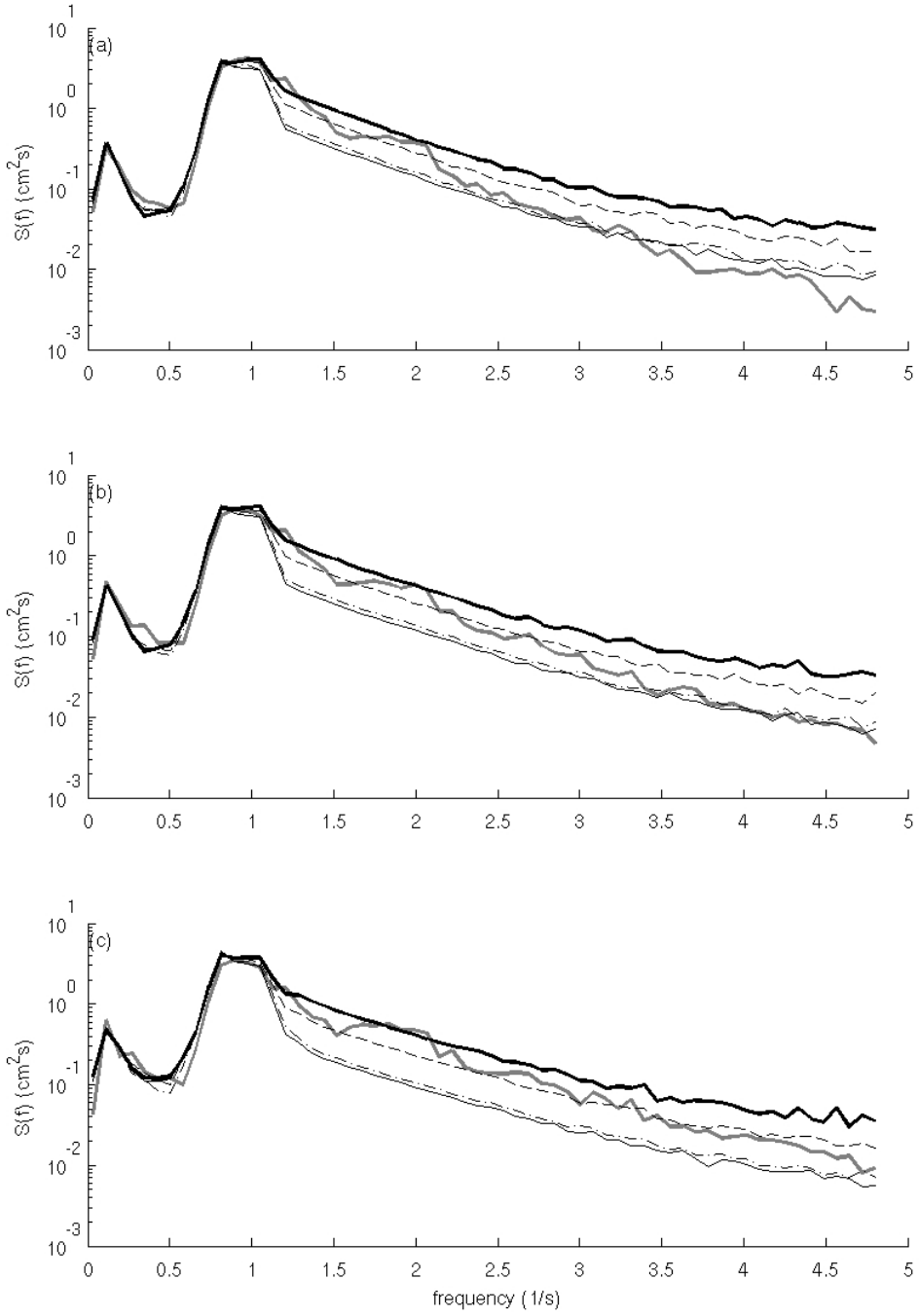

Figure 4.19 Comparison of observations (gray line) and hybrid model results (case 1, black solid; case 2, black dashed; case 3, black dash dotted; case 4 bold black solid). Results are given for the MK92 domain (a) 15 cm, (b) 12.5 cm, and (c) 10 cm.

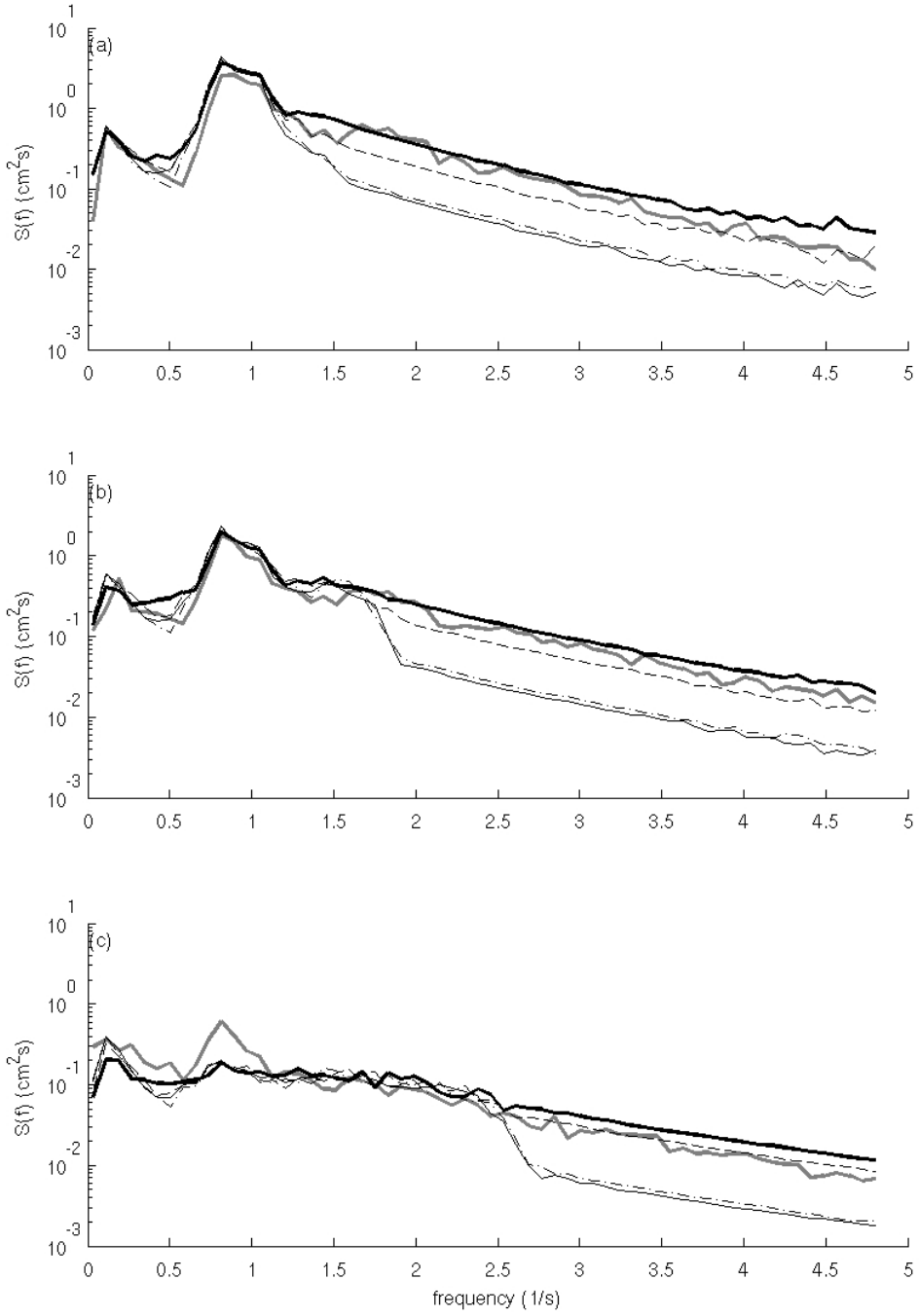

Figure 4.20 Comparison of observations (gray line) and hybrid model results (case 1, black solid; case 2, black dashed; case 3, black dash dotted; case 4 bold black solid). Results are given for the MK92 domain (a) 7.5 cm, (b) 5 cm, and (c) 2.5 cm.

As depth decreases, results of the hybrid model cases separate (Figures 4.18 and 4.19). Until a depth of approximately 15 cm where the effects of nonlinear interactions are evident in the observations, all cases of the hybrid model continue to overestimate the energy for most of a spectrum's Toba range.

In shallow water, cases 2 and 4 continue to replicate the observations well (Figure 4.20); however, cases 1 and 3 underestimate the energy of the Toba range. All cases of the hybrid model give good results for the region of the spectra outside the Toba range.

Quantitative Hybrid Model Results

Error analysis (Figure 4.21) of spectral energy in the long slope domain confirms only parts of the story told by the graphical results. Spectra resulting from the linear model never change shape, thus disagreeing with the full model shoreward of a depth of approximately 10 m where nonlinear interactions transfer energy primarily to high frequencies changing the shape of the spectra. In addition, shoreward of this depth, cases 2, 3, and 4 of the hybrid model replicate the full model significantly better than the instance when nonlinear interactions were ignored. Shoreward of approximately 3 m, error analysis suggests that all cases of the hybrid model possess equal ability to replicate the full model.

Error analysis (Figure 4.22) of spectral energy in the MK92 domain confirms that shoreward of a depth of approximately 17.5 cm, the full model replicates the observed spectra better than the model neglecting nonlinear interactions. In addition, cases 2 and 4 of the hybrid model perform better than

cases 1 and 3. In fact, until a depth of approximately 12.5 cm, the model neglecting nonlinear interactions performs better than cases 1 and 3. Shoreward of approximately 15 cm, cases 2 and 4 replicate the observations better than all other models. Case 4 gives the best hybrid model results.

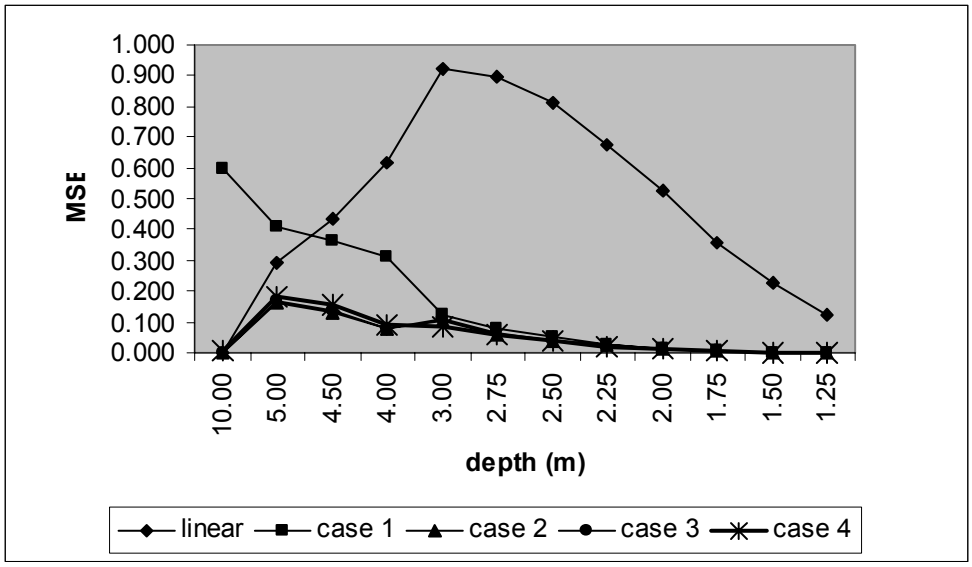

Figure 4.21 MSE for hybrid model comparisons to the full model in the long slope domain.

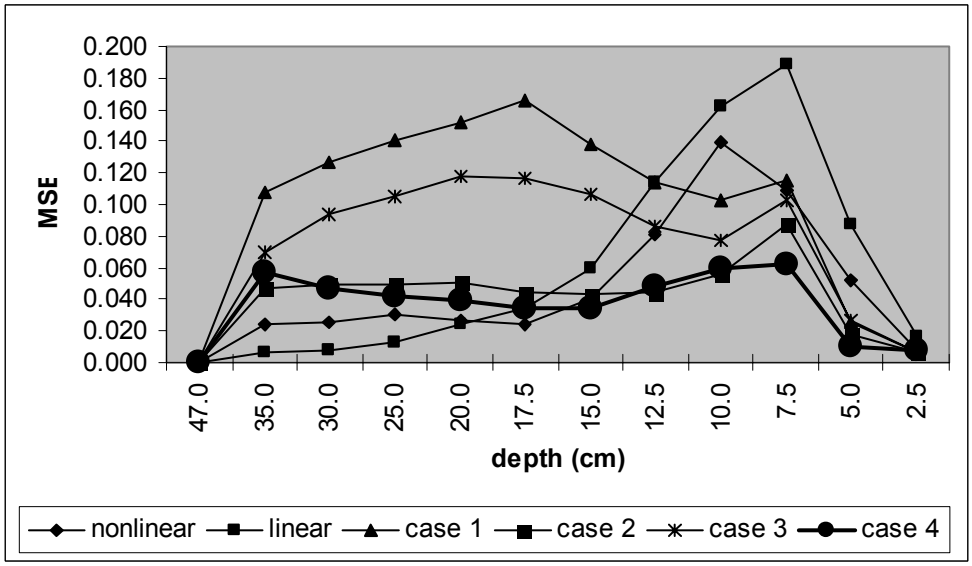

Figure 4.22 MSE for model comparisons to observations collected in the MK92 domain.

Resulting Wave Parameters

In this final section of the results, wave parameters determined from modeled spectra and available observations are presented. H_{rms}, skewness, and asymmetry are given for each domain.

For the long slope domain, case 1 of the hybrid model significantly overestimates H_{rms} determined from full model results (Figure 4.23). Although case 4 overpredicts H_{rms} through the domain, the overprediction is not as significant as that of case 1. Hybrid model cases 3 and 4 give the best results for H_{rms}. However these cases slightly underestimate H_{rms} in deeper water and overestimate H_{rms} after breaking.

For the MK92 domain, cases 1, 2, and 3 of the hybrid model appear to replicate H_{rms} better than the full model, with case 2 performing the best (Figure 4.24). Case 4 closely follows H_{rms} determined from the full model beyond breaking.

For both domains, skewness determined from hybrid model results mirrors skewness determined from full model results and available observations. In the long slope domain, skewness (Figure 4.25) determined from the full model increases until a depth of approximately 3 m. Shoreward of 3 m it decreases. Skewness determined from the full model in the long slope domain tends to decrease up to a depth of approximately 5 m and decrease shoreward of 5 m. For the MK92 domain, skewness (Figure 4.26) determined from observations increases to a depth of approximately 5 cm; then, it decreases. Skewness

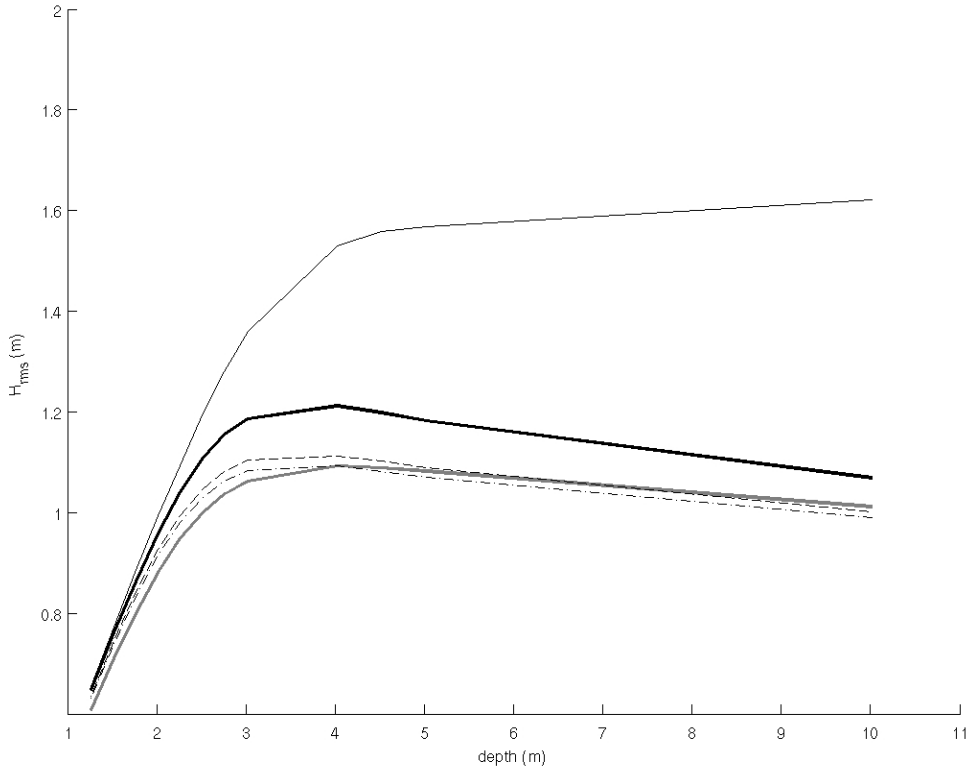

Figure 4.23 H_{rms} of the long slope domain determined from the full model results (gray line) and case 1 (black solid), case 2 (black dashed), case 3 (black dash dotted), and case 4 (bold black solid) of the hybrid model results.

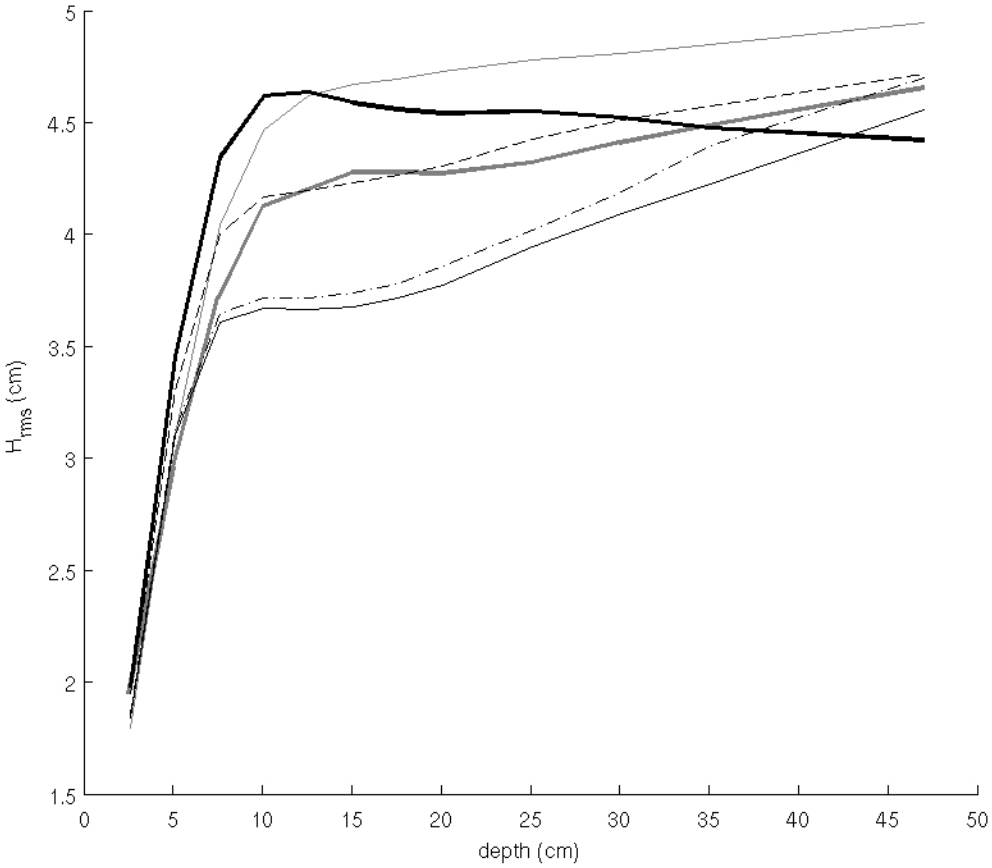

Figure 4.24 H_{rms} of the MK92 domain determined from observations (bold gray line), the full model results (gray line), and case 1 (black line), case 2 (black dashed), case 3 (black dash dotted), and case 4 (bold black solid) of the hybrid model results.

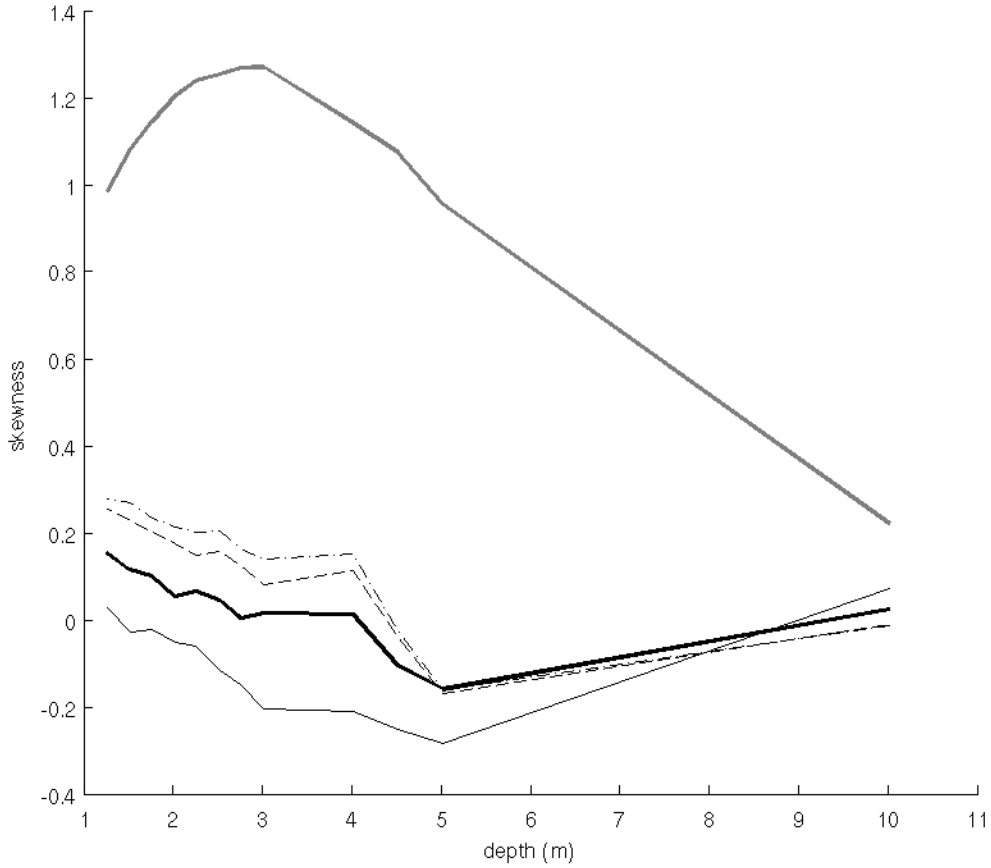

Figure 4.25 Skewness of the long slope domain determined from the full model results (gray line) and case 1 (black line), case 2 (black dashed), case 3 (black dash dotted), and case 4 (bold black solid) of the hybrid model results.

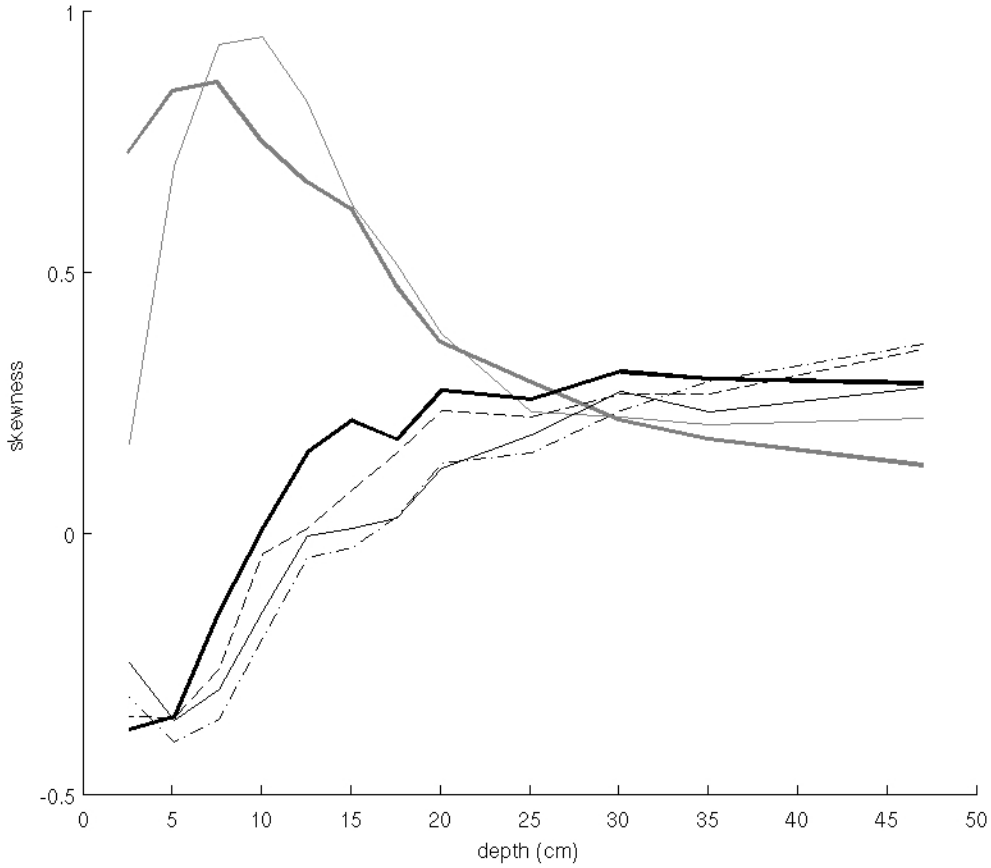

Figure 4.26 Skewness of the MK92 domain determined from observations (bold gray line), the full model results (gray line), and case 1 (black line), case 2 (black dashed), case 3 (black dash dotted), and case 4 (bold black solid) of the hybrid model results.

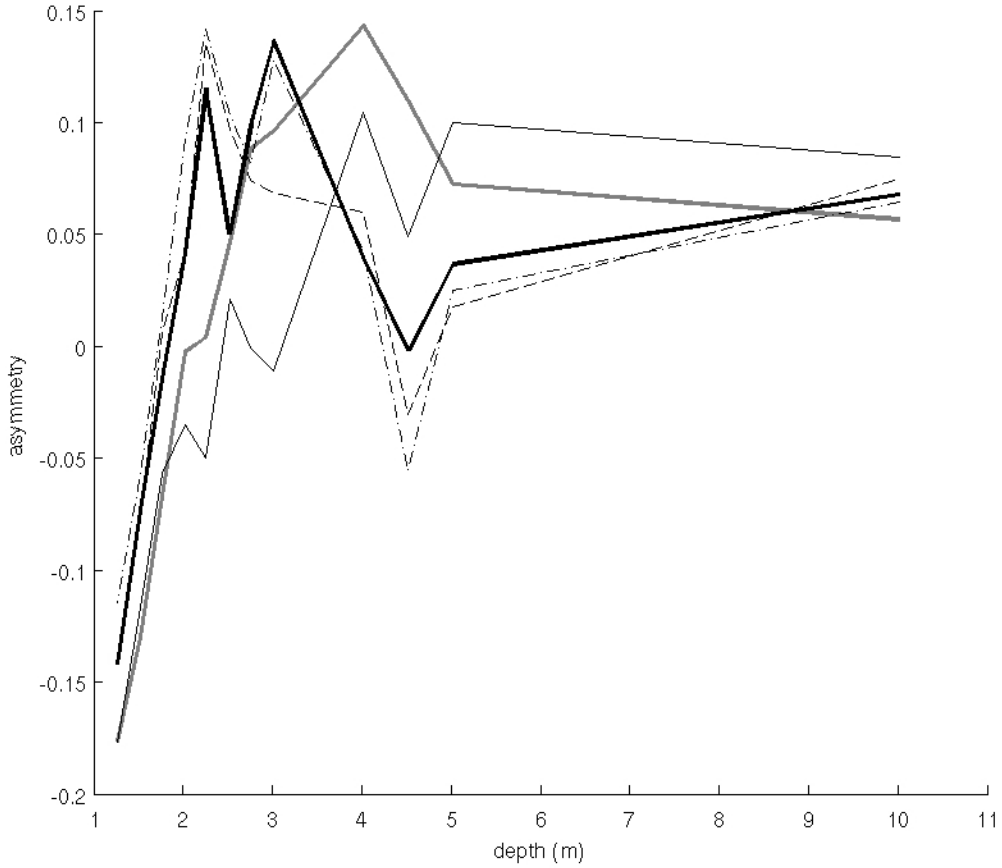

Figure 4.27 Asymmetry of the long slope domain determined from the full model results (gray line) and case 1 (black line), case 2 (black dashed), case 3 (black dash dotted), and case 4 (bold black solid) of the hybrid model results.

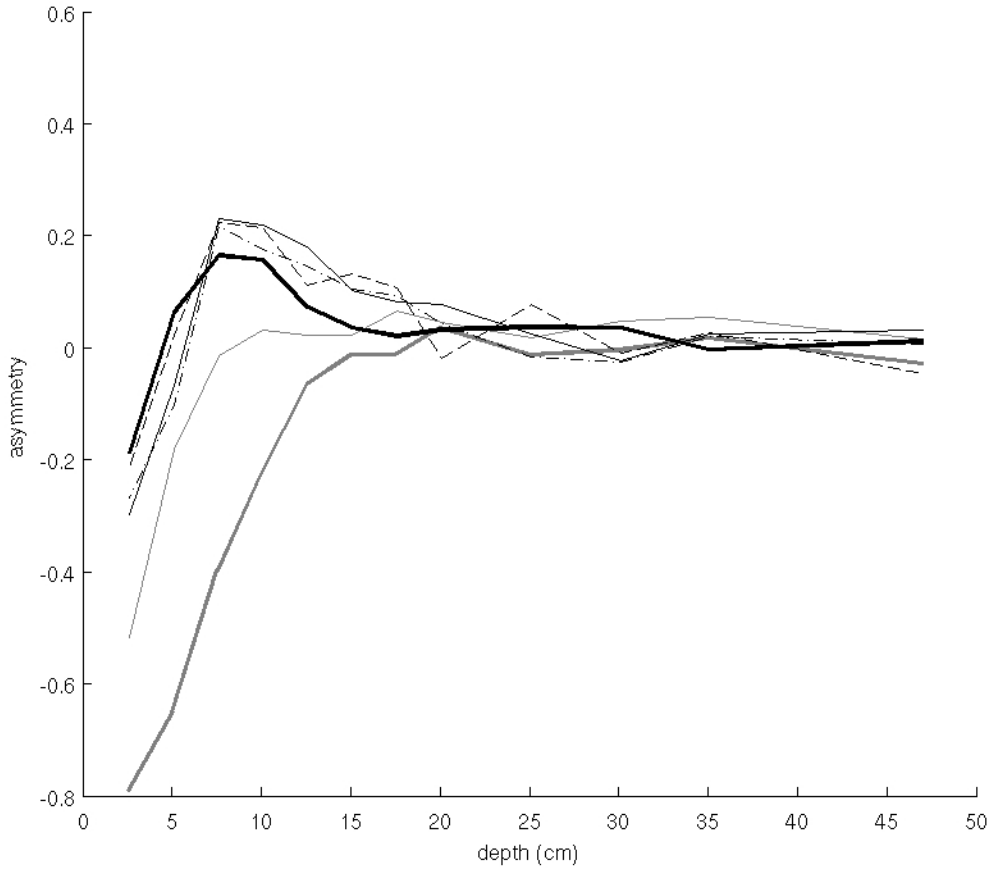

Figure 4.28 Asymmetry of the MK92 domain determined from observations (bold gray line), the full model results (gray line), and case 1 (black line), case 2 (black dashed), case 3 (black dash dotted), and case 4 (bold black solid) of the hybrid model results.

determined from full model results in the MK92 domain tends to follow the skewness determined from observations. However, skewness determined from all cases of the hybrid model decrease to a depth of approximately 5 cm and increases shoreward of 5 cm. All cases of the hybrid model results appear to determine skewness with the same skill.

For the long slope domain, asymmetry (Figure 4.27) determined from cases of the hybrid model shows no strong trends. For the MK92 domain, however, the hybrid models replicate asymmetry determined from observed spectra as good, if not better, than the full model up to approximately 20 cm (Figure 4.28). Shoreward of 20 cm, all cases of the hybrid model tend toward negative asymmetry but overestimate asymmetry determined from the full model results and observed spectra. No single hybrid model case appears to out-perform the others in determining asymmetry for the MK92 domain.

CHAPTER 5

CONCLUSIONS

This study considered two ways to reduce the number of computations of Kaihatu and Kirby's (1995) frequency domain model, thus reducing the computational expense. The first method was to completely eliminate the nonlinear interactions in Kaihatu and Kirby's model and the second method was to replace some of the direct computations in the equilibrium region of the spectra with a general parameterization. Both methods decreased the computational times but with different degrees of success. We used two domains to study the results: one was an idealized domain and the other was the domain used in a laboratory experiment.

Removing the nonlinear interactions from Kaihatu and Kirby (1995) dramatically reduced the time required to propagate the wavefield through both domains considered. However, nonlinear interactions play an important role in the evolution of shoaling and surf zone waves. While linear theory is sufficient for intermediate water depths where the nonlinear interactions are relatively weak, it is incapable of replicating shoaling and breaking waves, for which nonlinearity is important. As the waves begin to shoal and approach breaking, nonlinear interactions serve to change the wave shape from sinusoidal to one with peaked crests, shallow troughs and (during breaking) a steeper forward face. Furthermore, the shapes of wave spectra change because nonlinear interactions transfer energy between frequencies. Consequently, spectra become broader with more energy in the high frequency components. These effects are impossible to achieve with linear models.

Although its effect on computational expense is not as dramatic as the linear model, the hybrid model reduces the number of computations resulting in a significant decrease in computational time. Within the Toba range, a parameterization equivalent to an equilibrium spectra is used to replace the computations which accurately mimics the wave field evolution; these energies are then available for interaction with energies at frequencies outside this range. Therefore, the hybrid model more accurately replicates the evolution of waves from intermediate water depths through the shoaling and surf zones than the linear model but without the computational expense of the full nonlinear model. The extent of the hybrid model's ability to replicate wave propagation depends on the formulation of β_{Toba} in the parameterization.

The first case of the hybrid model utilizes β_{Toba} given by Smith and Vincent (2003) as $\beta_{SNV} = \alpha_{SNV} h^{0.5}$ with $\alpha_{SNV} = 0.0103$ for both testing domains. It overestimates the energy in the input spectrum in both the long slope and MK92 domains. The overestimation results because Smith and Vincent determined the Toba range parameterization from only surf zone spectra, which as a result of nonlinear interactions, contain more energy at high frequencies than spectra in the intermediate water range. Any misrepresentation of the wave energy offshore affects the solution throughout the domain. The overestimation in the beginning resulted in excess energy transfer to low frequencies and, thus, an inadequate replication of wave evolution. Keeping Smith and Vincent's parameterization's dependence on $k^{-2.5}$ and focusing on β_{Toba} results in

improving the parameterization's representation of the Toba range for the two domains considered.

The second case of the hybrid model defines β_{Toba} as $\beta_{con} = 0.0804$ and $\beta_{con} = 0.0041$ for the MK92 and long slope domains, respectively. These values of β_{Toba} represent the Toba range energy of the input spectrum and remain constant with a change in depth; therefore, the energy in the parameterized region does not change in either domain. This case of the hybrid model appears to do well in the MK92 domain because much of the domain has waves in the intermediate water range; thus, nonlinear interactions are relatively weak for most of the domain. In the long slope domain, however, the nonlinear interactions are stronger. Therefore, high frequency energy increases as the waves propagate toward shore, and the parameterized region increasingly deviates from the spectra. As a result, the second case of the hybrid model fails to adequately replicate the long slope domain.

Case three of the hybrid model substitutes $\beta_{emat} = \alpha_{emat} h^{0.5}$ for β_{Toba} in the parameterization. Determined from the Toba range energy of the offshore spectrum, $\alpha_{emat} = 0.0117$ and $\alpha_{emat} = 0.0011$ for the MK92 and long slope domains, respectively. Therefore, β is an explicit function of depth. In addition, this method does not take into account the energy transfer to the higher harmonics that result from nonlinear interactions. Consequently, as depth decreases, the energy of the parameterized portion of the hybrid model decreases. However, nonlinear interactions present in the full model and available observations feed energy into the high frequencies increasing the energy of the high frequency tail.

Therefore, regardless of the domain, the parameterized portion and the spectra's Toba ranges increasingly disagree with decreased depth.

Similar to case three of the hybrid model, the formulation of β_{Toba} for case four β_{alf} depends on α_{emat}. Furthermore, the nondimensional parameter H_{rms}/h is used in determining β_{alf} (equations 3.6 and 3.7). Because H_{rms}/h is equivalent to the nonlinearity parameter used in the development of nonlinear wave theory, this case accounts for energy transferred by wave-wave interactions. Including nonlinear interactions into the parameterization prevents case four of the hybrid model from dramatically underestimating the Toba range of shoaling and surf zone spectra as seen in the other depth dependent cases in the MK92 domain and the other long slope domain cases with energy matched variables. In both domains, case 4 of the hybrid model performs best. However, a drop in energy of the parameterization, although less dramatic, remains.

Determining β_{Toba} from the input spectra (cases 2, 3, and 4) prevents overestimation outside the surf zone and the resulting unwanted transfer of energy to low frequencies. However, the hybrid cases that use energy matching tend to underestimate the Toba range of the spectra. The underestimation is marked by a large drop in the Toba range parameterization with the formation of the secondary peak.

Determining the energy matched variable from only the Toba range at the offshore boundary causes the underestimation in energy when nonlinear interactions become important. At the offshore boundary, most of the energy is contained in low frequency bins; therefore, the Toba range contains relatively

little energy. As waves propagate shoreward and nonlinear interactions become important, the energy level of the high frequencies increases. As a result, the energy level determined from the offshore spectrum underestimates the high frequency energy of spectra affected by nonlinear interactions causing a large drop in energy in the hybrid model results. This drop is more pronounced in the long slope domain for two reasons. First, the nonlinear interactions are stronger than in the MK92 case. Second, the MK92 input spectrum is broader than the input spectrum of the long slope domain; therefore, a larger percent of the MK92 input spectrum's energy is present at high frequencies.

Determining β_{Toba} from total energy at every point in the domain, as opposed to only the Toba range energy of the input spectrum, creates an opportunity to alleviate the sudden drop in energy seen when nonlinear interactions intensify. At every point in the domain, the hybrid model determines dissipation, which balances the flux of energy between the point under consideration and the previous point in the domain. Knowing the calculated dissipation and the energy flux of the previous step makes the energy flux, thus total energy, of interest available for calculating β_{Toba}.

The results of the hybrid model show satisfactory computations of H_{rms}, a measure of total spectral energy. However, the wave parameters skewness and asymmetry, which result from nonlinear interactions, disagree with the full model and available observations. The wave-wave interactions depend on the phase mismatch between bound and free wavenumbers (Madsen & Sørensen, 1993). By assuming a random phase in the parameterized portion of the hybrid model,

the bound wavenumbers change, which in turn affects the phase mismatch and, thus, the nonlinear interactions that determine skewness and asymmetry.

In summary, a hybrid model is capable of reproducing shoaling and surf zone wave spectra. Furthermore, the hybrid model significantly reduces the computational expense of the nonlinear model required to reproduce wave spectra in areas where complex energy transfers occur. Further work will improve the hybrid model by determining β_{Toba} from total energy at each step in the domain, which will eliminate the energy drop seen in the Toba range of the hybrid model results. Also, a more consistent representation for the phase of the parameterization will be sought, which would improve the predictions of skewness and asymmetry in the shoaling region and the surf zone.

APPENDIX

Several methods were used to determine if the regressions adequately represent the spectra's Toba ranges of the observations in the MK92 domain and the full model results in the long slope domain.

Analysis of residuals and analysis of variance (ANOVA) were used to determine the adequacy of the regressions. Scatters of the residuals were used to determine if the regressions fulfilled the assumptions that the errors are independent and that the variance of the errors is constant. A group of randomly scattered residuals ensures that the regressions meet these assumptions. In addition, histograms of the residuals were considered. Normally distributed residuals are required of a sufficient linear regression. A final requirement is that the sum of the residuals be zero.

The regression model is numerically tested by ANOVA. ANOVA results in two important values, the mean square error (MSE) and the *F* ratio. A small MSE implies an adequate regression, and the *F* ratio is used to test the null hypothesis that no relation between the dependent and independent variables exist. Therefore, a large *F* ratio implies that the regression model represents the data. From the *F* ratios, *p*-values were determined. For values less than the significance level 5%, the regression adequately represents the observations.

For the MK92 domain, "fit" lines and corresponding observed spectra are well correlated (Figures A1—A4). Random scatters (Figure A5) and histograms indicative of normal distributions (Figure A6) of residuals show that the linear regressions used to determine the coefficients of the spectra's Toba ranges are

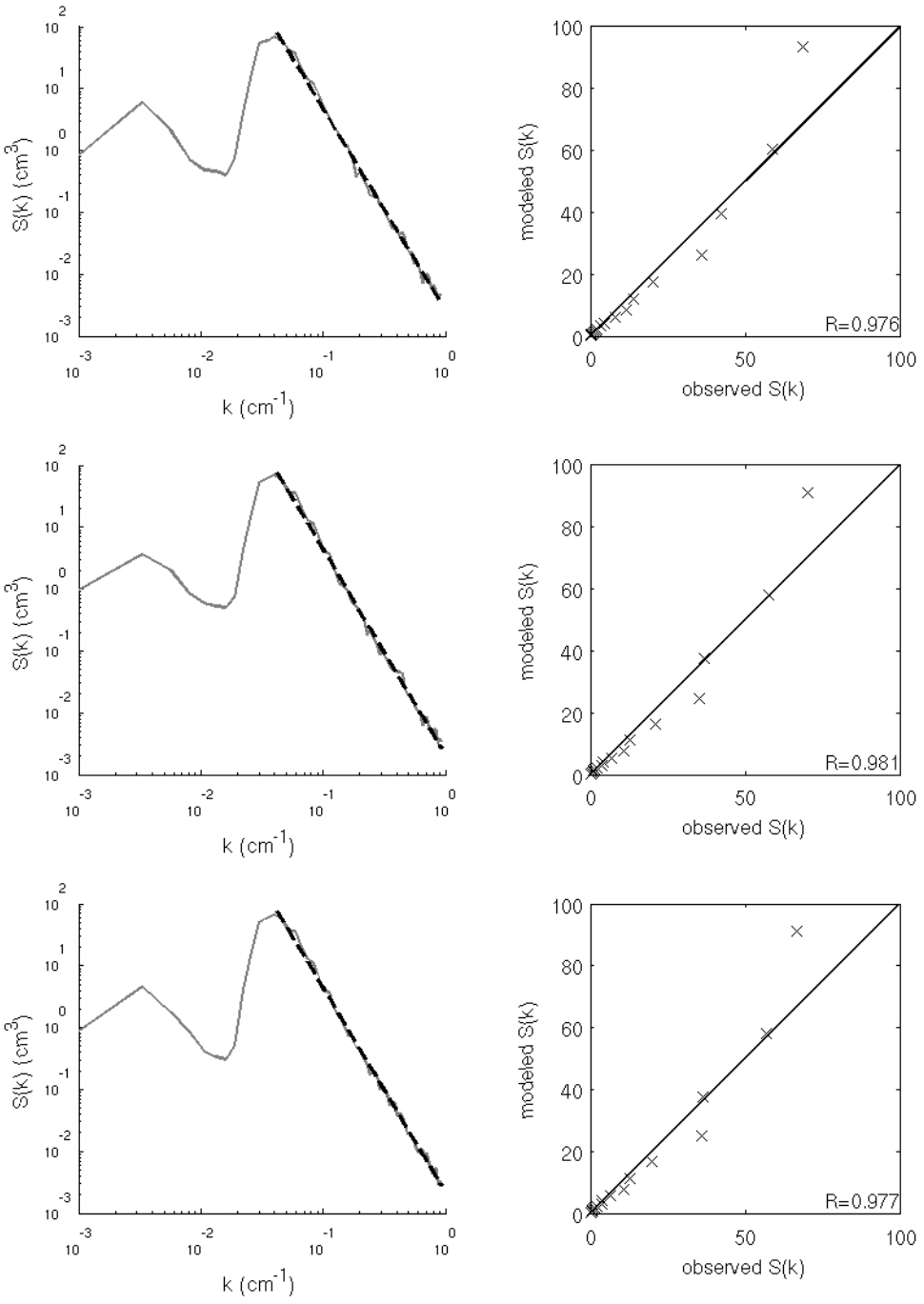

Figure A1 Comparisons of the observed wavenumber spectra (gray lines) and the "fit" lines (black dashed line) are shown in the left column. The correlation of the comparison is given in the right column. Comparisons are for depths of 47 (top), 35 (middle), and 30 (bottom) cm in the MK92 domain.

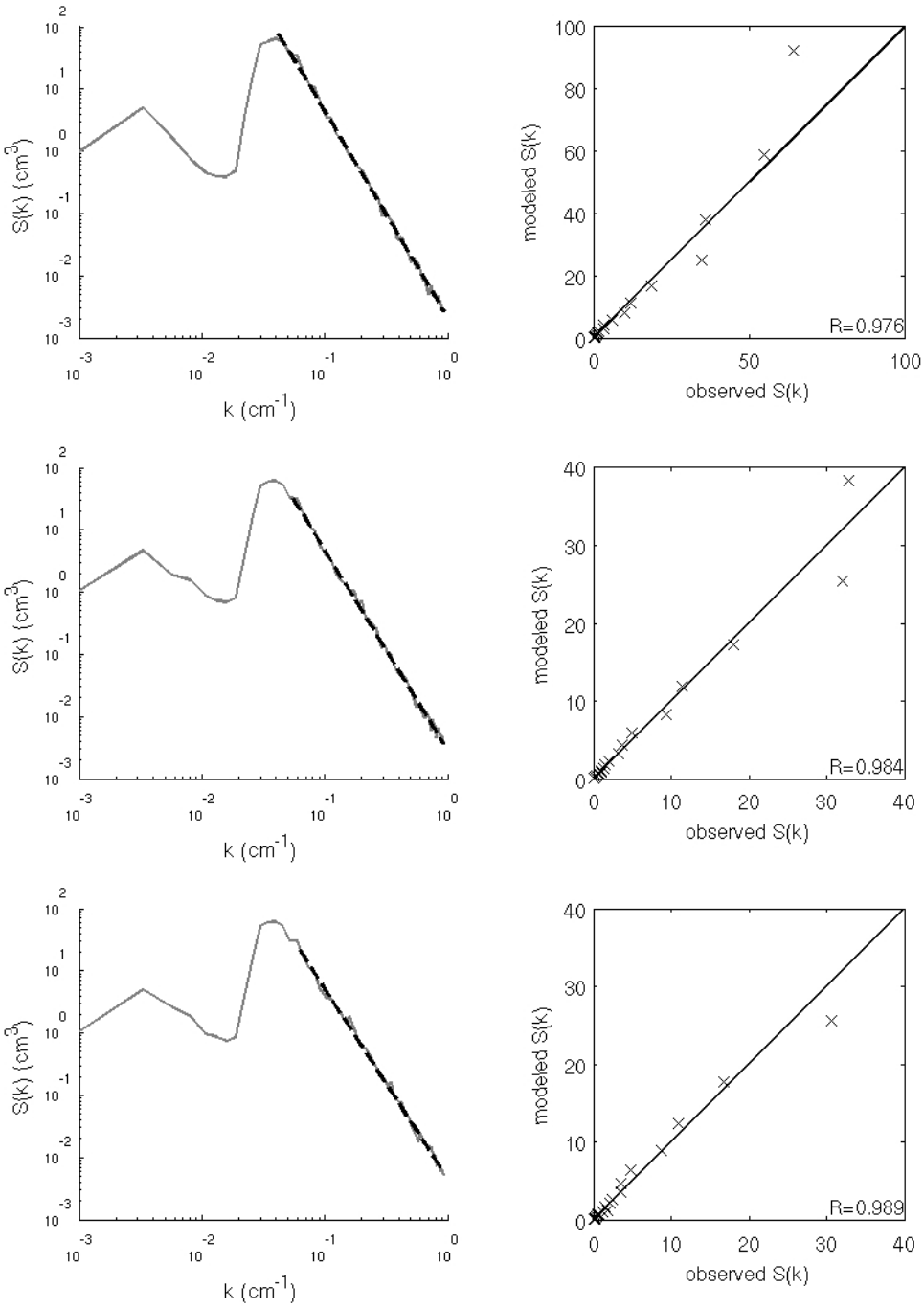

Figure A2 Comparisons of the observed wavenumber spectra (gray lines) and the "fit" lines (black dashed line) are shown in the left column. The correlation of the comparison is given in the right column. Comparisons are for depths of 25 (top), 20 (middle), and 17.5 (bottom) cm in the MK92 domain.

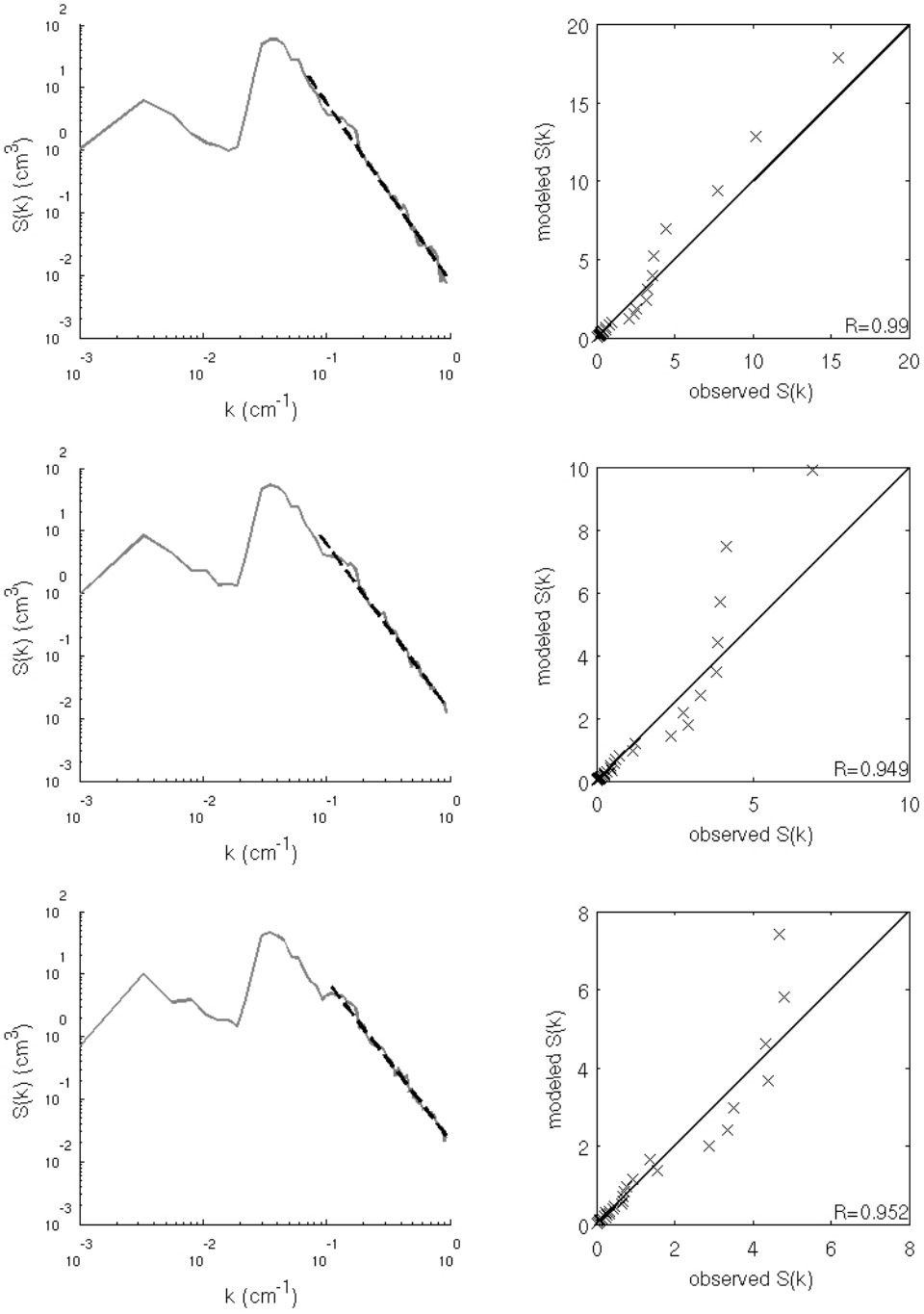

Figure A3 Comparisons of the observed wavenumber spectra (gray lines) and the "fit" lines (black dashed line) are shown in the left column. The correlation of the comparison is given in the right column. Comparisons are for depths of 15 (top), 12.5 (middle), and 10 (bottom) cm in the MK92 domain.

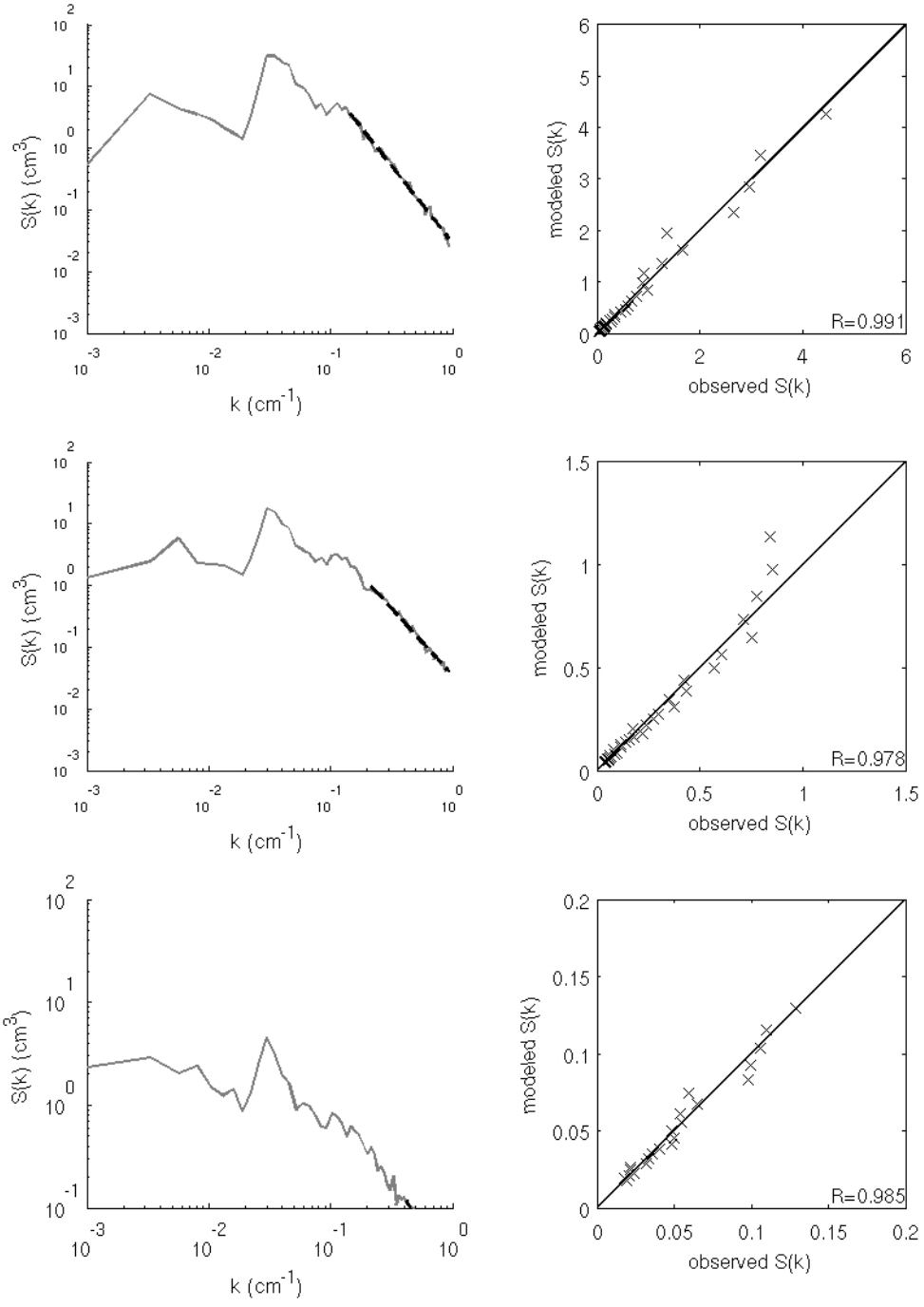

Figure A4 Comparisons of the observed wavenumber spectra (gray lines) and the "fit" lines (black dashed line) are shown in the left column. The correlation of the comparison is given in the right column. Comparisons are for depths of 7.5 (top), 5 (middle), and 2.5 (bottom) cm in the MK92 domain.

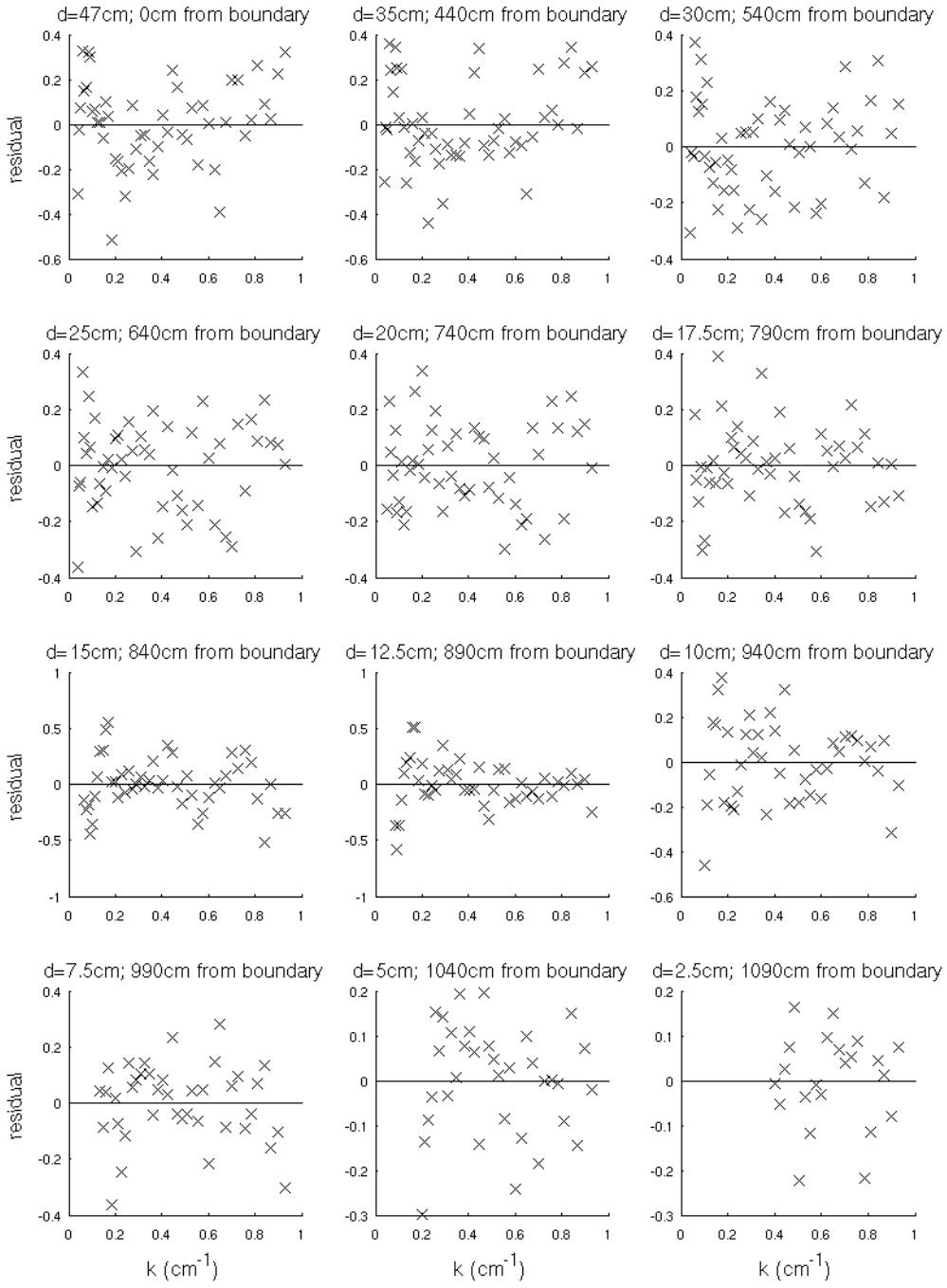

Figure A5 Scatter plots of the residuals resulting from the regression lines and observed spectra of the MK92 domain.

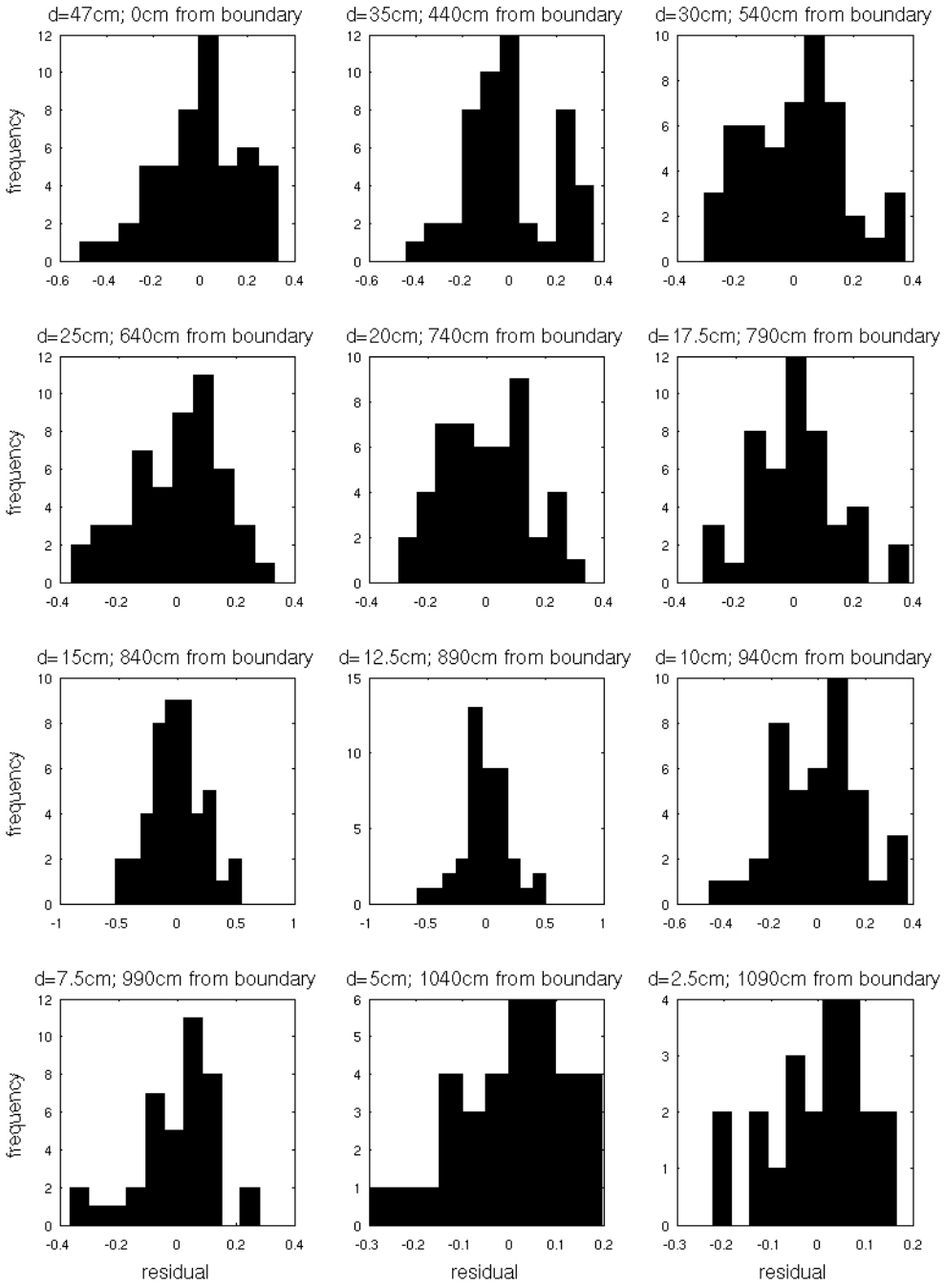

Figure A6 Distributions of residuals resulting from the regression lines and the observed spectra of the MK92 domain.

Table A1

ANOVA for the regressions of the MK92 domain.

d=47cm					
Source	**DOF**	**Sum of Squares**	**Mean Squares**	**F Ratio**	**p**
Error	*48*	*1.734*	*0.036*		
Regression	*48*	*415.924*	*415.924*	*11513.067*	*0.007*
d=35cm					
Source	**DOF**	**Sum of Squares**	**Mean Squares**	**F Ratio**	**p**
Error	*48*	*1.789*	*0.037*		
Regression	*48*	*432.071*	*432.071*	*11591.824*	*0.007*
d=30cm					
Source	**DOF**	**Sum of Squares**	**Mean Squares**	**F Ratio**	**p**
Error	*48*	*1.355*	*0.028*		
Regression	*48*	*427.975*	*427.975*	*15163.927*	*0.006*
d=25cm					
Source	**DOF**	**Sum of Squares**	**Mean Squares**	**F Ratio**	**p**
Error	*48*	*1.212*	*0.025*		
Regression	*48*	*431.827*	*431.827*	*17104.616*	*0.006*
d=20cm					
Source	**DOF**	**Sum of Squares**	**Mean Squares**	**F Ratio**	**p**
Error	*46*	*1.075*	*0.023*		
Regression	*46*	*328.875*	*328.875*	*14071.618*	*0.007*
d=17.5cm					
Source	**DOF**	**Sum of Squares**	**Mean Squares**	**F Ratio**	**p**
Error	*45*	*0.968*	*0.022*		
Regression	*45*	*266.604*	*266.604*	*12396.782*	*0.007*
d=15cm					
Source	**DOF**	**Sum of Squares**	**Mean Squares**	**F Ratio**	**p**
Error	*44*	*2.352*	*0.053*		
Regression	*44*	*209.235*	*209.235*	*3914.263*	*0.013*
d=12.5cm					
Source	**DOF**	**Sum of Squares**	**Mean Squares**	**F Ratio**	**p**
Error	*42*	*1.875*	*0.045*		
Regression	*42*	*149.817*	*149.817*	*3355.540*	*0.014*
d=10cm					
Source	**DOF**	**Sum of Squares**	**Mean Squares**	**F Ratio**	**p**
Error	*40*	*1.313*	*0.033*		
Regression	*40*	*110.387*	*110.387*	*3362.395*	*0.014*
d=7.5cm					

Source	DOF	Sum of Squares	Mean Squares	F Ratio	p
Error	*37*	*0.716*	*0.019*		
Regression	*37*	*76.050*	*76.050*	*3930.593*	*0.013*
		d=5cm			
Source	**DOF**	**Sum of Squares**	**Mean Squares**	**F Ratio**	**p**
Error	*32*	*0.488*	*0.015*		
Regression	*32*	*32.457*	*32.457*	*2126.388*	*0.017*
		d=2.5cm			
Source	**DOF**	**Sum of Squares**	**Mean Squares**	**F Ratio**	**p**
Error	*20*	*0.225*	*0.011*		
Regression	*20*	*7.819*	*7.819*	*693.615*	*0.030*

valid. In addition, the residuals cancel. ANOVA for the regressions results in small MSE values and large *F* ratios. *p*-values determined from the *F* ratios ensure that the regression model and the observations are significantly correlated at a level of 5% (Table A1).

In the long slope domain, the regressions and spectra appear well correlated, except for the depth of 1.25 m (Figures A7-A10). Furthermore, for comparisons that appear well correlated, the residuals randomly scatter (Figure A11). However, distributions of the residuals, as well as ANOVA, disagree with the correlations and residual scatters. Shoreward of a depth of approximately 2.75 m, the degrees of freedom (DOF) is low. The distribution of residuals (Figure A12) clearly deviates from a normal distribution. In addition, ANOVA (Table A2) results in MSE values and F ratios that give p-values larger than the significance level. Therefore, the null hypothesis is accepted making the regressions inadequate at depths shallower than approximately 2.75 m.

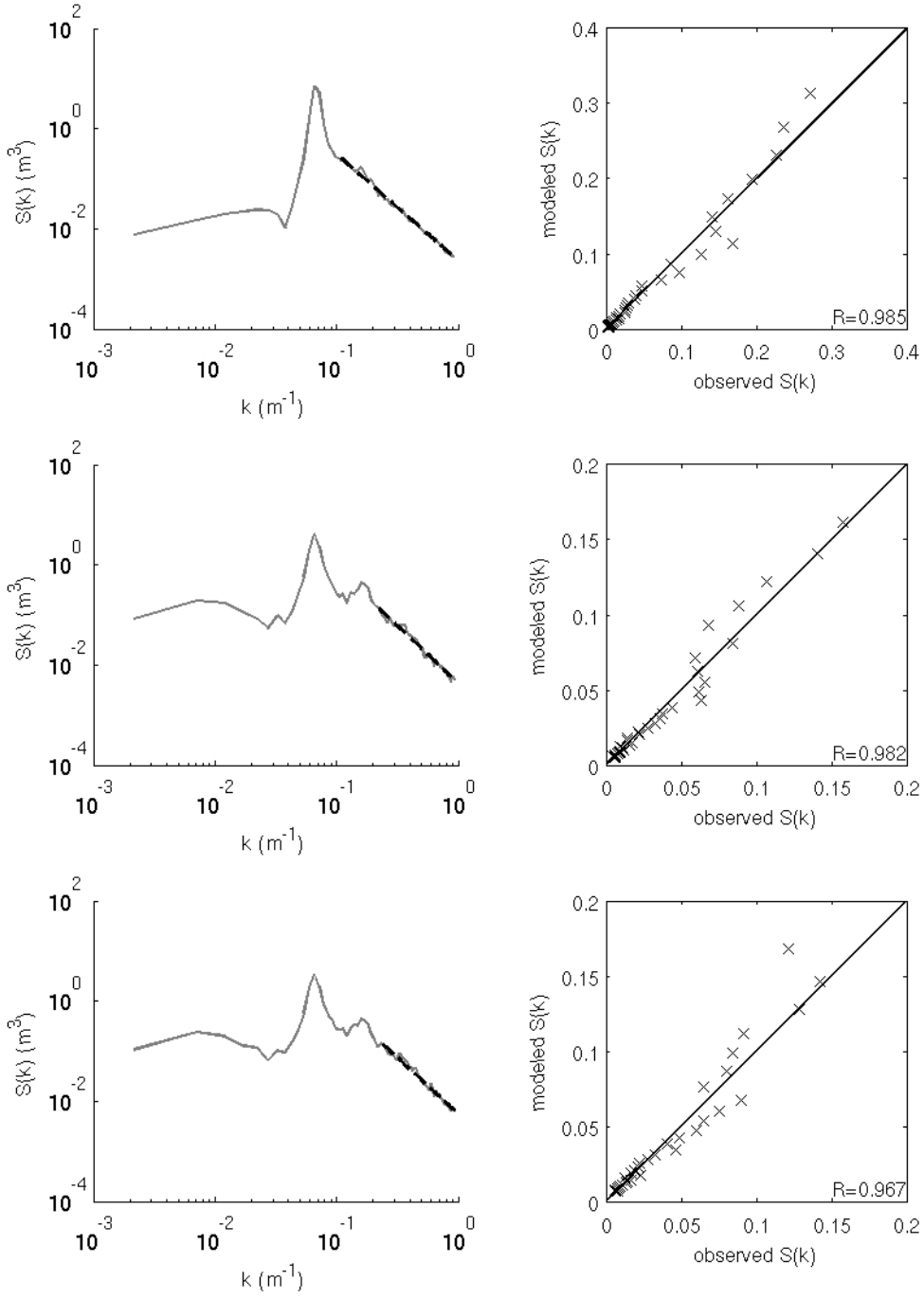

Figure A7 Comparisons of the observed wavenumber spectra (gray lines) and the "fit" lines (black dashed line) are shown in the left column. The correlation of the comparison is given in the right column. Comparisons are for depths of 10 (top), 5 (middle), and 4.5 (bottom) m in the long slope domain.

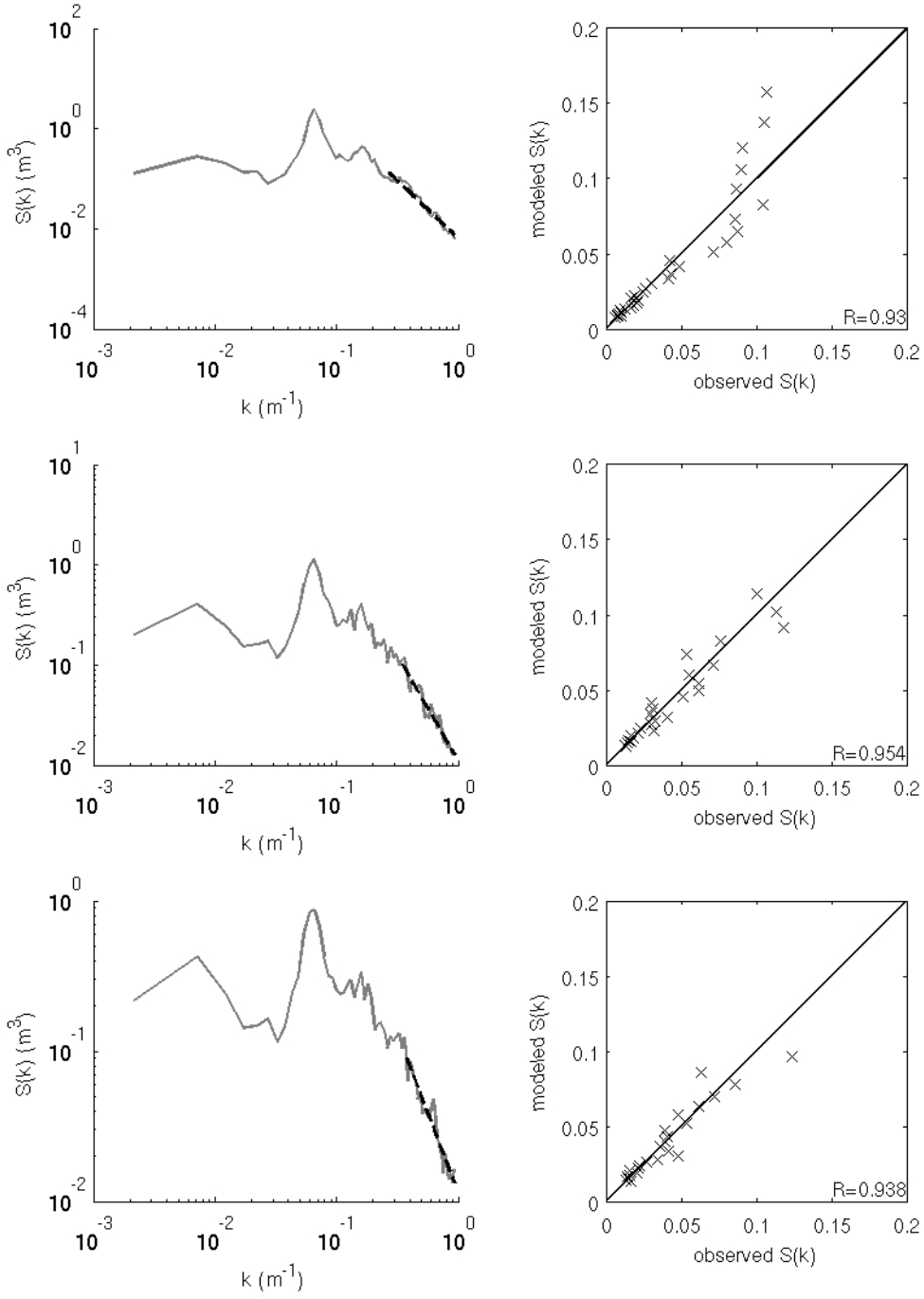

Figure A8 Comparisons of the observed wavenumber spectra (gray lines) and the "fit" lines (black dashed line) are shown in the left column. The correlation of the comparison is given in the right column. Comparisons are for depths of 4 (top), 3 (middle), and 2.75 (bottom) m in the long slope domain.

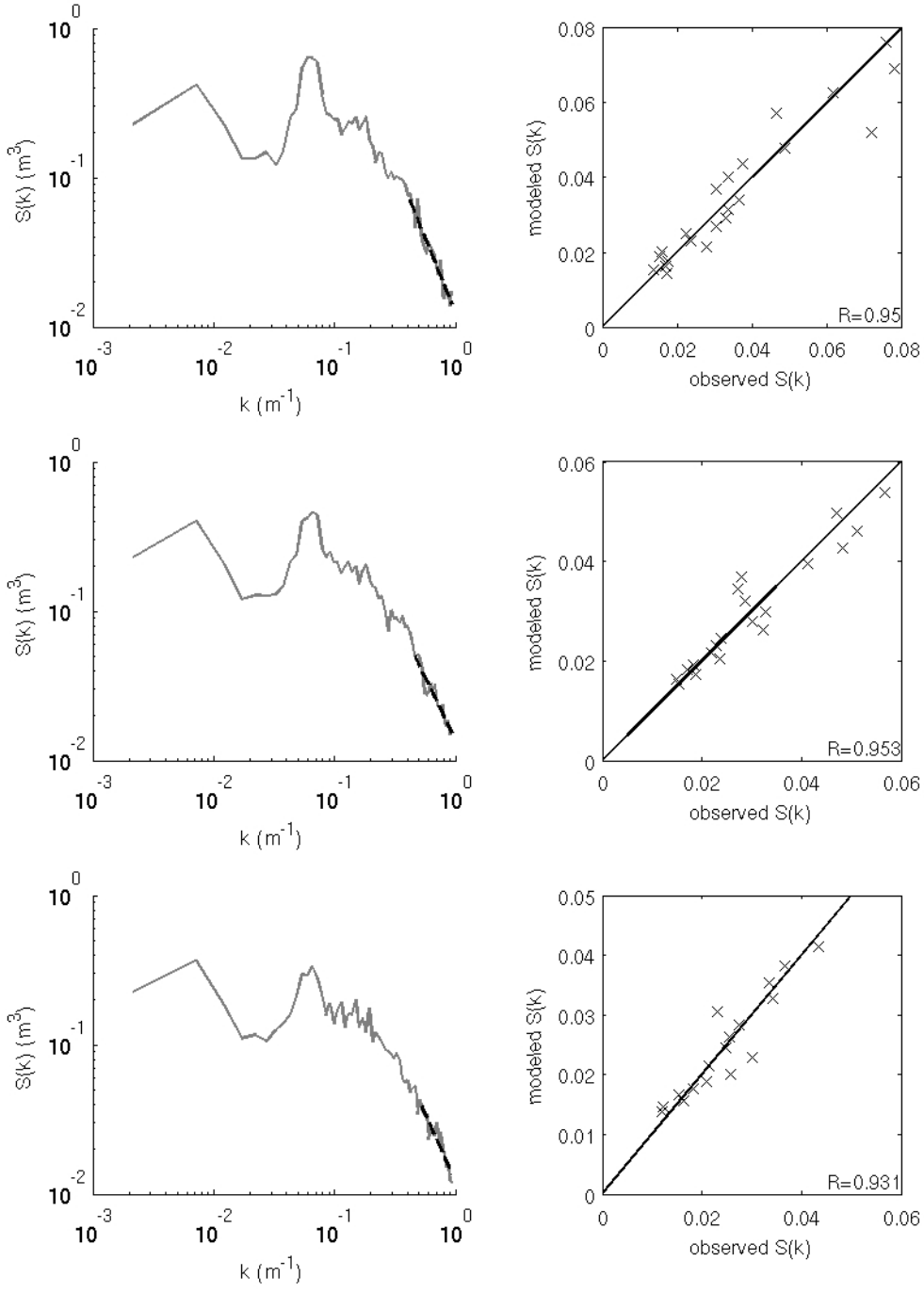

Figure A9 Comparisons of the observed wavenumber spectra (gray lines) and the "fit" lines (black dashed line) are shown in the left column. The correlation of the comparison is given in the right column. Comparisons are for depths of 2.5 (top), 2.25 (middle), and 2 (bottom) m in the long slope domain.

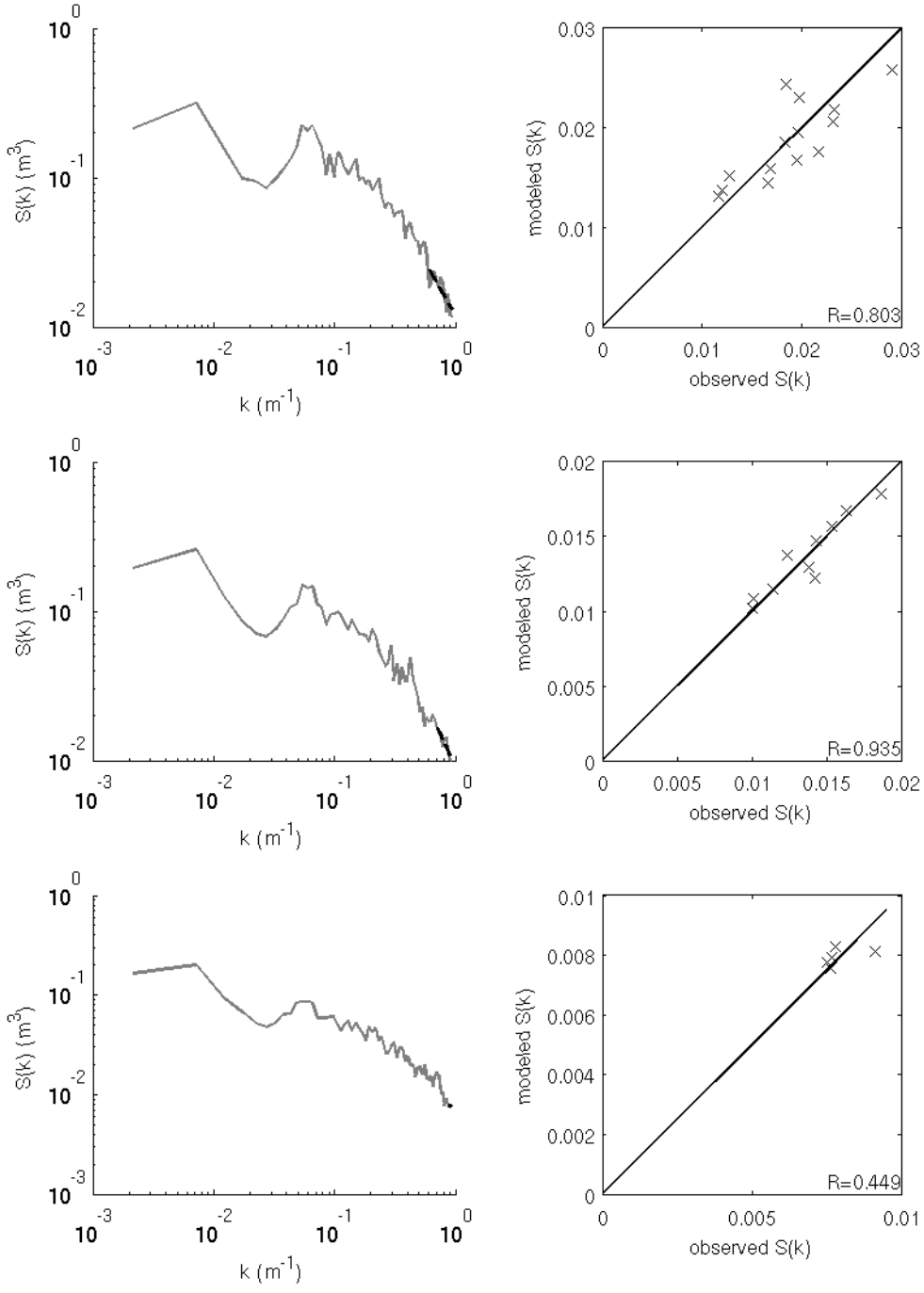

Figure A10 Comparisons of the observed wavenumber spectra (gray lines) and the "fit" lines (black dashed line) are shown in the left column. The correlation of the comparison is given in the right column. Comparisons are for depths of 1.75 (top), 1.5 (middle), and 1.25 (bottom) m in the long slope domain.

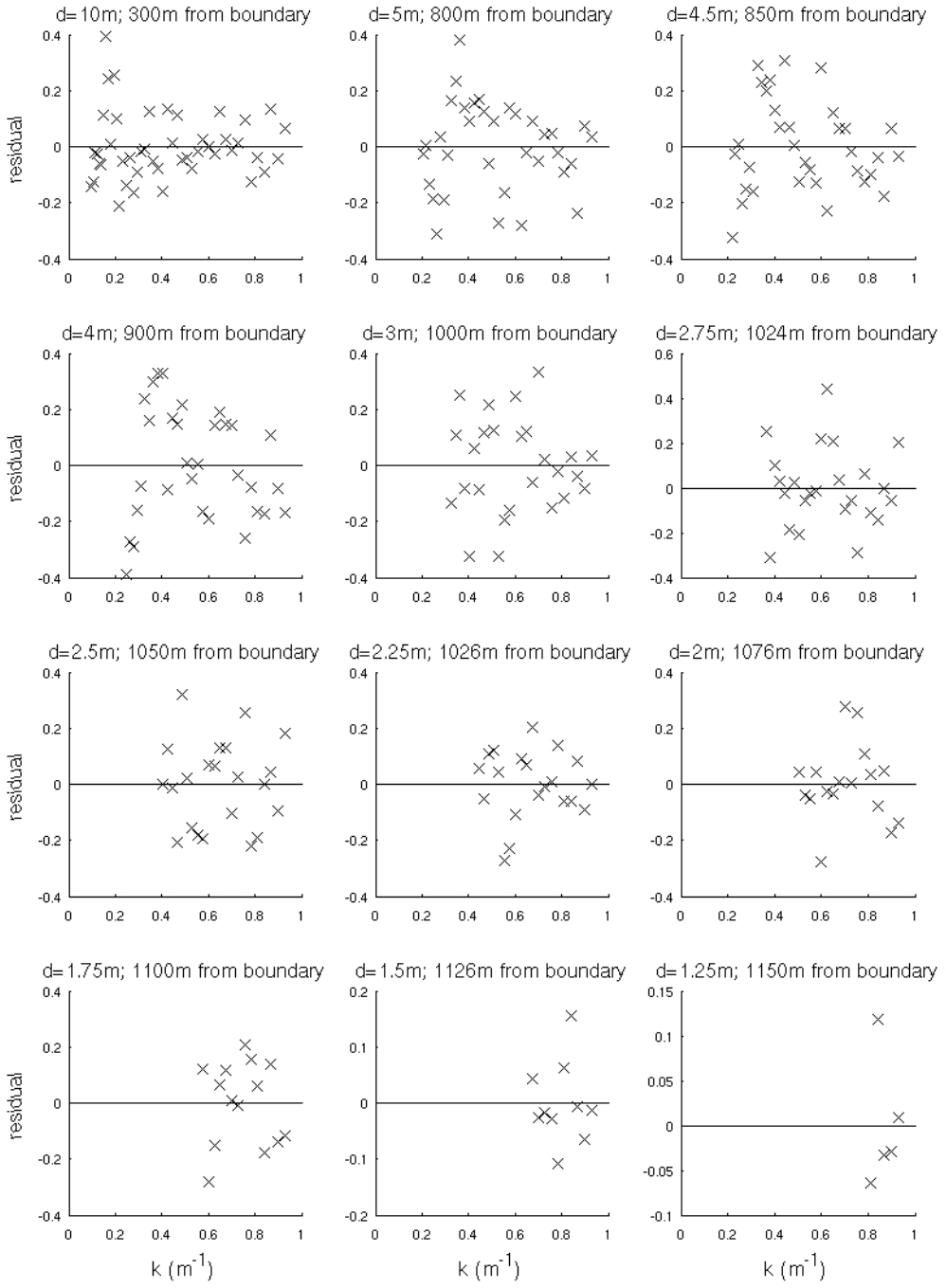

Figure A11 Scatter plots of the residuals resulting from the regression lines and full model results in the long slope domain.

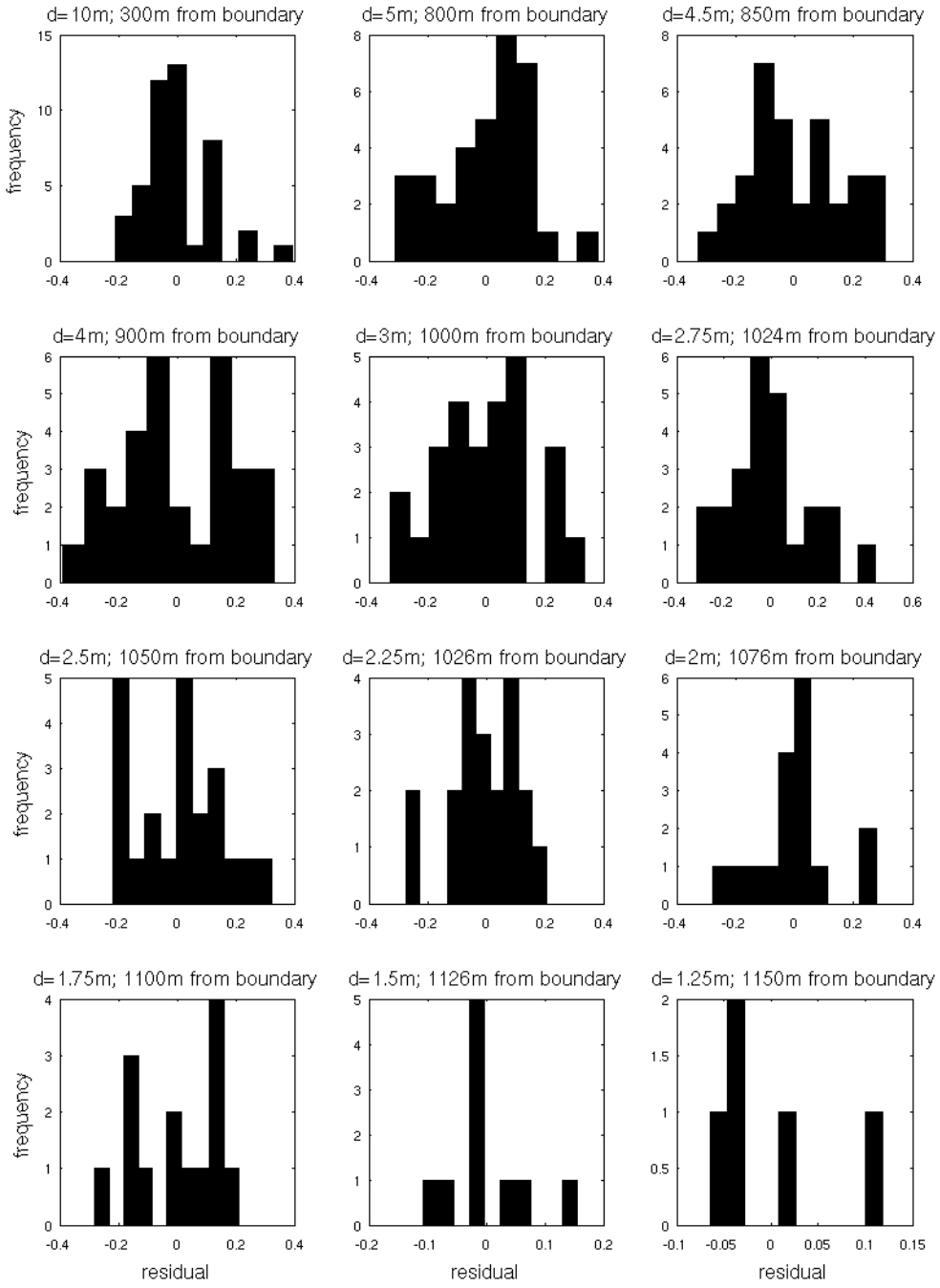

Figure A12 Distributions of residuals resulting from the regression lines and the full model results of the long slope domain.

Table A2

ANOVA for the regressions of the long slope domain.

d=10m					
Source	**DOF**	**Sum of Squares**	**Mean Squares**	**F Ratio**	**p**
Error	*43*	*0.616*	*0.014*		
Regression	*43*	*89.437*	*89.437*	*6246.505*	*0.010*
d=5m					
Source	**DOF**	**Sum of Squares**	**Mean Squares**	**F Ratio**	**p**
Error	*32*	*0.827*	*0.026*		
Regression	*32*	*35.879*	*35.879*	*1387.966*	*0.021*
d=4.5m					
Source	**DOF**	**Sum of Squares**	**Mean Squares**	**F Ratio**	**p**
Error	*31*	*0.822*	*0.027*		
Regression	*31*	*30.615*	*30.615*	*1154.023*	*0.023*
d=4m					
Source	**DOF**	**Sum of Squares**	**Mean Squares**	**F Ratio**	**p**
Error	*29*	*1.176*	*0.041*		
Regression	*29*	*25.170*	*25.170*	*620.530*	*0.032*
d=3m					
Source	**DOF**	**Sum of Squares**	**Mean Squares**	**F Ratio**	**p**
Error	*24*	*0.710*	*0.030*		
Regression	*24*	*11.194*	*11.194*	*378.261*	*0.041*
d=2.75m					
Source	**DOF**	**Sum of Squares**	**Mean Squares**	**F Ratio**	**p**
Error	*22*	*0.720*	*0.033*		
Regression	*22*	*8.423*	*8.423*	*257.315*	*0.049*
d=2.5m					
Source	**DOF**	**Sum of Squares**	**Mean Squares**	**F Ratio**	**p**
Error	*20*	*0.504*	*0.025*		
Regression	*20*	*5.579*	*5.579*	*221.282*	*0.053*
d=2.25m					
Source	**DOF**	**Sum of Squares**	**Mean Squares**	**F Ratio**	**p**
Error	*18*	*0.272*	*0.015*		
Regression	*18*	*2.871*	*2.871*	*189.918*	*0.057*
d=2m					
Source	**DOF**	**Sum of Squares**	**Mean Squares**	**F Ratio**	**p**
Error	*15*	*0.297*	*0.020*		
Regression	*15*	*1.928*	*1.928*	*97.246*	*0.079*
d=1.75m					

Source	DOF	Sum of Squares	Mean Squares	F Ratio	p
Error	*12*	*0.289*	*0.024*		
Regression	*12*	*0.611*	*0.611*	*25.421*	*0.154*
d=1.5m					
Source	**DOF**	**Sum of Squares**	**Mean Squares**	**F Ratio**	**p**
Error	*8*	*0.048*	*0.006*		
Regression	*8*	*0.319*	*0.319*	*52.967*	*0.106*
d=1.25m					
Source	**DOF**	**Sum of Squares**	**Mean Squares**	**F Ratio**	**p**
Error	*3*	*0.020*	*0.007*		
Regression	*3*	*0.005*	*0.005*	*0.810*	*0.652*

ACKNOWLEDGMENTS

I recognize and thank Dr. Jane McKee Smith of the US Army Engineer Research and Development Center's Coastal and Hydraulics Laboratory and Dr. James Kirby at the University of Delaware for providing data needed for the study. The work was supported by the Office of Naval Research through the 6.1 NRL Core Project "Nonlinear Interactions in Nearshore Environments," Program Element 61153N.

REFERENCES

Battjes, J. A. (1994). Shallow water wave modeling. In M. Isaacson & M. Quick (Eds.), *Proceedings of the International Symposium: Waves-Physical and Numerical Modeling* (pp.1-23). Vancouver, Canada: University of British Columbia.

Berkhoff, J. C. W. (1972). Computation of combined refraction-diffraction. In *Proceedings of the Thirteenth Coastal Engineering Conference* (pp. 471-490). New York: American Society of Civil Engineers.

Booij, N., Ris, R.C., & Holthuijsen, L.H. (1999). A third generation model for coastal regions. 1. Model description and validation. *Journal of Geophysical Research, 104,* 7649-7666.

Bouws, E., Gunther, H., Rosenthal, W., & Vincent, C. L. (1985). Similarity of the wind wave spectrum in finite depth water. 1. Spectral form. *Journal of Geophysical Research, 90*, 975-986.

Bredmose, H. (2002). *Deterministic modeling of water waves in the frequency domain*. PhD Thesis, Technical University of Denmark, Denmark.

Chen, Y., Guza, R. T., & Elgar, S. (1997). Modeling spectra of breaking surface waves in shallow water. *Journal of Geophysical Research, 102*, 25035-25046.

Cox, D. T., Kobayashi, N., & Wurjanto, A. (1991). Permeability effects on irregular wave runup and reflection. *Journal of Coastal Research*, *7*, 127-136.

Dean, R. G., & Dalrymple, R. A. (1991). *Water Wave Mechanics for Scientists and Engineers*. Singapore: World Scientific.

Dingemans, M. W. (1997). *Water Wave Propagation over Uneven Bottoms Part 1.* River Edge, NJ: World Scientific.

Eldeberky, Y., & Battjes, J. A. (1996). Spectral modeling of wave breaking: Application to Boussinesq equations. *Journal of Geophysical Research, 101*, 1253-1264.

Eldeberky, Y., & Madsen, P. A. (1999). Deterministic and stochastic evolution equations for fully-dispersive and weakly nonlinear waves. *Coastal Engineering, 38*, 1-24.

Herbers, T. H. C., & Burton, M. C. (1997). Nonlinear shoaling of directionally spread waves on a beach. *Journal of Geophysical Research, 102*, 21101-21114.

Herbers, T. H. C., Russnogle, N. R., & Elgar, S. (2000). Spectral energy balance of breaking waves within the surf zone. *Journal of Physical Oceanography,30*, 2723-2737.

Horikawa, K. (Ed.). (1988). *Nearshore Dynamics and Coastal Processes*. Japan: University of Tokyo Press.

Kaihatu, J. M. (1994). Frequency-domain models for nonlinear finite depth water wave propagation. PhD Thesis. University of Delaware.

Kaihatu, J. M. (2001). Improvement of parabolic nonlinear dispersive wave model. *Journal of Waterway, Port, Coastal, and Ocean Engineering, 127*, 113-121.

Kaihatu, J. M. (2003). Frequency domain wave models in the nearshore and surf zones. In V. C. Lakhan (Ed.), *Advances in Coastal Modeling* (pp. 43-72). Amsterdam: Elsevier.

Kaihatu, J. M., & Kirby, J. T. (1995). Nonlinear transformation of waves in finite water depth. *Physics of Fluids, 7*, 1903-1914.

Kaihatu, J.M., & Kirby, J.T. (1996) Effects of mode truncation and dissipation on predictions of higher order statistics. in B.L. Edge (Ed.), *Proceedings of the 25th International Conference of Coastal Engineering*, (pp. 123-136), Reston, VA: American Society of Civil Engineers.

Kirby, J.T. (1986). Higher order approximations in the parabolic equation method for water waves. *Journal of Geophysical Research, 91,* 933-952.

Kirby, J. T. (1997). Nonlinear, dispersive long waves in water of variable depth. In J. N. Hunt (Ed.), *Gravity Waves in Water of Finite Depth* (pp. 55-126). Great Britain: Computational Mechanics Publications.

Kirby, J. T. (2003). Boussinesq models and applications to nearshore wave propagation, surf zone processes and wave-induced currents. In V. C. Lakhan (Ed.), *Advances in Coastal Modeling* (pp. 1-41). Amsterdam: Elsevier.

Kirby, J.T., & Kaihatu, J.M. (1996). Structure of frequency domain models for random wave breaking. , in B.L. Edge (Ed.), *Proceedings of the 25th International Conference of Coastal Engineering*, (pp. 1144-1155), Reston, VA: American Society of Civil Engineers.

Madsen, P. A., & Sørensen, O. R. (1993). Bound waves and triad interactions in shallow water. *Ocean Engineering, 20*, 359-388.

Mase, H., & Kirby, J. T. (1992). Hybrid frequency-domain KdV equation for random wave transformation. In B. L. Edge (Ed.), *Proceedings of the 23rd International Conference of Coastal Engineering* (pp. 474-487). Reston, VA: American Society of Civil Engineers.

Peregrine, D. H. (1967). Long waves on a beach. *Journal of Fluid Mechanics, 27*, 815-827.

Phillips, O. M. (1980) *The Dynamics of the Upper Ocean* (2nd Ed.). Cambridge: Cambridge University Press.

Radder, A.C. (1979). On the parabolic equation method for water-wave propagation. *Journal of Fluid Mechanics, 95,* 159-176.

Resio, D. T., Pihl, J. H., Tracy, B. A., & Vincent, C. L. (2001). Nonlinear energy fluxes and the finite depth equilibrium range in wave spectra. *Journal of Geophysical Research, 106*, 6985-7000.

Smith, J. M., & Vincent, L. V. (2003). Equilibrium ranges in surf zone wave spectra. *Journal of Geophysical Research, 108*, 3366-3376.

Thornton, E. B. (1977). Rederivation of the saturation range in the frequency spectrum of wind-generated gravity waves. *Journal of Physical Oceanography, 7*, 137-140.

Thornton, E. B., & Guza, R. T. (1983). Transformation of wave height distribution. *Journal of Geophysical Research, 88*, 5925-5938.

Zakharov, V. (1999). Statistical theory of gravity and capillary waves on the surface of a finite-depth fluid. *European Journal of Mechanics-Fluids, 18*, 327-344.